THE IMPACT OF VESTIBULAR MODULATIONS ON WHOLE BRAIN STRUCTURE AND FUNCTION IN HUMANS

Judita Huber

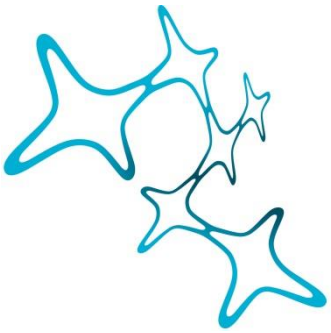

Graduate School of
Systemic Neurosciences

LMU Munich

Dissertation der
Graduate School of Systemic Neurosciences
der Ludwig-Maximilians-Universität München

October, 2020

Supervisor
Dr. Virginia L. Flanagin
German Center for Vertigo and Balance Disorders
Ludwig-Maximilians-Universität München

First Reviewer: Dr. Virginia L. Flanagin
Second Reviewer: Prof. Dr. Thomas Geyer
Third Reviewer: Prof. Dr. Dominik Straumann
Date of Submission: 8th of October, 2020
Date of Defense : 25th of January, 2021

Dedicated to my family

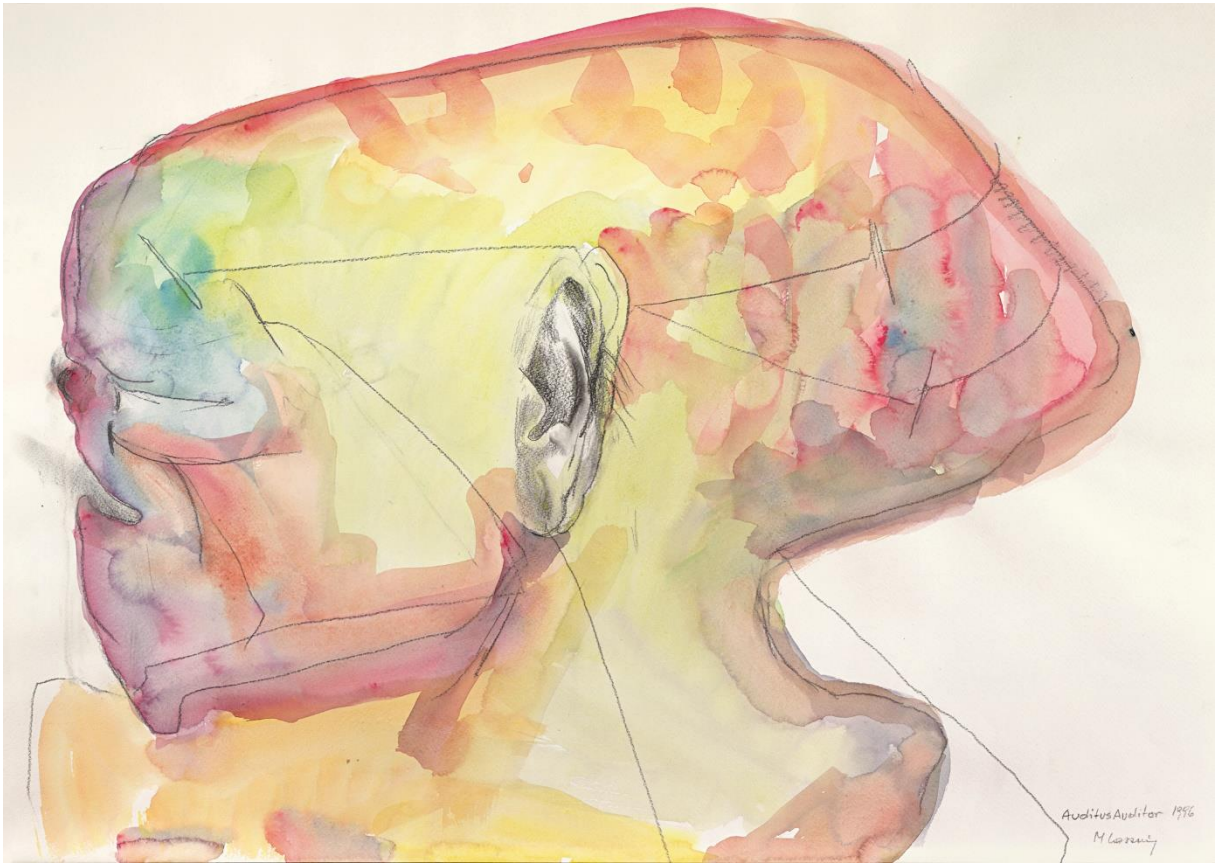

Maria Lassnig, Auditus Auditor, 1996 © Maria Lassnig Stiftung

Abstract

The vestibular system is a sensory system that monitors active and passive head movements while at the same time permanently sensing gravity. Vestibular information is important for maintaining balance and stabilisation of vision and ultimately for general orientation in space. A distributed set of cortical vestibular regions process vestibular sensory information, together with other sensory and motor signals. How these brain regions are influenced by or interact with each other, and how this depends on the context in which the system is acting is not well understood.

In my research I investigated the whole brain consequences of different vestibular sensory contexts by means of structural and functional magnetic resonance (MR) imaging on three different time scales (long-term, short-term, and medium-term). For the long-term time scale, I investigated functional brain connectivity in individuals experiencing a type of chronic dizziness that cannot be explained by structural damage within the nervous system. These patients exhibit chronic or long-term alterations in their processing of vestibular information, which leads to dizziness and vertigo. I found altered sensory and cerebellar network connectivity when they experience a dizziness-provoking stimulus. These two networks contain, but are not limited to, vestibular processing regions, demonstrating the importance of a whole-brain approach. The alterations correspond the notion that these patients have dysfunctional stimulus expectations.

The short-term vestibular processing I investigated was the effect of artificial vestibular stimulation, which is frequently used in vestibular research and treatment. For this, I analysed functional network connectivity in healthy participants. I found that short-term vestibular stimulation does not cause a cortical functional reorganisation, although a nociceptive stimulus, which was matched for the somatosensory component of this stimulation, led to a reorganisation. The fact that cortical reorganisation does not occur during exclusively vestibular stimulation may reflect subconscious nature of vestibular processing in that it does not induce a different internal brain state.

On the medium-term time scale, I investigated whole-brain structural changes as a result of gravity. Astronauts that travel to space for extended periods of time experience several physiological symptoms also affecting the fluid exchange of the brain. To characterise if these fluid exchanges also affect size of the spaces around brain blood vessels (perivascular spaces), I developed a semi-automatic detection pipeline which requires only one type of

structural MR image. I found that space travellers have enlarged perivascular spaces even before their mission, when compared to a control population. These spaces were to a small extend further increased shortly after a long duration space flight of 6 months. Astronaut training thus contributes to structural changes in the whole brain in combination with long-duration space flight. This further suggests that additional contextual factors such as sleep quality should be considered in the future.

Overall, in my thesis I show that investigating the whole brain during different vestibular modulations provides additional and novel insights about the underlying neural processes. I found that long-term vestibular states have an impact on functional networks, whilst short-term vestibular modulations do not seem to impact functional network organisation. In addition, I quantified the structural impact of microgravity and astronaut training in the whole brain using a new analysis pipeline. In the future, I expect that new advancements in the field of neuroimaging analysis, such as high sampling of individuals and dynamic network analysis will advance the field. This will potentially also provide new means to monitor disease progression or intervention success.

Content

List of Figures

List of Tables

List of Abbreviations

ANOVA	Analysis of variance
AUC	Area under the curve
BA	Brodmann area
BOLD	Blood oxygen level-dependent
CC	Clustering coefficient
CSF	Cerebrospinal fluid
CSv	Cingulate sulcus visual area
DC	Degree centrality
ECC	Eccentricity
EEG	Electroencephalography
ESA	European space agency
FA	Flip angle
FD	Framewise displacement
fMRI	Functional magnetic resonance imaging
FOV	Field of view
FWER	Family-wise error rate
GE-EPI	Gradient-echo echo planar imaging
GNS	Galvanic nociceptive stimulation
GVS	Galvanic vestibular stimulation
HC	Healthy controls
IQR	Interquartile range
ISF	Interstitial fluid
MEG	Magnetoencephalography
MNI-space	Montreal Neurological Institute standard space
MPRAGE	Magnetization prepared rapid acquisition gradient echo
MRI	Magnetic resonance imaging
MST	Medial superior temporal area
MT	Middle temporal area
NBS	Network-based statistics
OP	Parietal opercular area
PF	Inferior Parietal Lobule cytoarchitectonic area PF
PFcm	Inferior Parietal Lobule cytoarchitectonic area PFcm
Pfop	Inferior Parietal Lobule cytoarchitectonic area PFop
PIVC	Parieto-insular vestibular cortex

PPD	Persistent postural-perceptual dizziness
PPV	Phobic postural vertigo
PVS	Perivascular space
ROI	Region of interest
ROSCOSMOS	Roscosmos State Corporation for Space Activities
rs-fMRI	Resting state functional magnetic resonance imaging
SD	Standard deviation
SMA	Supplementary motor area
T1	T1 weighted image
TE	Echo time
TFCE	Threshold-free cluster enhancement
TR	Repetition time
V5	Visual area V5
VEMP	Vestibular evoked myogenic potentials
VIP	Ventral intraparietal area
VPS	Visual posterior sylvian area
WM	White matter

1. General Introduction

1.1 Perception in Context

In his essay on the topic of dizziness at the beginning of the 19th century, the Czech physiologist Jan Purkyně (better known today as Johann Purkinje, the discoverer of the large Purkinje cells of the cerebellum) described an observation which was later termed the 'motion aftereffect'. He reported that, after watching a directed motion continuously for a longer period of time, one perceives still objects to move in the opposite direction for a short amount of time (Anstis, Verstraten, & Mather, 1998; Purkinje, 1820). One way to experience this effect in nature is to look at a rock within a waterfall for a prolonged time and then to move the gaze quickly to the river bank, where the water will now seem to flow upwards (Anstis et al., 1998). Over a hundred years after Purkyně's description of the motion aftereffect, Barlow and Hill (1963) reported that activity of ganglion cells in the rabbit retina was closely related to the mentioned motion aftereffect phenomenon. They proposed a mechanism in which the perceived aftereffect results from a temporary imbalance of activity in cells which are responsive to motion in opposite directions. When motion stops, the activity of the responsive cell falls below baseline, the activity of the opposite cell thus becomes relatively stronger, which creates the perception of motion in the opposite direction.

Studying perceptual phenomena in isolation has provided an in depth knowledge of the principles of brain function, but studying sensory information in different contexts yields a more realistic understanding. Context here can be defined as internal or external state changes of the organism which persist for a certain duration (ranging from temporary to long-lasting). Internal state differences were for example found to influence the perception of the motion aftereffect: in patients who are suffering from chronic dizziness, perceived duration of the motion aftereffect was found to be longer when compared to healthy controls, and also brain activity differed between the two groups (Popp et al., 2017). Studying the neural basis of perception in context often requires going beyond investigating isolated brain structures. Using the example of the motion aftereffect, increased activity in the macaque cortical area middle temporal area (MT) (Van Wezel & Britten, 2002) and in the homologous area V5 of the occipital cortex in humans (Culham et al., 1999) was found to be related to the perceived motion aftereffect. However, a recent study by Rühl, Bauermann, Dieterich, and zu Eulenburg (2018) described that the motion aftereffect was also related to more complex whole brain activation and deactivation patterns.

Investigating the neural basis of vestibular perception in context is somewhat more difficult than studying the neural basis of visual illusions such as the motion aftereffect. A unique feature of the vestibular sense is that vestibular information is so ubiquitous: gravity for example is constantly sensed by the otolith organs, thus providing a stable vertical reference (Angelaki & Cullen, 2008). We cannot simply pause or modulate vestibular perception. Healthy humans also lack a distinct conscious quality (or 'qualia') about vestibular input. This is in contrast to other sensory modalities such as vision or audition, where we know what it means to see or to hear and we can pause or minimise sensory input by closing our eyes or plug our ears. Instead, if we become aware of vestibular stimulation it is mostly because a type of modulation in vestibular information processing. In this thesis, I will give examples of such changes of varying duration and discuss their contributions to our understanding of the involved neural processes in humans.

1.2 The Human Vestibular System

1.2.1 Peripheral vestibular processing

The vestibular labyrinth in the inner ear contains five sensory organs for detecting vestibular information: two otolith organs and three semicircular canals (see Figure 1.1). These sensory organs are endolymph-filled, interconnected chamber structures in which the mechanical energy originating from head movement is detected by hair cells. Hair cells contain mechanically gated ion channels, thus allowing the transduction of mechanical signal to neural signals which are then further propagated to the brain via the vestibular nerve, a branch of the eight cranial nerve (Bear, Connors, & Paradiso, 2007).

The semicircular canals detect angular rotations in three orthogonal planes. The sensory epithelium is contained in a bulge of each canal called the ampulla at one of its conjunctions with the utricle, the ampulla (Goldberg et al., 2012). The ampulla contains hair cells which are clustered, with the cilia projecting into the gelatinous cupula. Therefore, during rotation of the canal, the endolymph lags behind and applies force to the cupula, thus bending the cilia on the hair cells (Bear et al., 2007). Each functional pair of the semicircular canals has opposite discharge properties – i.e. rotation will cause an increase of activity in hair cells in the canal on one side and decrease of activity in hair cells located on the other side (Goldberg et al., 2012). This difference allows to compute the rotation direction.

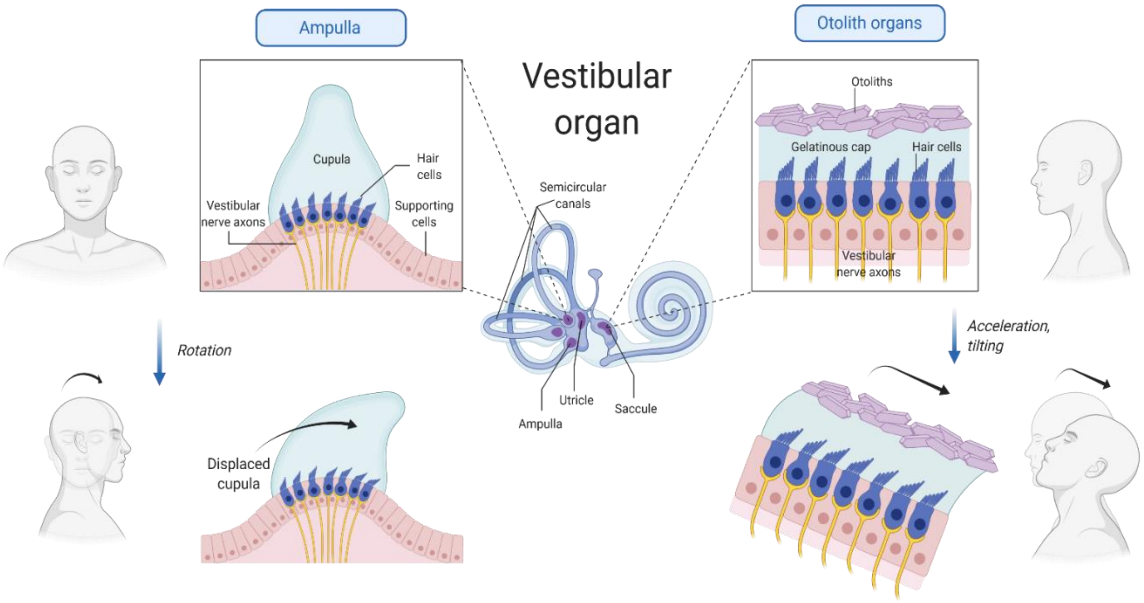

Figure 1.1 The vestibular organ.
Middle: The vestibular organ in the inner ear with sensory epithelium shown in purple. Left: Ampulla of the semicircular canals. Upon rotation of the head, the displacement of the cupula causes the hair cells to bend. Right: Otolith organs. Upon tilting of the head, the force of gravity pulls on the otoliths which deform the gelatinous cap, ultimately bending the embedded hair cells. Image created with BioRender.com.

The otolith organs consist of the saccule and the utricle. They detect the gravitational force vector and linear head translations. In the otolith organs, the macula is the actual sensory epithelium containing the hair cells. In an upright position, the macula is oriented vertically within the saccule, and horizontally within the utricle. The hair cell cilia are embedded in a gelatinous cap, which contains small calcium carbonate crystals called otoliths. When tilting the head, gravity creates a pulling force on the otoliths, which in turn deforms the gelatinous cap and thus causes the hair cell cilia to bend (Bear et al., 2007).

There are two types of primary vestibular sensor afferent neurons that carry the signals to the brain stem: those with regular and those with irregular resting discharge properties. These neurons differ in terms of their physiology, response dynamics and sensitivity to applied forces and electrical stimulation (Goldberg et al., 2012). Less is known about the efferents reaching the vestibular labyrinth, which arise from the brain stem. Evidence suggests a modulatory role, in that afferent discharge is modified by efferent activity (Goldberg et al., 2012).

1.1.1 Central vestibular processing pathways

The vestibular portion of the eighth cranial nerve terminates on ipsilateral secondary neurons in the vestibular complex of the brain stem. The vestibular complex of the brain stem consists of four main nuclei (medial, superior, lateral and descending/inferior nucleus), with no clear segregation of the inputs from afferents. In many species, inputs to

the vestibular complex originate in the brain stem, spinal cord, cerebellum and cerebral cortex (Goldberg et al., 2012). This demonstrates the multimodal nature of vestibular signal processing already at this first central processing stage.

The vestibular complex also projects to the brain stem, the spinal cord, the cerebellum and to the thalamus (Goldberg et al., 2012). The connections to the brain stem and the spinal cord are important for gaze and postural stabilisation respectively. The cerebellum receives connections from the vestibular complex to its anterior lobe, nodulus, ventral uvula, and also to the loculus and ventral para-flocculus (Goldberg et al., 2012). Each of these areas make a different contribution to vestibular processing such as posture, eye movements and multisensory integration (Barmack, 2003). Projections to the thalamus are further relayed to a wide range of cortical areas (Goldberg et al., 2012). Further integration with other sensory modalities occurs at these intermediate levels of processing.

At least two parallel ascending vestibular pathways send vestibular signals from the thalamus to the cortex: the anterior thalamocortical pathway and the posterior thalamocortical pathway (Cullen & Taube, 2017). The anterior pathway is important for the generation of the head direction signal, which is necessary for successful navigation and spatial memory (Yoder & Taube, 2014). Projections go to the retrosplenial and entorhinal cortical areas via the pre- and parasubiculum (Yoder & Taube, 2014). The posterior thalamocortical pathway is considered to be important for the perception and detection of self-motion and includes several cortical regions across all lobes, with partially overlapping functions in head motion detection (Smith, Greenlee, DeAngelis, & Angelaki, 2017). These cortical processing areas will be introduced in the following section.

1.1.2 Cortical vestibular processing

In contrast to other senses such as vision and audition, the identification of cortical areas in humans is somewhat complicated by methodological and technological restrictions. Most of our knowledge of cortical vestibular processing comes from single-cell recordings in the behaving monkey, which has revealed a widely distributed network of cortical regions that process different aspects of vestibular information. A combination of functional magnetic resonance imaging (fMRI) and artificial vestibular stimulation methods such as galvanic vestibular stimulation (see Section 1.3.2) have complimented our understanding of cortical vestibular processing in humans (see Figure 1.2).

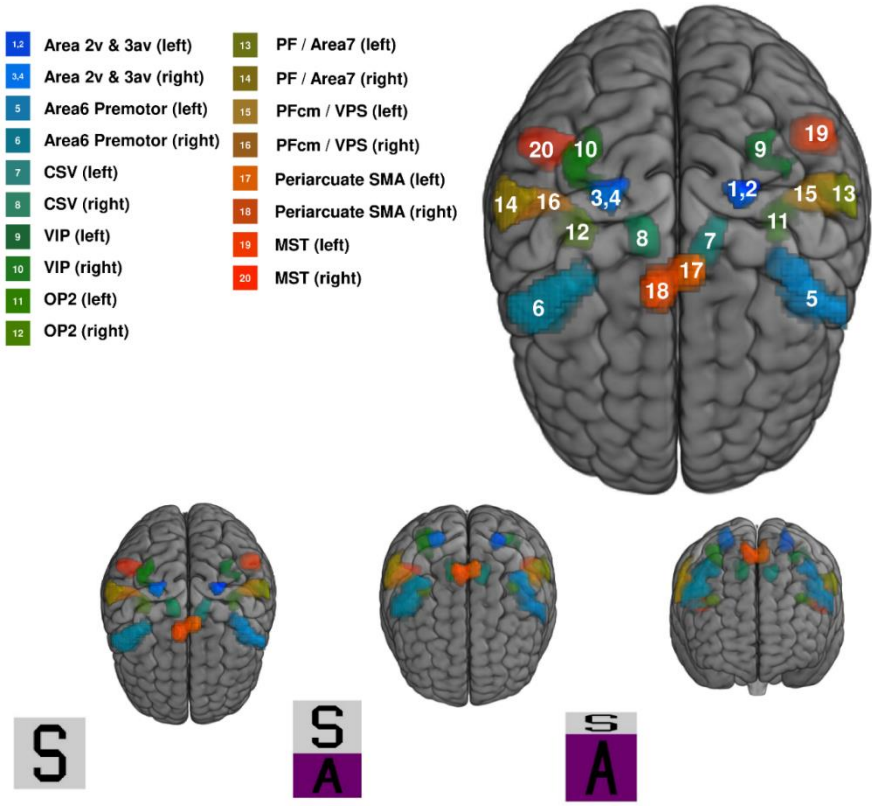

Figure 1.2 The vestibular cortical regions
Top: superior view with labelled regions. *Bottom*: rotation from superior to anterior view. CSV = cingulate sulcus visual area; VIP = Ventral intraparietal area; OP2 = parietal opercular area OP2 ; PF =Inferior Parietal Lobule cytoarchitectonic area PF; PFcm/VPS = Inferior Parietal Lobule cytoarchitectonic area PFcm/visual posterior sylvian area; SMA = supplementary motor area ; MST = medial superior temporal area. Figure created using MRIcroGL (Rorden, 2020). The regions shown are based on the atlas from zu Eulenburg et al. (2020).

The key region for cortical vestibular processing in the monkey is the parieto-insular vestibular cortex (PIVC), which contains a large amount of neurons responding to translational and rotational self-motion in the absence of visual input (i.e. in darkness) (Chen, DeAngelis, & Angelaki, 2010; Guldin & Grüsser, 1998). The human equivalent of this area was suggested to be located in the parietal opercular area OP2. This region is consistently activated in humans in response to various types of artificial vestibular stimulation (zu Eulenburg, Caspers, Roski, & Eickhoff, 2012).

Monkey PIVC is reciprocally interconnected with two areas: 2v at the tip of the intraparietal sulcus (Büttner & Buettner, 1978) and 3aV in the central sulcus. These connections were termed the 'inner cortical vestibular circuit' and have been suggested to be important for proprioceptive signal processing (Guldin, Akbarian, & Grüsser, 1992). In humans, area 3aV also shows a strong coupling with OP2 (zu Eulenburg et al., 2012).

Medial superior temporal area (MST) in the temporal lobe of the monkey contains neurons encoding both visual and vestibular stimuli (with a higher importance on the visual input)

(Smith et al., 2017). In human studies, the homologue brain region is thought to be located in the lateral occipital cortex, adjacent to the middle temporal area MT, also termed V5 (Smith et al., 2017). This region responds to both artificial vestibular stimulation as well as to visual motion stimuli (Smith, Wall, & Thilo, 2012).

The visual posterior sylvian area (VPS) at posterior tip of the sylvian sulcus receives input from MST and has known interconnections with PIVC in the macaque. It was also found to be responsive to both optic flow and vestibular stimuli (Chen, DeAngelis, & Angelaki, 2011). In contrast to MST, vestibular signalling dominates when both stimuli are presented together (Chen et al., 2011). In humans, cytoarchitectonic area PFcm of the inferior parietal lobule is suggested to be the homologue of VPS (zu Eulenburg, Stephan, Dieterich, & Ruehl, 2020).

In the macaque, area 7 in the inferior parietal lobule (a subdivision of the posterior parietal cortex) is important for encoding spatial relationships of objects in an allocentric coordinate system (Chafee, Averbeck, & Crowe, 2007). Area 7 is a heterogeneous region which is often separated into the area 7a and 7b, although other, more refined separations have been proposed on the basis of cytoarchitecture (Borra & Luppino, 2017; Rozzi et al., 2005; Scheperjans et al., 2007). These subregions have distinct connections and functions, some of which partially overlap with properties of PFcm in humans or VPS in monkeys (Rozzi et al., 2005). Other subregions of area 7 resemble connectivity and functional properties of cytoarchitectonic area PF of the inferior parietal lobule in humans (zu Eulenburg et al., 2020). Another cortical area in the parietal lobe of both macaque and human is the ventral intraparietal area (VIP). It is a highly multisensory region and was found to be involved in general multisensory integration (also in the absence of vestibular stimulation) (Smith et al., 2017).

In the frontal areas, area 6 and periarcuate cortex are involved in motor and oculomotor functions in the monkey (Ebata et al., 2004) and may be homologous to the human premotor cortex (Lopez & Blanke, 2011; zu Eulenburg et al., 2012) and supplementary motor area (SMA) respectively (zu Eulenburg et al., 2020).

The only vestibular cortical region that was first identified in humans is the cingulate sulcus visual area (CSv). This area responds to both artificial vestibular stimulation (Smith et al., 2012) and to optic flow stimulation indicative of egomotion (Wall & Smith, 2008). Using the same optic flow stimulus, Cottereau et al. (2017) located the corresponding region in macaque as being area 23c (or 23cv, see Shinder and Taube (2010)) in the posterior cingulate gyrus.

Considering these numerous regions located across the brain, one obvious question is: Why are so there so many cortical vestibular regions distributed across the brain? One explanation provided by Klingner, Axer, Brodoehl, and Witte (2016) is that these regions are brain regions of very different functioning which use information about head movement as an additional information for their respective tasks. Indeed, vestibular regions can often be differentiated in terms of the dominance of other (mostly visual) senses (Smith et al., 2017). Complementary to this notion, vestibular signalling was suggested to contribute to a range of cognitive processes, which also requires participation of distributed brain areas. Recent findings indicate a role not only in spatial navigation, but also in memory, object recognition and bodily self-consciousness (Hitier, Besnard, & Smith, 2014).

To summarise, cortical vestibular processing is very complex and involves many regions distributed across the brain, rather than one dedicated primary sensory cortex. In contrast to other senses, all of these regions are, at least to some extent, processing multisensory signals. It has been proposed that these regions participate in numerous, partially overlapping pathways (Hitier et al., 2014). It is not well understood how these brain regions are influenced by and interact with each other during different types of (or lack of) vestibular sensory input.

1.3 Probing the Vestibular System

Human neuroimaging and analysis methods allow the investigation of the full human brain and have been developed immensely in the last years. However, human vestibular research is made difficult by the fact that one of the most popular human neuroimaging methods, magnetic resonance imaging (MRI) requires the participants to lie still in a very narrow scanner bore, thus restricting the type of experiments being conducted. One way to circumvent this problem is to study groups of individuals who experience atypical vestibular input or processing, or to use artificial vestibular stimulation.

1.3.1 Disorders of the vestibular system

The most common impact of any perturbation to the vestibular system is dizziness (i.e. the sensation of feeling unsteady or faint) or vertigo (the sensation of spinning). Vertigo is commonly the result of a mismatch or conflict between the sensory systems encoding motion, i.e. the vestibular, visual an somatosensory systems (Brandt, 2013). Clinically, vertigo is defined as a combination of phenomena which include perceptual, ocular motor, postural and autonomic symptoms (Brandt, 2013). Ocular motor symptoms include ocular

deviations or nystagmus (i.e. involuntary eye movements), postural symptoms include abnormalities in posture or gait and autonomic symptoms include nausea, vomiting and anxiety (Brandt, 2013). Vestibular disorders are typically associated with vertigo, which can have extremely debilitating effect on daily functioning (Brandt & Dieterich, 2017).

One of the most obvious causes of vestibular system disorders is physical damage to the underlying structure. Damage can occur at any point of the vestibular processing pathway and can thus affect the peripheral vestibular system or the central vestibular system. The duration of symptoms can also be categorised into acute, episodic and chronic. The most frequent cause for vestibular symptoms is benign paroxysmal vertigo. This is a common condition of the peripheral vestibular system, where loosened otoliths move to the semicircular canals, thus causing episodes of strong rotatory vertigo (Brandt & Dieterich, 2017; Furman & Cass, 1999). Once the freely moving otoliths are moved to the ampulla of the vestibular organs, vertigo terminates (Furman & Cass, 1999). In some cases, recovery of vestibular function can also occur in cases of permanent damage to the vestibular pathway due to the bilateral organisation of the vestibular system. In unilateral peripheral vestibulopathy for example, the peripheral damage on one side can be compensated by central structures and can thus lead to recovery of vestibular function after appropriate therapy (Brandt & Dieterich, 2017). Bilateral vestibulopathy on the other hand is a chronic condition characterised by bilateral reduction or absence of function, with very poor recovery rates (Brandt et al., 2010).

Not all cases of episodic and chronic dizziness can be explained by structural damage though. In fact, one of the most common diagnoses in specialised neurological clinics is functional dizziness. Symptoms include chronic dizziness (i.e. feelings of unsteadiness and faintness) with no structural origin, thus suggesting a somatoform origin (Dieterich & Staab, 2017). The symptoms can be triggered by certain situations or visual stimulation (Dieterich & Staab, 2017). Despite the lack of physical origin, chronic dizziness does have an impact on behaviour and on central nervous system functioning. For example, postural performance is abnormal during simple standing, but normalises when a distraction task is presented (Querner, Krafczyk, Dieterich, & Brandt, 2000; Schniepp et al., 2014; Wuehr, Brandt, & Schniepp, 2017). Moreover, grey matter volume changes in distributed sets of brain regions (the thalamus, the prefrontal gyrus and the cerebellum, amongst others) were found to correlate with disease markers, suggesting neural reorganisation. Using fMRI task activation studies, a distributed pattern of brain activation was found in previous studies, suggesting differences in anterior cingulate cortex activations (Indovina et al., 2015; Popp et al., 2017), but also insula and hippocampus (Indovina et al., 2015).

1.3.2 Artificial vestibular stimulation

A few artificial vestibular stimulation techniques exist that are very useful for furthering the understanding of the neural processing of vestibular information, since they allow for within-participant controls and testing in controlled environments. Examples of these techniques include caloric irrigation, vestibular evoked myogenic potentials (VEMPs) and galvanic vestibular stimulation.

Galvanic vestibular stimulation (GVS) directly activates the vestibular nerve by means of electrical current. Electrodes are placed on the two mastoid processes and a weak direct current (typically not stronger than 5 mA (Curthoys & MacDougall, 2012)) is passed through the electrodes. This depolarises the vestibular primary afferents on the side on the cathode, while it hyperpolarises the vestibular afferent on the side of the anode (Goldberg, Smith, & Fernandez, 1984). The result is a strong perception of head and partial upper body movements towards the anode (Fitzpatrick & Day, 2004). Evidence that indeed the peripheral vestibular system is being stimulated comes from postural and oculomotor responses to GVS (Forbes et al., 2016; Nashner & Wolfson, 1974; Schneider, Glasauer, & Dieterich, 2002; Zink et al., 1998).

The precise mechanism of GVS has been the subject of several scientific enquiries. Behavioural responses in humans have been inconclusive, with some studies suggesting that GVS preferably stimulates the otoliths at low currents (Zink et al., 1998), although other studies propose equal contributions of otoliths and semicircular canals (Fitzpatrick & Day, 2004). Recently, vestibular afferents were recorded during sinusoidal GVS in the behaving primate (Kwan et al., 2019). They found that both otoliths and semicircular canals are stimulated by GVS. Whilst there was no difference in terms of vestibular organ activation, Kwan et al. (2019) found that irregular afferents of both organs were more responsive to GVS compared to the regular afferents. Still, these afferents transferred equivalent levels of information to the central vestibular pathways (Kwan et al., 2019). Interestingly, GVS has been successfully used in treating clinical disorders such as vestibulopathy (Schniepp et al., 2018) and even Parkinson's disease (Samoudi, Jivegård, Mulavara, & Bergquist, 2015) and stroke (Wilkinson et al., 2014). Application of GVS was further found to influence higher cognitive functions (for example Hilliard et al., 2019; Wilkinson et al., 2008). This further corroborates the notion that vestibular information is processed in higher-order brain regions.

GVS has been frequently used in vestibular research since it provides the possibility to deliver a customisable, consistent and bilateral stimulus. Other types of artificial vestibular

stimulation also exist, but these mostly only activate portions of the vestibular organs. Sound induced vestibular stimulation is provided by means of clicks or short tone bursts, which trigger VEMPs, reflecting the activation of the sacculus (Schlindwein et al., 2008). Caloric vestibular stimulation is performed by injection of cold or warm water, which mostly activates the horizontal semicircular canals, with a weaker contribution of the vertical canals (Lopez, Blanke, & Mast, 2012).

1.3.3 Microgravity

In the more unusual case, perturbations to vestibular signal processing can also occur due to different gravitational environments, such as during spaceflight. In space, gravity is reduced to 10^{-6} of the gravity experienced on earth, a condition called microgravity. This leads to a substantial change in the input to the vestibular organ, but it also has a range of effects on general physiology. In the following, I will discuss these physiological effects of temporarily reduced exposure to gravity on the brain.

Microgravity has wide ranging effects which may also persist after exposure. In terms of specific changes to the vestibular system, otolith organ function (but not semicircular canal function) seems to be temporarily affected by exposure to microgravity (Clément et al., 2020; Tanaka, Nishimura, & Kawai, 2017). In particular, ocular counter-rolling, an otolith-driven reflex, is decreased when astronauts return from a space mission of 6 months, but normalises after 9 days (Hallgren et al., 2016). Other temporary effects not directly related to vestibular functioning, but impacting general physiology included sleep deprivation (Barger et al., 2014) and bone and muscle loss (Tanaka et al., 2017), nausea, changes in spatial orientation, sensorimotor coordination and cardiovascular dynamic (Clément et al., 2020; Morita, Kaji, Ueta, & Abe, 2020). Notable long lasting effects of prolonged exposure to microgravity are visual acuity changes (Mader et al., 2011), and increased ventricle volume in the brain (Van Ombergen et al., 2019). Current theories suggest that these changes are related to circulatory changes in brain fluids induced by the lack of gravity.

Such cephalic fluid shift has been suggested as a driving component of changes in the central nervous system. In healthy humans, the force of hydrostatic pressure drives circulation of body fluids and the body's alignment to the gravitational field will change fluid circulation (Hinghofer-Szalkay, 2011). The lack of the gravitational force removes this pressure, thus resulting in fluid movement to the head (Lathers et al., 1989; Nelson, Mulugeta, & Myers, 2014). Due to this cephalic fluid shift, the resorption of the

cerebrospinal fluid into the venous cranial vasculature and hence the interstitial tissue flow of the brain may be disturbed, causing changes across the entire brain.

This system responsible for fluid exchange in the brain was termed glymphatic (glial-lymphatic) system. It is an astrocyte-mediated cerebrospinal fluid (CSF) and interstitial fluid (ISF) system which clears the brain from metabolic waste (Abbott et al., 2018; Mestre, Mori, & Nedergaard, 2020). In the healthy organism, this is accomplished by bulk flow of CSF into arterial perivascular spaces (the spaces that surround small blood vessels, also known as Virchow-Robin spaces). Astrocytes connect to these perivascular spaces, promoting the fluid to flow through the neural tissue. Here, CSF mixes with IST and subsequently exits through venous perivascular spaces (Mestre, Kostrikov, Mehta, & Nedergaard, 2017). Egress pathways include the cribriform plate around the olfactory nerve, the cranial nerves, meninges and the spinal nerves. The specific contribution of these sites in humans is not known (Rasmussen, Mestre, & Nedergaard, 2018). Interestingly, body posture was found to influence brain glymphatic transport. In sleeping rats it was found that CSF – ISF exchange and metabolite clearance was higher in the lateral, natural sleeping position, when compared to prone or supine positioning (Lee et al., 2015). Whilst several physiological reasons may underlie this effect, gravity modulating CSF drainage may also play a role.

1.4 The Brain as a Network

Human neuroscience research spent a number of years ascribing functions to individual brain regions, based on task-based fMRI to evaluate which brain regions, for each data point or voxel separately, exhibit increased / decreased blood-oxygen-level dependent (BOLD) signal changes in relation to a specific cognitive or behavioural task. Brain regions do not work in isolation though. Instead, they interact by means of connections, forming networks. The complete set of connections between the elements of the nervous system is also known as the connectome (Bullmore & Sporns, 2009; Sporns, Tononi, & Kötter, 2005). The connections can be studied structurally connected by examining the anatomical tracts or functionally by measuring the statistical associations of brain signals. Using MRI, structural connectivity usually involves studying white matter tracts by means of diffusion weighted imaging, whilst functional connectivity is studied by means of statistical associations of the BOLD signal. Research on the human connectome does not only reveal general principles and properties of brain architecture and computation, but also provides means to quantify differences between patients and control groups.

Both model-dependent and model-free methods can be used to examine connectivity (van den Heuvel & Hulshoff Pol, 2010). With the model-dependent (also seed-based) approach, brain regions of interest (ROIs, also termed 'seeds') are defined *a priori* and examined in respect to their connections to other ROIs or the whole remaining brain. The advantage of these analyses is that they are simple to execute and can provide clear answers to simple, specific research questions. On the other hand, by using the model-dependent approach, relevant network changes in the remaining brain may be overlooked.

In contrast, model-free approaches are not restricted to predefined regions but instead consider regions across the whole brain (see Figure 1.3). Owing to the increasing availability of large imaging data sets and the computational power, developments in whole brain network analysis have been rapid in the recent years. Currently, one of the most popular methods for studying networks is graph theory (Bassett & Sporns, 2017; Rubinov & Sporns, 2010). Here, a network is represented as a graph, which is defined as a set of nodes (vertices) and the links (edges) between them. A network can be described by means of adjacency matrices, where nodes are represented by the rows and columns, and the presence of edges are represented with a numerical value in the matrix elements. The representation of a graph in a matrix allows a range of mathematical operations and quantification of the network.

The definition of both nodes and edges are subject to wide discussion in the field of network neuroscience and a wide range of methods have been discussed and developed to define both entities. Node definition depends on a meaningful spatial partition of brain regions, which has been achieved via several approaches (Eickhoff, Yeo, & Genon, 2018). Edge definition in functional networks, depends on reducing the contributions of non-neuronal fluctuations in order to make the results biologically meaningful (Caballero-Gaudes & Reynolds, 2017).

Likewise, the underlying cognitive state of the participant is important. Intrinsic network organisation of the brain is typically determined from resting-state paradigms where no dedicated task is presented and participants are only required to lie in the scanner (Biswal, Kylen, & Hyde, 1997; van den Heuvel & Hulshoff Pol, 2010). Functional connectivity is then computed on the basis of spontaneous, mostly low-frequency BOLD (<0.1 Hz) signal fluctuations. Recently, researchers have also started studying network architecture during task states (Cole et al., 2014). Such task-state (also task-induced or task-derived) functional connectivity changes are connectivity measures derived from signal changes

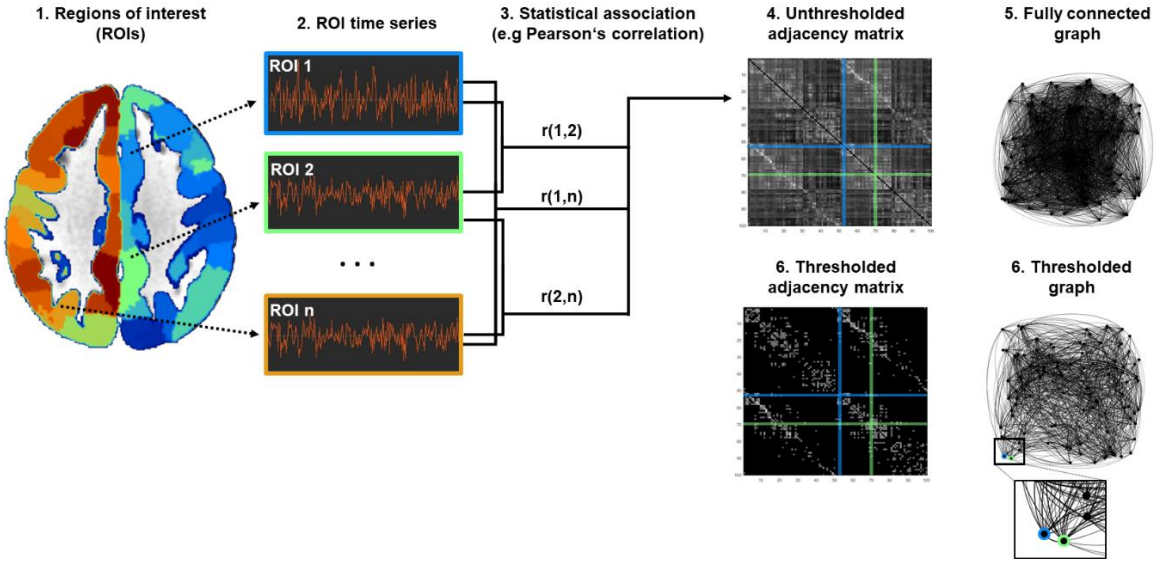

Figure 1.3 Schematic showing the computation of functional networks.
1: A parcellation atlas is used for defining regions of interest (ROIs) (in this example the parcellation by Schaefer et al. (2018) is shown). 2: The atlas is used to partition the brain into meaningful entities from which the BOLD time series are extracted. 3: Statistical associations are calculated between each time series (most commonly, Pearson's correlation is used). It is assumed that the strength of statistical association corresponds to a strength in functional connectivity. 4: A square adjacency matrix is created, where each brain region corresponds to one row and one column (the rows and columns for ROI 1 (blue) and ROI 2 (green) regions are highlighted). The elements of the matrix consist of the numerical value of the functional connection between the two respective regions (in this example, the Pearson's correlation coefficient r). In the case of functional connectivity, the matrix is symmetrical since we cannot deduce the direction of the connection (i.e. we cannot say if ROI 1 is connected to ROI 2 or vice versa, the value of the connection will be the same in both elements of the matrix). 5: The matrix can also be depicted as a graph or network, with brain regions represented as nodes (also *vertices*), and the functional connection between them as links (also *edges*). A functional network is initially fully connected. 6: Only once weak connections are removed (e.g. after thresholding), the network will become sparse. In this example, the connection between ROI 1 and ROI 2 survives the thresholding. Summarising brain activity in such a way allows for the calculation of a wide range of metrics from the network. This makes quantitative description and statistical comparisons possible (see Rubinov & Sporns (2010) for an introduction to network measures). Figure was created after Baggio et al (2015) using MRIcroGL (Rorden, 2020), Gephi (Bastian et al., 2014) and Matlab 2019b (MathWorks Inc.).

occurring during one or several cognitive or perceptual tasks. Increasing evidence suggests that task-state network organisation provide more information than resting-state (Bolt, Nomi, Rubinov, & Uddin, 2017) or task-activations alone (Di & Biswal, 2019; Greene et al., 2020), although the added informational value may be small in magnitude and may vary substantially across individuals (Cole et al., 2014; Gratton et al., 2018).

1.5 Aims of Thesis

In summary, vestibular information is ubiquitous in our daily lives, with gravity for example being processed continuously. Vestibular information is conveyed to brain areas distributed across the cortex, however to what extent these areas interact with eachother and with the remaining brain is not well understood. Studying the whole brain network

can provide an insight to such interactions. In my thesis I used perturbations and modulations of the vestibular system as different vestibular sensory contexts to gain a deeper understanding into the neural underpinnings of this sense. I investigated perturbations on three different time scales: long-term, short-term, and medium-term. To study the whole brain effects of these vestibular modulations I used structural and functional MRI, as well as current image and network analysis methods.

In terms of long-term perturbations, I investigated network changes in individuals suffering from functional dizziness. As discussed in Section 1.3.1, symptoms in this chronic condition occur in the absence of structural damage. It is therefore possible that functional network changes may underlie this condition instead. Previous studies have found some, partially contradictory differences in functional connectivity in these patients, when compared to healthy participants. These studies either used a resting-state fMRI approach, thus not taking into account the often stimulus-dependent onset of dizziness in these patients (Van Ombergen et al., 2017), or used model-based approaches thus potentially overlooking relevant effects in the remaining brain (Popp et al., 2017). Since symptoms of functional dizziness in patients are often task-dependent, I investigated functional connectivity during episodes in which dizziness is triggered using a model free graph-theoretical approach.

In terms of short-term perturbations, a wide range of task-activation studies have used artificial vestibular stimulation to determine cortical areas related to vestibular processing (as discussed in Section 1.1.2 and Section 1.3.2). However, whole brain functional network effects of artificial galvanic stimulation on the are not well understood. The few studies conducted have not aimed at determining the general processes occurring in healthy participants, but instead focused on individuals with vestibular symptoms (Helmchen et al., 2020; Toschi et al., 2017). In order to deepen the understandings of the principle effects that artificial vestibular stimulation has on network architecture, I studied healthy participants. To delineate property changes uniquely associated with vestibular processing, I compared network changes during vestibular stimulation to network changes during non-vestibular painful stimulation.

In terms of medium-term perturbations, microgravity has wide-ranging effects on brain physiology, particularly impacting the movement of brain fluids (as discussed in Section 1.3.3). Therefore, I aimed at examining whether microgravity also influences size of perivascular spaces in space travellers. For this I also developed an easy to use detection pipeline which quantifies these spaces across the whole brain.

2. Network Changes in Patients with Phobic Postural Vertigo

Received: 22 August 2019 | Revised: 29 January 2020 | Accepted: 15 March 2020

DOI: 10.1002/brb3.1622

ORIGINAL RESEARCH

Brain and Behavior Open Access WILEY

Network changes in patients with phobic postural vertigo

Judita Huber[1,2] | **Virginia L. Flanagin**[1,2,3] | **Pauline Popp**[1,3] | **Peter zu Eulenburg**[1,3,4] | **Marianne Dieterich**[1,2,3,4,5]

[1]Graduate School of Systemic Neurosciences, Department Biology II Neurobiology, Ludwig-Maximilians-Universität München, Planegg-Martinsried, Germany

[2]Research Training Grant 2175, Department Biology II, LMU Munich, Ludwig-Maximilians-Universität München, Planegg-Martinsried, Germany

[3]German Center for Vertigo and Balance Disorders, Ludwig-Maximilians-Universität München, Klinikum Großhadern, München, Germany

[4]Neurologische Klinik und Poliklinik (Department of Neurology), Ludwig-Maximilians-Universität München, Klinikum Großhadern, München, Germany

[5]Munich Cluster of Systems Neurology (SyNergy), München, Germany

Correspondence
Judita Huber, Department of Neurology, University Hospital, Ludwig-Maximilians-Universität München, Klinikum Großhadern, Feodor Lynen Straße 19, D-81377 München, Germany.
Email: Judita.huber@campus.lmu.de

Funding information
Deutsche Forschungsgemeinschaft; German Ministry for Education and Research, Grant/Award Number: IFB01EO1401

Abstract

Introduction: Functional dizziness comprises a class of dizziness disorders, including phobic postural vertigo (PPV), that cause vestibular symptoms in the absence of a structural organic origin. For this reason, functional brain mechanisms have been implicated in these disorders.

Methods: Here, functional network organization was investigated in 17 PPV patients and 18 healthy controls (HCs) during functional magnetic resonance imaging with a visual motion stimulus, data initially collected and described by Popp et al. (2018). Graph theoretical measures (degree centrality [DC], clustering coefficient [CC], and eccentricity) of 160 nodes within six functional networks were compared between HC and PPV patients during visual motion and static visual patterns.

Results: Graph theoretical measures analyzed during the static condition revealed significantly different DC in the default-mode, sensorimotor, and cerebellar networks. Furthermore, significantly different group differences in network organization changes between static visual and visual motion stimulation were observed. In PPV, DC and CC showed a significantly stronger increase in the sensorimotor network during visual stimulation, whereas cerebellar network showed a significantly stronger decrease in DC.

Conclusion: These results suggest that the altered visual motion processing seen in PPV patients may arise from a modified state of sensory and cerebellar network connectivity.

KEYWORDS

connectome, dizziness, functional magnetic resonance imaging, vertigo, visual stimulation

Abbreviations: AUC, area under the curve; CC, clustering coefficient; DC, degree centrality; ECC, eccentricity; FD, framewise displacement; fMRI, functional magnetic resonance imaging; HC, healthy controls; PPPD, persistent postural-perceptual dizziness; PPV, phobic postural vertigo; ROI, region of interest; rs-fMRI, resting-state functional magnetic resonance imaging.

Peter zu Eulenburg and Marianne Dieterich have contributed equally.

The peer review history for this article is available at https://publons.com/publon/10.1002/brb3.1622

1 | INTRODUCTION

One of the most common diagnoses in neuro-otology centers is functional dizziness with an estimated prevalence of 10% (Dieterich & Staab, 2017). Functional dizziness, previously known as somatoform or psychogenic dizziness, refers to a class of chronic dizziness disorders with a highly overlapping etiology (Dieterich & Staab, 2017). Although the disorder may be precipitated by a structural vestibular syndrome, the chronic manifestation of vertigo, dizziness, or unsteadiness symptoms has no structural origin. Key symptoms include persistent dizziness and unsteadiness that is usually exacerbated by upright posture, motion, or visual motion stimulation (Dieterich & Staab, 2017). Furthermore, functional dizziness often co-occurs with obsessive-compulsive personality traits and symptoms of anxiety and depression (Brandt, 1996; Staab et al., 2017).

Functional dizziness includes phobic postural vertigo (PPV) (Brandt, 1996), chronic subjective dizziness (Ruckenstein & Staab, 2009), visually induced dizziness (Bisdorff, Von Brevern, Lempert, & Newman-Toker, 2009; Bronstein, 1995), and space and motion discomfort (Jacob, Lilienfeld, Furman, Durrant, & Turner, 1989). The disorders typically differ in their provocative factors, temporal profile, or the focus of the diagnosis. Recently, the Bárány Society Classification Committee developed diagnostic criteria that incorporate all these dizziness disorders into a common disorder called persistent postural-perceptual dizziness (PPPD) (Dieterich & Staab, 2017; Popkirov, Staab, & Stone, 2018; Staab et al., 2017). In the current study, patients were recruited before 2017 and thus used the original PPV criteria (Brandt, 1996; Lempert, Brandt, Dieterich, & Huppert, 1991). Patients are therefore referred to as PPV patients here, although they would fall under the new PPPD classification. Because PPPD is a recent classification and less well established in the literature, we use the term functional dizziness to discuss previous literature using patient populations described having chronic subjective dizziness, visually induced dizziness, or space and motion discomfort.

One of the hallmark features of functional dizziness is the task dependency of symptoms such as postural performance. While patients show increased body sway during simple standing tasks, they typically improve during more difficult balance tasks. In contrast, healthy individuals typically worsen with an increasing difficulty in balancing tasks (Holmberg, Tjernström, Karlberg, Fransson, & Magnusson, 2009; Querner, Krafczyk, Dieterich, & Brandt, 2000). Furthermore, when a balance task is combined with a distraction task, PPV patients showed the same amount of body sway and co-contraction of leg antigravity muscles as healthy controls (HCs), that is, their balancing behavior normalizes (Wuehr, Brandt, & Schniepp, 2017). This has led to the idea that functional changes in monitoring, predicting, and attention to bodily perceptions are altered in these patients.

Although the behavioral characteristics of functional dizziness disorders have been identified, their neural attributes are not yet understood. Since evaluation and interpretation of sensory stimuli appear disrupted in functional dizziness patients, information processing is likely affected in sensory brain areas. Furthermore, the cerebellum is often considered as a key structure in predicting perceptual events (Baumann et al., 2015) and as being a control structure for automatic movements (Jahn, Deutschländer, Stephan, Kalla, Hüfner, et al., 2008; Jahn, Deutschländer, Stephan, Kalla, Wiesmann, et al., 2008). Cerebellar activity and connectivity might thus also be related to the dysfunctional behavior in functional dizziness.

Few imaging studies have investigated the neural characteristics of functional dizziness disorders. For example, in the study by Indovina et al. (2015) functional connectivity changes between visual, vestibular, and anxiety-related brain regions in functional dizziness patients were investigated. They found more negative functional connectivity changes in these regions upon sound-evoked vestibular stimulation, when compared to HCs. This suggests an altered coordination between sensory and higher cortical regions in these patients (Indovina et al., 2015). Alterations in sensory and cerebellar brain connectivity were found in functional dizziness patients during resting-state functional magnetic resonance imaging (rs-fMRI) (Van Ombergen et al., 2017). Another recent rs-fMRI study differentiating comorbid anxiety and depression from PPPV suggested that increased connectivity in the occipital areas was more related to comorbid disorders, while decreased connectivity among vestibular, frontal regulatory, and visual cortices, as well as decreased connectivity between cerebellar regions, was rather related to functional dizziness itself (Lee et al., 2018). A task-based fMRI approach using a visual motion aftereffect paradigm to study task-related activity and task-based connectivity was performed in PPV patients (Popp et al., 2018). Here, the prefrontal cortex showed increased gray matter volume and increased connectivity with associated thalamic projections and primary motor areas. Conversely, decreased gray matter and connectivity were found in cerebellar vermis, posterior lobules, and the supramarginal gyrus. These results pointed to a higher weighting of cognitive-based control of motor areas during a sensory task that induced dizziness in PPV patients (Popp et al., 2018).

These results suggest that brain function and connectivity differ in functional dizziness patients, even in the absence of an organic dysfunction. So far, however, no specific region or mechanism has emerged from the studies. Instead, a distributed array of regions appears to be implicated in functional dizziness, pointing toward network differences in these patients. Furthermore, considering that normal posture and gait can occur in these patients under certain conditions immediately after dysfunctional balancing (Querner et al., 2000; Schniepp et al., 2014; Wuehr et al., 2017), network organization may be influenced by differential sensory processing. Therefore, we examined the whole-brain network architecture during episodes of visual motion, compared to a static visual stimulus. To this aim, we used a graph theoretical approach to extensively analyze the network properties of the whole brain in PPV patients using the data collected in Popp et al. (2018). Six well-known functional subnetworks were characterized in terms of their importance, segregation, and functional integration of the network (degree centrality [DC], clustering coefficient [CC], and eccentricity [ECC], respectively) (Bullmore & Sporns, 2009; Rubinov &

Sporns, 2010). These measures during visual motion stimulation were then compared with those during a static visual stimulation as well as between PPV patients and HCs.

2 | METHODS

2.1 | Participants

This study used the data from Popp et al. (2018) to analyze differences in functional connectivity between PPV patients and HC. Overall, 34 patients and 37 HC were included in the original study (Popp et al., 2018). Patients were recruited from the Dizziness Clinic of the University Hospital Munich (German Center for Vertigo and Balance Disorders). The study was approved by the local ethics committee of the Ludwig-Maximilians-Universität München, Germany. All subjects gave their informed written consent to participate in the study.

Phobic postural vertigo was diagnosed based upon the criteria by Brandt (1996) as determined after diagnostic testing at the German Center for Vertigo and Balance Disorders (DSGZ) in Munich. Patients presented with (a) persistent nonspinning dizziness or unsteadiness while standing or walking despite normal clinical balance tests; (b) perceptual or social factors typically exacerbate the symptoms leading to conditioning and avoidance behavior; (c) fluctuating unsteadiness from seconds to minutes; (d) frequent onset after a serious illness, a vestibular disorder, or a period of emotional stress; (e) vegetative symptoms or anxiety during or after vertigo; and (f) an obsessive-compulsive personality type, mild depression, or a labile affect. These symptoms must present either in the absence of a structural origin or as a secondary symptom after an acute but now compensated vestibular pathology. The absence of a structural pathology was determined by a clinical neurological examination and a neuro-orthoptic examination including video head impulse test (vHIT), caloric irrigation, measurements of subjective visual vertical, posturography, and structural magnetic resonance imaging of the brain.

A high number of patients terminated the experiment early and displayed high head motion, particularly in later sessions of the experiment. Therefore, participants had to complete the first session and had a maximum head motion of 3 mm or maximum head motion of 3 degrees to be included in the analysis so as not to introduce additional variability due to differences in the number of samples for the network analysis (18 patients and 18 HCs). One additional patient had to be excluded for excessive head movements (see Section 2.4.1). We thus ended up with 17 right-handed patients (8 female) diagnosed with PPV patients and 18 right-handed HC (7 female) in the current analyses. The mean age of PPV patients was 41.47 years (*SD* = 11.33 years). In HC, the mean age was 36.11 years (*SD* = 12.93 years). Groups did not significantly differ in terms of age ($t_{(32.82)} = -1.306$, $p = .201$), but because of the potentially still relevant difference in mean age between the cohorts, we used age as a relevant covariate in our analysis.

2.2 | MR parameters

MR data were acquired on a 3T MRI machine (GE, Signa Excite HD), using a 12-channel head coil. A T2*-weighted gradient-echo echo-planar imaging sequence sensitive to blood-oxygen-level-dependent (BOLD) contrast was used to collect functional images (TR 2.45 s, TE 40 ms, FA 90°, voxel size 3 mm isotropic, 38 transversal slices). Three consecutive functional runs were acquired, each containing 260 volumes covering the whole brain. The total number of volumes did not include the first four volumes, which were not reconstructed because they contain transient T1 effects. Slices were collected in an ascending interleaved fashion. We analyzed the first completed session for each participant. A T1-weighted anatomical image (FSPGR, slice thickness = 0.7 mm, matrix size = 256 × 256, FOV = 220 mm, phase encoding = anterior/posterior, FA = 15 ms, bandwidth = 31.25, voxel size = 0.86 × 0.86 0.7 mm) was acquired at the start of the MRI session.

2.3 | Task description

Participants received earplugs in combination with sound-isolating headphones for a profound noise reduction inside the MRI machine. Our visual stimulus consisted of 600 black and white dots (diameter = 0.5°) randomly positioned on a gray background. The dots moved coherently at a constant speed (7°/sec) for the duration of 27.5 s (herewith called "motion" stimulus). After this time period, static dots were shown for another 27.5 s (herewith called "static" stimulus). Each run was 11 min long with 12 blocks of the motion stimulus. The motion stimulus could move to the left, right, counterclockwise, or clockwise and change from one block to the other. Participants were asked to passively look straight ahead *through* the visual stimulus. Instantly after the end of the motion stimulus, participants had to press a button when they no longer experienced the motion aftereffect (the feeling that the static dots were moving into the opposite direction from the precedent stimulus). MATLAB 8.0 (The MathWorks, Inc., Natick, Massachusetts, US) was used together with the Cogent 2000 toolbox (http://www.vislab.ucl.ac.uk/cogent_2000.php) to present the visual stimuli. The field of view was ±24.9° in the horizontal and ±18.9° in the vertical plane. The visual field was kept small to prevent sensations of vection.

2.4 | Preprocessing

Image preprocessing was performed using DPARSF (RRID:SCR_002372, version 4.3_170105) toolbox with MATLAB 2016 (RRID:SCR_001622, The MathWorks, Inc.). Functional images of each participant were realigned to the first. The T1 images were segmented using the affine regularization in DARTEL and subsequently coregistered to the mean functional image. Both functional and structural images were normalized using DARTEL into MNI space at a voxel size of 2 mm^3. Functional images were additionally smoothed during the normalization process using a Gaussian smoothing kernel with FWHM of 4 mm.

2.4.1 | Head motion

Head movements may induce spurious correlations of the fMRI time courses with each other (Power, Barnes, Snyder, Schlaggar, & Petersen, 2012) and distort graph measures (Yan, Craddock, He, & Milham, 2013). Therefore, mean motion and correlations of head movement with task on- and offsets were inspected and compared between PPV patients and HC. Head motion was determined using framewise displacement (FD) calculated according to Jenkinson (Jenkinson, Bannister, Brady, & Smith, 2002) as implemented within the DPARSF toolbox. This measure was recommended over other head motion parameters by Yan, Cheung, et al. (2013).

For all participants, the following two FD measures were used. First, mean FD was calculated across the whole scanning session (260 time points). Second, the correlation between FD and the task was determined as the Pearson correlation between the binary vector representing task on- and offsets and the FD vector across the scanning session. Therefore, we determined not only whether participants moved excessively in general but also to what degree head movement coincided with the task. Values with a normalized *z*-score of >±3 within each group led to exclusion of the subject's data set.

In the PPV group, one patient had to be excluded due to high mean FD (mean FD = 0.153, $z = 3.191$). No other individual from the PPV group had to be excluded due to excessive task–motion correlation. Within the HC group, no outlier values were found. No HC was therefore excluded from further analysis.

Differences in head motion between groups were analyzed to assure validity of the network analysis. Assumptions for homogeneity of variances were tested for each group using *F* test; assumptions of normality were tested using Shapiro–Wilk normality test. If assumptions of homogeneity and normality were met, two-sample *t* test was used for group comparison; else, nonparametric Wilcoxon rank test was used.

Nonparametric tests were used to determine differences of mean FD between groups; groups did not differ significantly in mean FD ($W = 124$, $p = .351$) (Figure 2c). Group differences between task–movement correlations were tested using a parametric two-sample *t* test since all necessary assumptions were met. Indeed, group differences were found ($t_{(33)} = -2.203$, $p = .035$) with correlation of motion with task onsets being significantly higher in PPV patients compared to HC (Figure 2d). To take this into consideration, we removed motion parameters from the original BOLD signal, as described in the following section.

2.4.2 | Data extraction and cleaning

Subsequent processing was performed using the CONN toolbox (RRID:SCR_009550, version 17.f) (Whitfield-Gabrieli & Nieto-Castanon, 2012). For each participant, inputs to the CONN processing pipeline included the preprocessed functional and structural images, as well as the normalized gray matter, white matter (WM), and cerebrospinal fluid (CSF) masks. The mean BOLD signal was extracted from 160 region of interest (ROIs) (4.5-mm-radius spheres), according to the Dosenbach atlas (Dosenbach et al., 2010) (Figure 1a). The atlas was downloaded from ABIDE Open Connectomes Project website (http://preprocessed-connectomes-project.org/abide/Pipelines.html). Six motion parameters (three rotation and three translation parameters) were entered as first-level covariates, and group identity vectors (patients and controls) were entered as second-level parameters. A principal component analysis (PCA) was performed to determine the signals explaining the most variance in the WM and CSF.

The time series were then denoised. First, the first five principal components from the PCA and the 6 motion parameters were removed via linear regression. Because we were interested in functional connectivity which cannot be explained by task-specific co-activations, the time series convolved with the hemodynamic response function for the task effects of the "motion" and "static" conditions were also regressed out of the BOLD signals. After regression, data were high-pass-filtered with a cutoff of 0.008 Hz to remove any scanner-related drifts in the signal. No low-pass filter was applied to avoid possible signal spillage of the BOLD signal between different conditions and to avoid filtering out possible task signals at higher frequencies (Cole, Bassett, Power, Braver, & Petersen, 2014). Finally, the time series were detrended and despiked, as implemented in the CONN toolbox. The resulting BOLD signals from the 160 regions were used for data analysis.

2.5 | Data analysis

Graph theory was used to characterize brain network connectivity. In this method, the brain is defined as a set of nodes connected to each other via edges, thus forming a graph (Fornito, Zalesky, & Bullmore, 2016). In the context of fMRI, edges are derived from the Pearson correlation between BOLD signal time courses of the two respective nodes (Fornito et al., 2016). In the following, the analysis steps will be specified (also see Figure 1 for a graphical representation).

2.5.1 | Adjacency matrix

We were interested in investigating potential differences in connectivity separately during static and motion conditions. To achieve this, we used the standard approach implemented in CONN to determine "condition-dependent" functional connectivity. Specifically, a weighted GLM was performed to determine the BOLD signals specific for the static and the motion conditions, respectively. For this, the block regressors are convolved with the hemodynamic response function, thus creating a measure of how each scan is expected to be affected by each task. This regressor is then further used to weight each scan in order to compute a weighted correlation across all time points (also see Whitfield-Gabrieli & Nieto-Castanon, 2012). The correlations computed for each ROI were included in two 160x160 adjacency matrices for

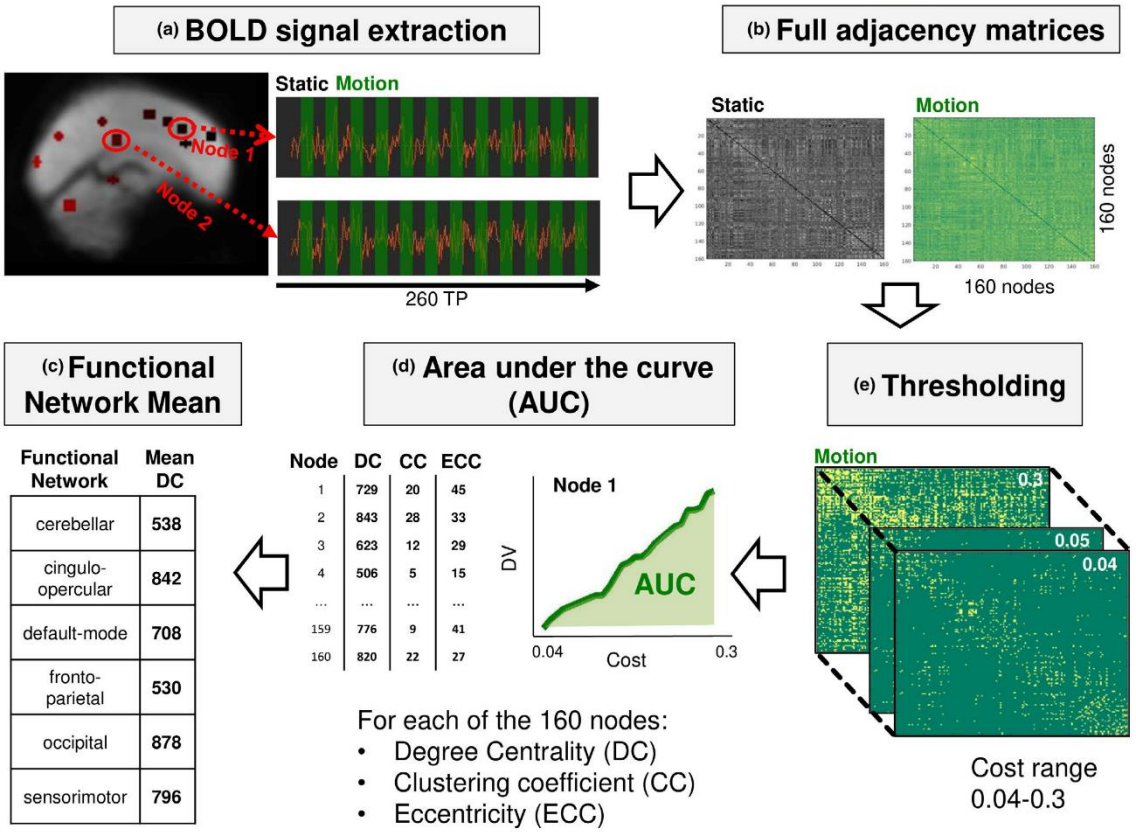

FIGURE 1 The analysis pipeline used in this study, shown for one example participant. The analysis pipeline was loosely based on previous analysis approaches (e.g., Bassett et al. (2012) and Markett, Montag, Melchers, Weber, and Reuter (2016). (a) The BOLD signal was extracted from 160 Dosenbach nodes for all 260 time points. Signal includes periods where participants were shown a visual motion stimulus ("motion"), interspersed with periods with a static visual stimulus ("static"). (b) Adjacency matrices for each participant were created for the static and motion condition by using hemodynamic response function weighting and bivariate correlation. (c) Binarized matrices were created with a range of costs (0.04–0.3, steps of 0.01), which was determined as being the thresholds where small-world dynamics were preserved. (d) For each threshold, three measures were calculated: degree centrality, clustering coefficient, and eccentricity. Area under the curve (AUC) was calculated for each node and each graph measure. (e) Mean over nodes belonging to the same network, for each of the graph measures. Here, only values for mean DC are shown; however, they were calculated for clustering coefficient and shortest path as well. DC, degree centrality

each participant, one for each condition (static and motion) with the correlation value between all nodes described as a *z*-score (Figure 1b). Note that anticorrelations were not considered for the analysis; therefore, only positive z-scores were used for the subsequent calculations.

2.5.2 | Graph measures

Three graph measures were chosen to describe network properties: DC, CC, and ECC. DC is the total number of edges that connect the node to the remaining network (Bullmore & Sporns, 2009). A node with a high DC will interact highly with the remaining nodes of the network (Fornito et al., 2016; Rubinov & Sporns, 2010). CC measures the number of pairs of a node's neighbors that are connected with each other as a fraction of the total amount of pairs that particular node has (Fornito et al., 2016). Paths in a network are a distinct sequence of a route of information flow. ECC is a nodal measure for path length and is defined as the maximum shortest path length between a node and any other node, thus describing how functionally integrated a node is (Rubinov & Sporns, 2010).

2.5.3 | Thresholding

In order to calculate graph theory measures from the adjacency matrices, thresholding is usually performed to remove spurious links with low correlation values (Fornito et al., 2016). It has been

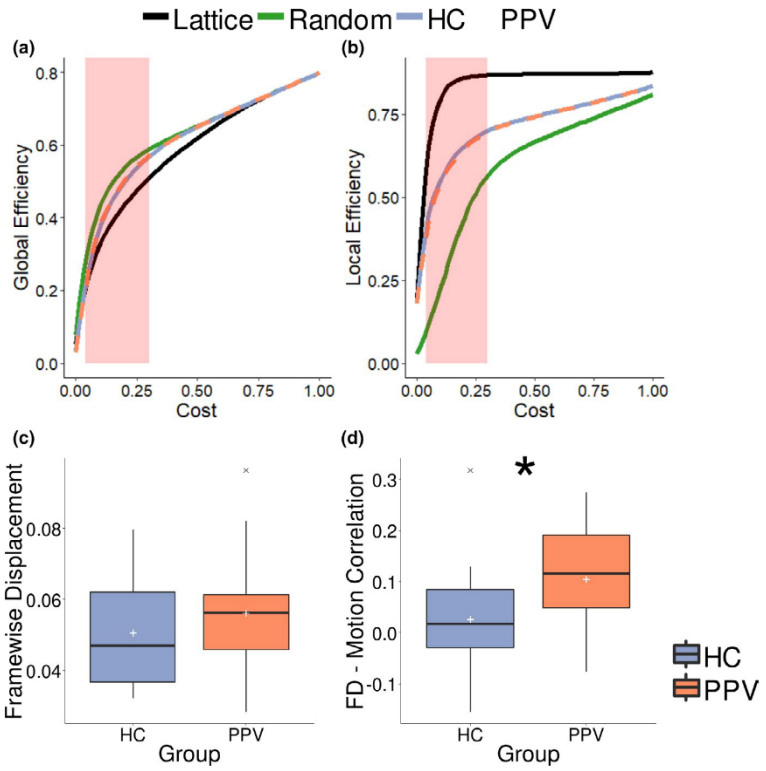

FIGURE 2 (a) Global efficiency for real graphs (healthy controls [HCs] and patients [PPV]) and shuffled graphs (random and lattice) at different costs. Small-world regime occurs between thresholds of 0.04 and 0.3 (highlighted in red). (b) Local efficiency for real graphs (HC and PPV patients) and shuffled graphs (random and lattice) at different costs. (c) Box plot showing mean framewise displacement (FD) over the course of the whole session for HC and PPV patients (white cross indicates mean). (d) Box plot showing correlation between FD and a vector modeling onset and offset of visual stimulation for HC and PPV patients (white cross indicates mean). PPV, phobic postural vertigo

suggested that density thresholding is more appropriate than absolute thresholding to keep the number of links in the graph stable. This way, possible differences in graph properties do not merely emerge due to different connection density. Relative thresholding is thus particularly suited for comparing brain graphs between groups of participants (De Vico Fallani, Richiardi, Chavez, & Achard, 2014; Fornito et al., 2016). However, often only one arbitrary proportional threshold (or "network cost") is chosen for a network which might also lead to erroneous results.

We therefore adopted the approach of calculating graph measures over a range of threshold values (similar to Bassett, Nelson, Mueller, Camchong, & Lim, 2012; Ginestet, Nichols, Bullmore, & Simmons, 2011) instead of choosing one arbitrary network cost. The range of threshold values was chosen such that networks had small-world properties, as would be expected from a biologically plausible network (Achard & Bullmore, 2007). A small-world network should have a global efficiency greater than a lattice graph but smaller than a random graph (Achard & Bullmore, 2007). Furthermore, local efficiency of a small-world network should be lower than a lattice graph and higher than a random graph. For this, global and local efficiency of all participants during static periods were compared with global and local efficiency of randomized and lattice graphs. Using the *randmio_und* and *latmio_und* functions of the Brain Connectivity Toolbox (Rubinov & Sporns, 2010, RRID:SCR_004841, version from 15.01.2017), the graph of each participant was both permuted to a random and a lattice graph for costs in the interval of 0.01–0.60 using a step size of 0.02 and a rewiring parameter of 100. Global and local efficiency were calculated for each cost (Figure 2a,b). Small-world properties were found in the range of costs between 0.04 and 0.3 (Figure 2a), similar to Achard and Bullmore (2007). This cost range was used for all subsequent calculations (Figure 1c).

For each thresholded matrix (0.04–0.3, steps of 0.01), adjacency matrices were binarized using the functions *threshold_proportional* and *weight_conversion* from the Brain Connectivity Toolbox (Figure 1c). For ECC, a distance matrix was calculated using the function distance_bin. DC, CC, and ECC were calculated using functions for undirected binary networks from the Brain Connectivity toolbox, respectively. Therefore, each node could be described with three graph measures calculated using 35 different thresholds.

To summarize these values, for each of the 160 atlas nodes and for each graph measure, the area under the curve (AUC) was calculated, resulting in 160 × 3 values for each participant (Figure 1d). Since we were mainly interested in characterizing network properties of functional networks, we grouped every node into one of six networks: cingulo-opercular, fronto-parietal, default-mode, sensorimotor, occipital, and cerebellum (Figure 1e) (according to Dosenbach et al., 2010). For each network, we thus calculated the mean AUC from the respective nodes. Therefore, in the end, each participant had 18 summary network measures for each condition: the AUC for the three graph measures for the six networks. These were calculated for both static and motion periods, thus resulting in 36 measures overall for each participant.

2.5.4 | Group statistics

We first tested for differences between network properties in each stimulation condition separately, and then by subtracting the summary graph measures of the static condition from the motion condition (motion–static). In both cases, we used a mixed-design ANCOVA with "group" as between-group factor, "network" as within-group factor, and age of participants as a covariate. In case of a significant Mauchly test of sphericity, Greenhouse–Geisser correction for departure from sphericity was reported. We were interested in differences between groups, rather than differences solely explained by the heterogeneity of networks across groups. Therefore, only in the case of significant main effects of "group" or an interaction of "group" with "network," post hoc pairwise *t* tests were used to determine the nature of the difference using FWE correction using Tukey's method. All calculations were performed using lsmeans (Lenth, 2016), afex (Singmann, Bolker, Westfall, & Aust, 2018), plyr (Wickham, 2011), and reshape (Wickham, 2007) libraries in R 3.4.0 (RRID:SCR_001905, 2018). Human brain networks were visualized using BrainNet Viewer (Xia, Wang, & He, 2013, RRID:SCR_009446). All analysis and plotting of results were performed using R 3.4.0, Python 3, and MATLAB 2016 (The MathWorks, Inc.).

3 | RESULTS

3.1 | Connectivity group effects during static and motion condition

To test for the presence of general differences in any of the measures, we performed a MANCOVA to determine the overall group, network, or interaction effect on any graph measure during static and motion conditions, as well as the effect of age. By including the factor "network" as a repeated-measure factor and "group" as an independent-measure factor, we aimed to minimize unexplained variance from the model. Three graph measures (DC, CC, and ECC) were included as dependent variables, and group of participants and six functional networks were included as independent variables. Age was added as a covariate. Note that the main significant results below remain, even if we correct our initial significant p-value for multiple testing using Bonferroni correction since three MANCOVAs were tested (i.e., if we adjust the criterion to $p = .0167$).

To additionally investigate effects of motion, an alternative model was tested that included a subject-specific nuisance regressor for regressing out the signal related to time points with excessive motion (see Supplementary Information, Analysis 1). We also conducted the same analysis with normalized values by the estimated values for a random graph (see Supplementary Information, Analysis 2). Unless otherwise stated, the results in these alternative analyses yielded the same results.

During the visual motion condition, no significant interaction (Pillai's trace = 0.062 $F_{(5,15)} = 0.658$, $p = .826$) or main group effects were found (Pillai's trace = 0.087, $F_{(3,29)} = 0.924$, $p = .441$). The main effect of age (Pillai's trace = 0.370, $F_{(3,29)} = 5.681$, $p = .003$), as well as the factor of network, was found to be significant using MANCOVA (Pillai's trace = 0.844, $F_{(5,15)} = 12.143$, $p < .001$). No subsequent ANCOVAs were thus performed for this condition (Figure 3b,d).

For the static condition, however, the interaction between group and network effects was significant (Pillai's trace = 0.187, $F_{(15,465)} = 2.057$, $p = .011$). There was no significant main effect of group (Pillai's trace = 0.023, $F_{(3,29)} = 0.234$, $p = .871$) and no main effect of age (Pillai's trace = 0.159, $F_{(3,29)} = 1.834$, $p = .163$). Furthermore, a significant main effect of the factor network was found (Pillai's trace = 0.740, $F_{(15,465)} = 10.145$, $p < .001$).Consequently,

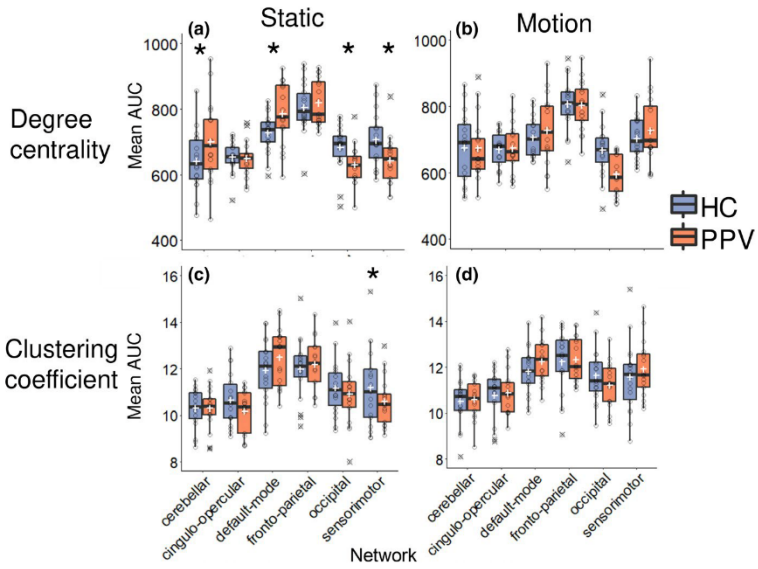

FIGURE 3 Box plots comparing degree centrality mean area under the curve (AUC) and clustering coefficient AUC between healthy controls (HCs) and patients (PPV) both in static and in motion, for each of the six functional brain networks given by Dosenbach (2010). White crosses indicate means, stars indicate a significant ($p < .05$) group effect, and outliers are marked with a black cross. (a) Degree centrality during static conditions. (b) Degree centrality during motion conditions. (c) Clustering coefficient during static conditions. (d) Clustering coefficient during visual motion conditions. PPV, phobic postural vertigo

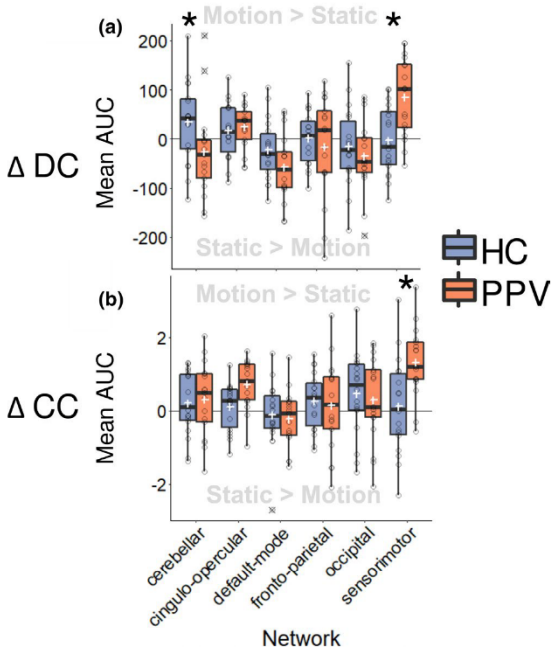

FIGURE 4 Box plots showing (a) change in degree centrality (ΔDC) and (b) clustering coefficient (ΔCC) across tasks (i.e., graph values during static subtracted from motion condition) for six functional networks of the Dosenbach atlas for healthy controls (HCs) and patients (PPV). Values above zero indicated nodes in the respective network had an AUC value during motion on average, whereas values below zero mean nodes in the network had a higher AUC value on average during the static condition. White cross indicates mean, stars indicate a significant ($p < .05$) group effect, and outliers are marked with a black cross. AUC, area under the curve; PPV, phobic postural vertigo

TABLE 1 Coordinates and labels of nodes in the sensorimotor network (after Dosenbach et al., 2010)

Coordinates			Node	Number
58	11	14	Frontal	1
60	8	34	dFC	2
−55	7	23	vFC	3
10	5	51	Pre-SMA	4
43	1	12	vFC	5
0	−1	52	SMA	6
53	−3	32	Frontal	7
58	−3	17	Precentral gyrus	8
−42	−3	11	Mid-insula	9
−44	−6	49	Precentral gyrus	10
−26	−8	54	Parietal	11
46	−8	24	Precentral gyrus	12
−54	−9	23	Precentral gyrus	13
44	−11	38	Precentral gyrus	14
−47	−12	36	Parietal	15
33	−12	16	Mid-insula	16
−36	−12	15	Mid-insula	17
59	−13	8	Temporal	18
−38	−15	59	Parietal	19
−47	−18	50	Parietal	20
46	−20	45	Parietal	21
−55	−22	38	Parietal	22
−54	−22	22	Precentral gyrus	23
−54	−22	9	Temporal	24
41	−23	55	Parietal	25
42	−24	17	Posterior insula	26
18	−27	62	Parietal	27
−38	−27	60	Parietal	28
−24	−30	64	Parietal	29
−41	−31	48	Posterior parietal	30
−41	−37	16	Temporal	31
−53	−37	13	Temporal	32
34	−39	65	Superior parietal	33

Abbreviations: dFC, dorsal frontal cortex; SMA, supplementary motor area; vFC, ventral frontal cortex.

a subsequent post hoc analysis was used to determine what network properties show differences between PPV patients and HC in specific networks. For this, three separate mixed-design ANCOVAs were performed, one for each of the network measures, DC, CC, and ECC during the static condition.

For DC, the factor group and network showed a significant interaction ($F_{(3.41,109.12)} = 3.266$, $p = .019$, where degrees of freedom were adjusted using Greenhouse–Geisser estimates of sphericity ($\varepsilon = 0.683$) after Mauchly's test indicated that the assumption of sphericity had been violated [$W_{(14)}=0.355$, $p = .005$]). Both the factor of group ($F_{(1,32)}=0.062$, $p = .435$) and the main effect of age ($F_{(1,32)}=0.136$, $p = .715$) were not found significant. The main effect of network was found significant ($F_{(3.41,109.12)}=20.068$, $p < .001$ after adjusting degrees of freedom as above). Because of the significant interaction, post hoc t tests were performed using Tukey's method to test in which networks the group effect was most pronounced. Indeed, DC of cerebellar network nodes ($t_{(168.32)} = -2.245$, $p = .0260$) and default-mode network nodes ($t_{(168.32)} = -2.201$, $p = .0291$) was higher in PPV patients compared to HC (Figure 3a). In contrast, DC of sensorimotor nodes ($t_{(168.32)} = 2.389$, $p = .018$) was lower in PPV patients when compared to HC (Figure 3a). PPV patients also had a lower DC of occipital nodes, compared to HC ($t_{(168.32)} = 1.996$, $p = .048$), but this result did not survive in the model for subject-specific motion (see Analysis 1 in Supplementary Information). Individual within-participant changes in DC can be seen in Figure A.1.

For CC, a significant interaction between the factor of group and network was also found ($F_{(3.57,114.24)} = 2.560$, $p = .046$). Degrees of freedom were adjusted using Greenhouse–Geisser estimates of

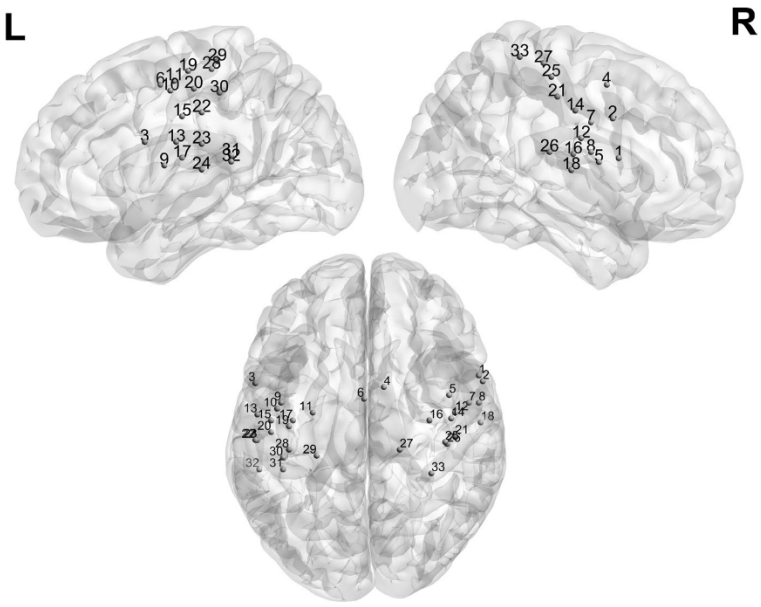

FIGURE 5 Nodes of the sensorimotor network defined according to Dosenbach (2010)

sphericity (ε = 0.714), since Mauchly's test indicated that the assumption of sphericity was violated, $W_{(14)}$ = 0.385, p = .012. No main effect of group was found ($F_{(1,32)}$ = 0.219, p = .643). However, the main factor of age was found to be significant ($F_{(1,32)}$ = 0.029, p = .029). The main effect of network was also significant ($F_{(3.57,114.24)}$ = 26.817, p < .001), degrees of freedom were adjusted as above). Because of the significant interaction, we performed post hoc t tests using Tukey's method to determine in which networks CC significantly differed between HC and PPV patients. The only significant effect was found in the sensorimotor network ($t_{(95.73)}$ = 2.014, p = .047); HC showed a higher CC in the sensorimotor network (Figure 3c) than PPV patients. For an overview of within-participant changes in CC, see Figure A.2.

For ECC, no significant main effect or interaction was found during the static condition (Figure A.3a). Within-participant ECC values for each network can be seen in Figure A.4.

3.2 | Change of graph measures between conditions

We were further interested in the relative change in network properties between the visual motion and static visual conditions. For this, for each participant and graph measure, the values of each node during the static condition were subtracted from the motion condition, thus resulting in values representing the change of degree centrality (ΔDC), clustering coefficient (ΔCC), and eccentricity (ΔECC). This resulting value indicates whether the mean AUC for one graph measure of a certain network remained the same between conditions (and thus has a value close to zero), or whether it increased during motion (positive) or decreased during motion (negative).

An initial MANCOVA resulted in a significant interaction between the factors group and network (Pillai's trace = 0.176, $F_{(15,465)}$ = 1.933, p = .019), as well as a main effect of group (Pillai's trace = 0.313, $F_{(3,29)}$ = 4.409, p = .0113) and a main effect of network (Pillai's trace = 0.182, $F_{(15,465)}$ = 2.008, p = .0135). The covariate of age was not significant (Pillai's trace = 0.066, $F_{(3,29)}$ = 0.679, p = .572). As before, the specific effects for each graph measure was determined via mixed-design ANCOVAs for ΔDC, ΔCC, and ΔECC. Only ΔDC and ΔCC showed significant differences between HC and PPV patients. For ΔECC, no significant interaction or main group effect was found (Figure A.5). For ΔDC, a significant interaction was found between the factor of group and network ($F_{(3.97,\ 127.04)}$ = 3.456, p = .010). Degrees of freedom were adjusted using Greenhouse–Geisser estimates of sphericity (ε = 0.794) after Mauchly's test indicated that the assumption of sphericity was violated ($W_{(14)}$ = 0.422, p = .027). A significant main effect of network ($F_{(3.97,\ 127.04)}$ = 4.477, p = .002 degrees of freedom were adjusted as described above) and group ($F_{(1,32)}$ = 7.096, p = .012) was also found. No significant main effect of age was found ($F_{(1,32)}$ = 0.017, p = .897).

Subsequent t tests using Tukey's method revealed that the difference between groups was significant for the sensorimotor network ($t_{(167.99)}$ = −3.467, p = .0007). PPV patients showed a significantly higher positive change, compared to HC. Conversely, HC showed a significantly higher positive change of DC in the cerebellar network ($T_{(167.99)}$ = 2.389, p = .018). No significant group difference changes were found in the other networks for DC (Figure 4a).

For ΔCC, a significant interaction between the factor of group and network ($F_{(5,160)}$ = 3.003, p = .013) was found. There was no significant group ($F_{(1,32)}$ = 2.167, p = .151) or age effect ($F_{(1,32)}$ = 0.928, p = .343). A significant main effect of network ($F_{(5,160)}$ = 3.500, p = .005) was also found. Because of the significant interaction,

post hoc *t* tests were performed. A significant difference of ΔCC between groups in the sensorimotor network was found again ($t_{(185.94)} = -3.627$, $p = .0004$). PPV patients displayed a significantly higher positive change of CC, compared to HC. No other significant group differences were found in other networks (Figure 4b).

The results for ΔCC were maintained when the analysis performed on the values that were normalized to random networks. However, an additional significant interaction of network and group was found in ΔECC, with post hoc *t* tests showing that PPV patients had a significantly increased ECC in the sensorimotor network compared to the HC group ($t_{(63.51)} = -2.217$, $p = .030$) (see Supplementary Information, Analysis 2 for details). An overview of the nodes from the sensorimotor and cerebellar networks can be found in Table 1 and Figure 5 and Table 2 and Figure 6, respectively.

3.3 | Sources of differences in connectivity within cerebellar and sensorimotor network

Considering that cerebellar and sensorimotor networks showed significant network property changes between experimental condition and across groups, the question arises: What about these networks led to a change in DC? Three options were conceivable: an increase/decrease in connections (a) with nodes within the same network, (b) between nodes of the cerebellar and sensorimotor network specifically, and (c) to nodes of all the remaining networks in the brain (i.e., to the cingulo-opercular, fronto-parietal, default-mode, and occipital networks).

To determine this, the same adjacency matrix values were used for the analyses described before, but the matrices were reduced in size to test each of the three options. To test for within-network connectivity, DC for nodes of only one network (either cerebellar or sensorimotor) was calculated. To examine connectivity between the cerebellar and sensorimotor network, DC only between nodes of these networks was calculated (i.e., adjacency matrices were created containing only the correlation values of sensorimotor nodes to cerebellar nodes or vice versa). To determine the connectivity to the remaining networks, adjacency matrices containing only correlation values of either cerebellar or sensorimotor networks to nodes in the remaining networks were calculated. Other than the reduction of the adjacency matrices, the methodology was the same as described in Section 2.5 (also see Figure 1). To determine how PPV patients differed from HC, a 2 × 2 mixed-design ANOVA with the repeated-measure factors of connectivity type (within-network connectivity, reciprocal connectivity, and other remaining connectivity) and the independent factor of group (HC and PPV) was performed for DC values during static and for ΔDC values.

For cerebellar connectivity during static vision, no main effect of group was found (HC and PPV patients) ($F_{(1,33)} = 2.678$, $p = .11$). Therefore, differences in cerebellar DC between groups seem not to be driven by distinct patterns in within or between connectivity (Figure A.6a). In sensorimotor connectivity during static vision, a significant effect of the factor group was found $F_{(1,33)} = 5.68$, $p = .023$). In subsequent post hoc tests, a significant effect of within-connectivity was found with PPV showing significantly lower within-network connectivity ($t_{(98.39)} = 2.893$, $p = .005$). Therefore, differences in DC between groups seem to be driven by connectivity changes within the somatosensory network (Figure A.6b).

When analyzing ΔDC values, again for cerebellum, no group effect was found ($F_{(1,33)} = 1.72$, $p = .20$). Again, this suggests that no distinct connectivity changes occur (Figure A.4a) in the cerebellar network. For sensorimotor connectivity, a main effect for the factor group was found ($F(_{1,33)} = 11.786$, $p = .002$). Post hoc *t* tests revealed a significant effect both in within-sensorimotor connectivity ($t_{(98.35)} = -2.934$, $p = .004$) and in remaining connectivity to other brain networks ($t_{(98.35)} = -3.157$, $p = .002$), with PPV patients showing higher ΔDC than HC. Therefore, both within-connectivity and connectivity to the remaining brain contributed to differences in ΔDC between groups (Figure A.7b).

TABLE 2 Coordinates and labels of nodes in the cerebellar network (after Dosenbach et al., 2010)

Coordinates			Node	Number
−28	−44	−25	Lateral cerebellum	A
−24	−54	−21	Lateral cerebellum	B
−37	−54	−37	Inferior cerebellum	C
−34	−57	−24	Lateral cerebellum	D
−6	−60	−15	Medial cerebellum	E
−25	−60	−34	Inferior cerebellum	F
32	−61	−31	Inferior cerebellum	G
−16	−64	−21	Medial cerebellum	H
21	−64	−22	Lateral cerebellum	I
1	−66	−24	Medial cerebellum	J
−34	−67	−29	Inferior cerebellum	K
−11	−72	−14	Medial cerebellum	L
33	−73	−30	Inferior cerebellum	M
5	−75	−11	Medial cerebellum	N
14	−75	−21	Medial cerebellum	O
−21	−79	−33	Inferior cerebellum	P
−6	−79	−33	Inferior cerebellum	Q
18	−81	−33	Inferior cerebellum	R

4 | DISCUSSION

The aim of the current analysis was to study the whole-brain network properties in functional dizziness. We further wished to disentangle intrinsic network effects related to visual motion processing from network effects during static visual processing. For this, graph theory was used to characterize six functional brain networks (cingulo-opercular, fronto-parietal, default-mode, sensorimotor, occipital, and cerebellar network) during periods of visual motion and interjacent periods of a static visual stimulation. Importantly, the

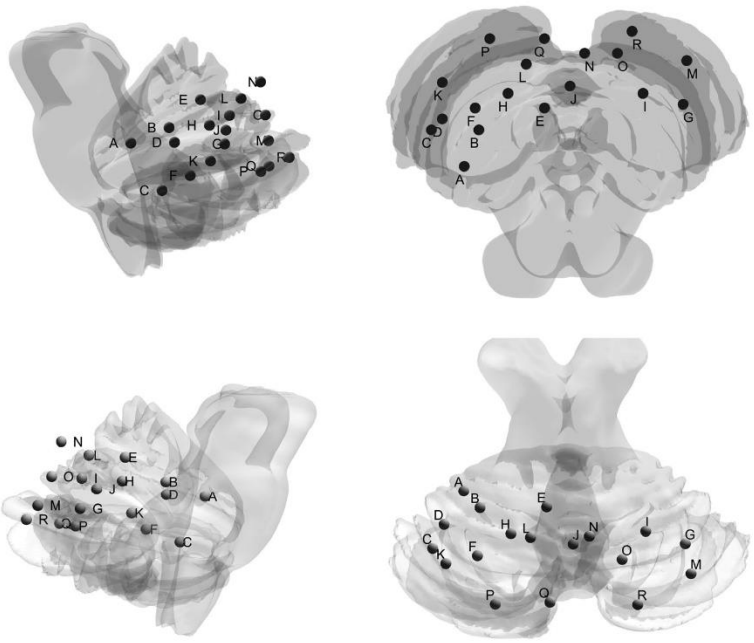

FIGURE 6 Nodes of the cerebellar network defined according to Dosenbach (2010)

effect of the task was regressed out from the main signal to study interaction of regions above and beyond task co-activations. Based on previous behavioral findings (Holmberg et al., 2009; Querner et al., 2000; Wuehr et al., 2017), we expected the sensory systems and the cerebellum to show the strongest changes in network properties.

To summarize, we found that brain networks of PPV patients are connected differently (i.e., they differed in their DC) in the two conditions studied, compared to HC. During static visual stimulation, the default-mode network as well as the cerebellar network was found to be more strongly connected in PPV. This was accompanied by a lower connectivity of the sensorimotor network. Upon visual motion stimulation, the sensorimotor network of PPV patients became significantly more connected, while the cerebellar network became less connected compared to HC. Building on the previous study by Popp et al. (2018), we also find different connectivity of cerebellum. The significant changes of network properties within the sensorimotor network during the two visual stimulation periods in PPV patients are particularly notable. We found that the sensorimotor network initially displayed decreased DC and CC during static visual stimulation, but that these measures increased to a greater extent in PPV patients during visual motion. The significant differences in DC and CC suggest changes in importance and functional segregation of the sensorimotor network, respectively. To understand these results, it is helpful to understand that sensorimotor nodes are located in, amongst others, premotor regions, the supplementary motor area, and precentral gyrus (see Table 1 and Figure 5). These regions are thought to belong to the action-oriented motor network and are active during imagined vestibular sensation (zu Eulenburg, Müller-Forell, & Dieterich, 2013).

The cerebellar network also had different network properties in PPV patients. The cerebellar network was connected more strongly in the static condition of PPV patients, and it did not display the same increase in DC upon motion stimulation, as is seen in HC. Aberrant cerebellar connectivity in functional dizziness has been also found during resting state, with an increase in connectivity to the thalamus (Van Ombergen et al., 2017) and a decrease in connectivity to other brain regions (Lee et al., 2018). The cerebellum is, amongst others, considered to be responsible for predicting sensory information to optimize perception (Baumann et al., 2015), displaying enhanced activity upon the absence of an expected somatosensory stimulus (Tesche & Karhu, 2000). Based on these findings, it would be interesting to investigate whether increased DC of the cerebellum during static conditions is related to a dysfunctional stimulus prediction in PPV patients. Specifically, in a state without specific motion input, increased cerebellar integration to the remaining brain network may reflect inappropriate stimulus expectations, a possible mechanism for the overpreparedness of PPV patients for motion stimuli.

The default-mode network was found to have a higher mean DC in PPV patients during the static visual condition, when compared to HC, but no different dynamics were found between the two visual conditions. This network consists of nodes extracted from precuneus, prefrontal cortex, anterior cingulate cortex, frontal cortex, and occipital regions (see Dosenbach et al., 2010). These regions were reported to support emotional processing, self-referential mental activity, and recollection of previous experiences (Raichle, 2015), and aberrant default-mode resting-state connectivity was also found in patients diagnosed with major depressive disorders (Sheline, Price, Yan, & Mintun, 2010;

Whitfield-Gabrieli & Ford, 2012). Depression as well as anxiety disorders often displays with functional dizziness (Staab et al., 2017). It would be interesting to test whether anxiety and depression are related to default-mode network connectivity changes in PPV—since we were not specifically interested in affective disorders, this research question was, however, out of the scope of our current study. Other sensory networks did not differ in terms of their modulation between groups. The differences found in the occipital network were not statistically robust when correcting for motion, thus suggesting no direct involvement of the occipital network in PPV. This is contrary to previous findings (Lee et al., 2018; van Ombergen et al., 2017).

The presented findings are an extension of the initial analysis by Popp et al. (2018), who conducted a voxel-based morphometry (VBM) analysis, task-based fMRI, and task-based functional connectivity of selected seed regions. In the latter study, structural differences between PPV patients and HC were found in cerebellum, as well as precentral gyrus and primary motor cortical areas (largely part of the sensorimotor network), but also thalamus, left supramarginal gyrus, and middle frontal gyrus. Interestingly, in the task-based fMRI analysis only a significant increased BOLD signal in the subgenual anterior cingulate cortex was seen in PPV, hinting at more complex functional differences. Using task-based functional connectivity of six selected seeds (based on the findings of the VBM analysis), differences in the cerebellum and precentral gyrus were found amongst others (Popp et al., 2018). In the current study, we expanded on these findings using a functional network analysis across the whole brain (rather than extracting seeds) and took advantage of the different task episodes (static and motion). Indeed, we also found an involvement of premotor areas and cerebellar networks, particularly upon visual motion stimulation.

Taken together, we hypothesize that network changes found in PPV patients can be connected to the mechanistic models of sensory efference copy (von Holst & Mittelstaedt, 1950) or the related Bayesian modeling approach (Henningsen et al., 2018; Petzschner, Weber, Gard, & Stephan, 2017). The first model explains the tendency of vertigo patients to perceive involuntary bodily fluctuations and individual head movements as a disturbing external acceleration by a transient uncoupling of efference and efference copy, leading to a mismatch between anticipated and actual motion (Brandt, 1996; Henningsen et al., 2018; Petzschner et al., 2017). In the latter model, perception or beliefs are considered to be an inferred process. Here, abnormal signaling or computation of priors, prediction errors, or precision ratios leads to functional somatic syndromes such as PPV (see Petzschner et al., 2017 for more details). Connecting this to the present findings, we suggest that in the absence of visual motion stimulation, networks associated with stimulus expectations (cerebellar network) and increased focus on internal processes (default-mode network) are overprioritized in PPV. Conversely, the sensorimotor network is less important in PPV during static visual input. Upon visual motion, regions involved with action-oriented evaluation of sensory stimuli become overprioritized upon sensory input in patients. To test the hypothesis that the differences in network dynamics are related to differences in stimulus expectation and evaluation, it would be necessary to include behavioral measures which test for dysfunctional interpretation of sensory input and to connect them to changes in connectivity measured by means of fMRI.

Overall, in the present study we took a whole-brain, network-level approach to characterize changes in the brain of PPV patients when compared to HCs. Therefore, we did not aim to reach any conclusions regarding how individual nodes/brain regions are implicated. We restricted our graph theoretical approach to three simple and widely used measures (DC, CC, and ECC) to investigate importance, functional segregation, and functional integration of the networks. We did not find any differences in ECC in any of our measurements.

A limitation of our study is that eye movements were monitored but not recorded. Although relevant ocular motor phenomena or neuroophthalmological pathologies have already been excluded in the diagnosis process, we cannot completely exclude that subtle differences in ocular motor behavior explain the differences in functional connectivity. In future studies, it would be interesting to record and analyze eye movements during such a visual motion paradigm to determine potential influences on connectivity. Another limitation of the study is that the presented findings may not be unique to PPV. Firstly, due to the comorbidity of PPV with depression and anxiety the network-level changes found in PPV may not be specific to functional dizziness, but rather depression or anxiety in general. Future studies should include populations of individuals with similar levels of trait anxiety and depression (but without dizziness symptoms) to evaluate specificity of the described results. Furthermore, previous studies suggested that visual dependency is related to chronic functional dizziness symptoms (Cousins et al., 2014, 2017). In future, recording visual dependency in a similar manner would be useful to determine the relation of our reported functional brain changes to such visual motion sensitivity.

5 | CONCLUSIONS

Distinct changes in functional brain networks in PPV patients during static visual stimulation were found in nodes of the sensorimotor network, the cerebellar network, and the default-mode network. Upon visual motion, nodes in the sensorimotor network become more connected in PPV, whereas cerebellar nodes become more connected in HC. We hypothesize that the underlying network differences may be related to dysfunctional stimulus expectations and suggest combining functional brain network analysis with psychophysical approaches in PPV patients using Bayesian modeling.

ACKNOWLEDGMENTS

This research was supported by a grant from the German Ministry for Education and Research (http://www.bmbf.de, Grant number: IFB 01EO1401). It was further funded by the Deutsche Forschungsgemeinschaft (DFG) via the RTG 2175 "Perception in

context and its Neural Basis" and the Graduate School of Systemic Neurosciences (GSC 82/1), Munich, Germany.

CONFLICT OF INTEREST

All authors declared no conflict of interest.

AUTHOR CONTRIBUTION

JH conceived the analysis, analyzed and interpreted the data, wrote the manuscript, and created the figures. VLF provided support with data analysis, and drafted and reviewed the manuscript and figures. PP acquired the data. PzE conceived the analysis, interpreted the data, and drafted and reviewed the manuscript and figures. MD conceived and designed the study, and drafted and reviewed the manuscript and figures.

DATA AVAILABILITY STATEMENT

The data that support the findings of this study are available from the corresponding author upon reasonable request.

ORCID

Judita Huber https://orcid.org/0000-0002-5452-063X
Virginia L. Flanagin https://orcid.org/0000-0002-6677-459X
Peter zu Eulenburg https://orcid.org/0000-0002-3729-4570

REFERENCES

Achard, S., & Bullmore, E. (2007). Efficiency and cost of economical brain functional networks. *PLOS Computational Biology*, *3*(2), e17. https://doi.org/10.1371/journal.pcbi.0030017

Bassett, D. S., Nelson, B. G., Mueller, B. A., Camchong, J., & Lim, K. O. (2012). Altered resting state complexity in schizophrenia. *NeuroImage*, *59*(3), 2196–2207. https://doi.org/10.1016/j.neuroimage.2011.10.002

Baumann, O., Borra, R. J., Bower, J. M., Cullen, K. E., Habas, C., Ivry, R. B., … Sokolov, A. A. (2015). Consensus paper: The role of the cerebellum in perceptual processes. *The Cerebellum*, *14*(2), 197–220. https://doi.org/10.1007/s12311-014-0627-7

Bisdorff, A., Von Brevern, M., Lempert, T., & Newman-Toker, D. E. (2009). Classification of vestibular symptoms: Towards an international classification of vestibular disorders. *Journal of Vestibular Research*, *19*(1,2), 1–13. https://doi.org/10.3233/VES-2009-0343

Brandt, T. (1996). Phobic postural vertigo. *Neurology*, *46*(6), 1515–1519. https://doi.org/10.1212/wnl.46.6.1515

Bronstein, A. M. (1995). Visual vertigo syndrome: Clinical and posturography findings. *Journal of Neurology, Neurosurgery & Psychiatry*, *59*(5), 472–476. https://doi.org/10.1136/jnnp.59.5.472

Bullmore, E., & Sporns, O. (2009). Complex brain networks: Graph theoretical analysis of structural and functional systems. *Nature Reviews Neuroscience*, *10*, 186. https://doi.org/10.1038/nrn2575

Cole, M. W., Bassett, D. S., Power, J. D., Braver, T. S., & Petersen, S. E. (2014). Intrinsic and task-evoked network architectures of the human brain. *Neuron*, *83*(1), 238–251. https://doi.org/10.1016/j.neuron.2014.05.014

Cousins, S., Cutfield, N. J., Kaski, D., Palla, A., Seemungal, B. M., Golding, J. F., … Bronstein, A. M. (2014). Visual dependency and dizziness after vestibular neuritis. *PLoS ONE*, *9*(9), e105426. https://doi.org/10.1371/journal.pone.0105426

Cousins, S., Kaski, D., Cutfield, N., Arshad, Q., Ahmad, H., Gresty, M. A., … Bronstein, A. M. (2017). Predictors of clinical recovery from vestibular neuritis: A prospective study. *Annals of Clinical and Translational Neurology*, *4*(5), 340–346. https://doi.org/10.1002/acn3.386

De Vico Fallani, J., Chavez, M., & Achard, S. (2014). Graph analysis of functional brain networks: Practical issues in translational neuroscience. *Philosophical Transactions of the Royal Society B: Biological Sciences*, *369*(1653), 20130521. https://doi.org/10.1098/rstb.2013.0521

Dieterich, M., & Staab, J. P. (2017). Functional dizziness: From phobic postural vertigo and chronic subjective dizziness to persistent postural-perceptual dizziness. *Current Opinion in Neurology*, *30*(1), 107–113. https://doi.org/10.1097/WCO.0000000000000417

Dosenbach, N. U. F., Nardos, B., Cohen, A. L., Fair, D. A., Power, J. D., Church, J. A., … Schlaggar, B. L. (2010). Prediction of individual brain maturity using fMRI. *Science*, *329*(5997), 1358–1361. https://doi.org/10.1126/science.1194144

Fornito, A., Zalesky, A., & Bullmore, E. (2016). *Fundamentals of brain network analysis*. London, UK: Academic Press.

Ginestet, C. E., Nichols, T. E., Bullmore, E. T., & Simmons, A. (2011). Brain network analysis: Separating cost from topology using cost-integration. *PLoS ONE*, *6*(7), e21570. https://doi.org/10.1371/journal.pone.0021570

Henningsen, P., Gündel, H., Kop, W. J., Löwe, B., Martin, A., Rief, W., … Van den Bergh, O. (2018). Persistent physical symptoms as perceptual dysregulation: A neuropsychobehavioral model and its clinical implications. *Psychosomatic Medicine*, *80*(5), 422–431. https://doi.org/10.1097/psy.0000000000000588

Holmberg, J., Tjernström, F., Karlberg, M., Fransson, P. A., & Magnusson, M. (2009). Reduced postural differences between phobic postural vertigo patients and healthy subjects during a postural threat. *Journal of Neurology*, *256*(8), 1258–1262. https://doi.org/10.1007/s00415-009-5110-x

Indovina, I., Riccelli, R., Chiarella, G., Petrolo, C., Augimeri, A., Giofrè, L., … Passamonti, L. (2015). Role of the insula and vestibular system in patients with chronic subjective dizziness: An fMRI study using sound-evoked vestibular stimulation. *Frontiers in Behavioral Neuroscience*, *9*, 334. https://doi.org/10.3389/fnbeh.2015.00334

Jacob, R. G., Lilienfeld, S. O., Furman, J. M. R., Durrant, J. D., & Turner, S. M. (1989). Panic disorder with vestibular dysfunction: Further clinical observations and description of space and motion phobic stimuli. *Journal of Anxiety Disorders*, *3*(2), 117–130. https://doi.org/10.1016/0887-6185(89)90006-6

Jahn, K., Deutschländer, A., Stephan, T., Kalla, R., Hüfner, K., Wagner, J., … Brandt, T. (2008). (2008). Supraspinal locomotor control in quadrupeds and humans. *Progress in Brain Research*, *171*, 353–362. https://doi.org/10.1016/s0079-6123(08)00652-3

Jahn, K., Deutschländer, A., Stephan, T., Kalla, R., Wiesmann, M., Strupp, M., & Brandt, T. (2008). Imaging human supraspinal locomotor centers in brainstem and cerebellum. *NeuroImage*, *39*(2), 786–792. https://doi.org/10.1016/j.neuroimage.2007.09.047

Jenkinson, M., Bannister, P., Brady, M., & Smith, S. (2002). Improved optimization for the robust and accurate linear registration and motion correction of brain images. *NeuroImage*, *17*(2), 825–841. https://doi.org/10.1006/nimg.2002.1132

Lee, J. O., Lee, E. S., Kim, J. S., Lee, Y. B., Jeong, Y., Choi, B. S., … Staab, J. P. (2018). Altered brain function in persistent postural perceptual dizziness: A study on resting state functional connectivity. *Human Brain Mapping*, *39*(8), 3340–3353. https://doi.org/10.1002/hbm.24080

Lempert, T., Brandt, T., Dieterich, M., & Huppert, D. (1991). How to identify psychogenic disorders of stance and gait. A video study in 37 patients. *Journal of Neurology*, *238*(3), 140–146.

Lenth, R. V. (2016). Least-squares means: The R package lsmeans. *Journal of Statistical Software*, *69*(1), 1–33.

Markett, S., Montag, C., Melchers, M., Weber, B., & Reuter, M. (2016). Anxious personality and functional efficiency of the insular-opercular network: A graph-analytic approach to resting-state fMRI.

Cognitive, Affective & Behavioral Neuroscience, *16*(6), 1039–1049. https://doi.org/10.3758/s13415-016-0451-2

Petzschner, F. H., Weber, L. A. E., Gard, T., & Stephan, K. E. (2017). Computational psychosomatics and computational psychiatry: Toward a joint framework for differential diagnosis. *Biological Psychiatry*, *82*(6), 421–430. https://doi.org/10.1016/j.biopsych.2017.05.012

Popkirov, S., Staab, J. P., & Stone, J. (2018). Persistent postural-perceptual dizziness (PPPD): A common, characteristic and treatable cause of chronic dizziness. *Practical Neurology*, *18*(1), 5–13. https://doi.org/10.1136/practneurol-2017-001809

Popp, P., zu Eulenburg, P., Stephan, T., Bögle, R., Habs, M., Henningsen, P., … Dieterich, M. (2018). Cortical alterations in phobic postural vertigo–A multimodal imaging approach. *Annals of Clinical and Translational Neurology*, *5*, 717–729. https://doi.org/10.1002/acn3.570

Power, J. D., Barnes, K. A., Snyder, A. Z., Schlaggar, B. L., & Petersen, S. E. (2012). Spurious but systematic correlations in functional connectivity MRI networks arise from subject motion. *NeuroImage*, *59*(3), 2142–2154. https://doi.org/10.1016/j.neuroimage.2011.10.018

Querner, V., Krafczyk, S., Dieterich, M., & Brandt, T. (2000). Patients with somatoform phobic postural vertigo: The more difficult the balance task, the better the balance performance. *Neuroscience Letters*, *285*(1), 21–24. https://doi.org/10.1016/S0304-3940(00)01008-9

R Core Team (2018). *R: A language and environment for statistical computing*. Vienna, Austria: R Foundation for Statistical Computing.

Raichle, M. E. (2015). The brain's default mode network. *Annual Review of Neuroscience*, *38*, 433–447. https://doi.org/10.1146/annurev-neuro-071013-014030

Rubinov, M., & Sporns, O. (2010). Complex network measures of brain connectivity: Uses and interpretations. *NeuroImage*, *52*(3), 1059–1069. https://doi.org/10.1016/j.neuroimage.2009.10.003

Ruckenstein, M. J., & Staab, J. P. (2009). Chronic subjective dizziness. *Otolaryngologic Clinics of North America*, *42*(1), 71–77. https://doi.org/10.1016/j.otc.2008.09.011

Schniepp, R., Wuehr, M., Huth, S., Pradhan, C., Brandt, T., & Jahn, K. (2014). Gait characteristics of patients with phobic postural vertigo: Effects of fear of falling, attention, and visual input. *Journal of Neurology*, *261*(4), 738–746. https://doi.org/10.1007/s00415-014-7259-1

Sheline, Y. I., Price, J. L., Yan, Z., & Mintun, M. A. (2010). Resting-state functional MRI in depression unmasks increased connectivity between networks via the dorsal nexus. *PNAS*, *107*(24), 11020–11025. https://doi.org/10.1073/pnas.1000446107

Singmann, H., Bolker, B., Westfall, J., & Aust, F. (2018). afex: Analysis of Factorial Experiments. R package version 0.21-2. Retrieved from https://CRAN.R-project.org/package=afex

Staab, J. P., Eckhardt-Henn, A., Horii, A., Jacob, R., Strupp, M., Brandt, T., & Bronstein, A. (2017). Diagnostic criteria for persistent postural-perceptual dizziness (PPPD): Consensus document of the committee for the classification of Vestibular Disorders of the Bárány Society. *Journal of Vestibular Research*, *27*(4), 191–208. https://doi.org/10.3233/VES-170622

Tesche, C. D., & Karhu, J. J. T. (2000). Anticipatory cerebellar responses during somatosensory omission in man. *Human Brain Mapping*, *9*(3), 119–142. https://doi.org/10.1002/(SICI)1097-0193(200003)9:3%3C119:AID-HBM2%3E3.0.CO;2-R

Van Ombergen, A., Heine, L., Jillings, S., Roberts, R. E., Jeurissen, B., Van Rompaey, V., … Wuyts, F. L. (2017). Altered functional brain connectivity in patients with visually induced dizziness. *NeuroImage: Clinical*, *14*, 538–545. https://doi.org/10.1016/j.nicl.2017.02.020

von Holst, E., & Mittelstaedt, H. (1950). Das Reafferenzprinzip. *Naturwissenschaften*, *37*(20), 464–476. https://doi.org/10.1007/BF00622503

Whitfield-Gabrieli, S., & Ford, J. M. (2012). Default mode network activity and connectivity in psychopathology. *Annual Review of Clinical Psychology*, *8*, 49–76. https://doi.org/10.1146/annurev-clinpsy-032511-143049

Whitfield-Gabrieli, S., & Nieto-Castanon, A. (2012). Conn: A functional connectivity toolbox for correlated and anticorrelated brain networks. *Brain Connectivity*, *2*(3), 125–141. https://doi.org/10.1089/brain.2012.0073

Wickham, H. (2007). Reshaping data with the reshape package. *Journal of Statistical Software*, *21*(12).

Wickham, H. (2011). The split-apply-combine strategy for data analysis. *Journal of Statistical Software*, *40*(1), 1–29. https://doi.org/10.18637/jss.v040.i01

Wuehr, M., Brandt, T., & Schniepp, R. (2017). Distracting attention in phobic postural vertigo normalizes leg muscle activity and balance. *Neurology*, *88*(3), 284–288. https://doi.org/10.1212/wnl.0000000000003516

Xia, M., Wang, J., & He, Y. (2013). BrainNet viewer: A network visualization tool for human brain connectomics. *PLoS ONE*, *8*(7), e68910. https://doi.org/10.1371/journal.pone.0068910

Yan, C. G., Cheung, B., Kelly, C., Colcombe, S., Craddock, R. C., Di Martino, A., … Milham, M. P. (2013). A comprehensive assessment of regional variation in the impact of head micromovements on functional connectomics. *NeuroImage*, *76*, 183–201. https://doi.org/10.1016/j.neuroimage.2013.03.004

Yan, C. G., Craddock, R. C., He, Y., & Milham, M. P. (2013). Addressing head motion dependencies for small-world topologies in functional connectomics. *Frontiers in Human Neuroscience*, *7*, 910. https://doi.org/10.3389/fnhum.2013.00910

zu Eulenburg, P., Müller-Forell, W., & Dieterich, M. (2013). On the recall of vestibular sensations. *Brain Structure and Function*, *218*(1), 255–267. https://doi.org/10.1007/s00429-012-0399-0

SUPPORTING INFORMATION

Additional supporting information may be found online in the Supporting Information section.

How to cite this article: Huber J, Flanagin VL, Popp P, zu Eulenburg P, Dieterich M. Network changes in patients with phobic postural vertigo. *Brain Behav*. 2020;10:e01622. https://doi.org/10.1002/brb3.1622

Appendices

Appendix A: Supplementary Figures

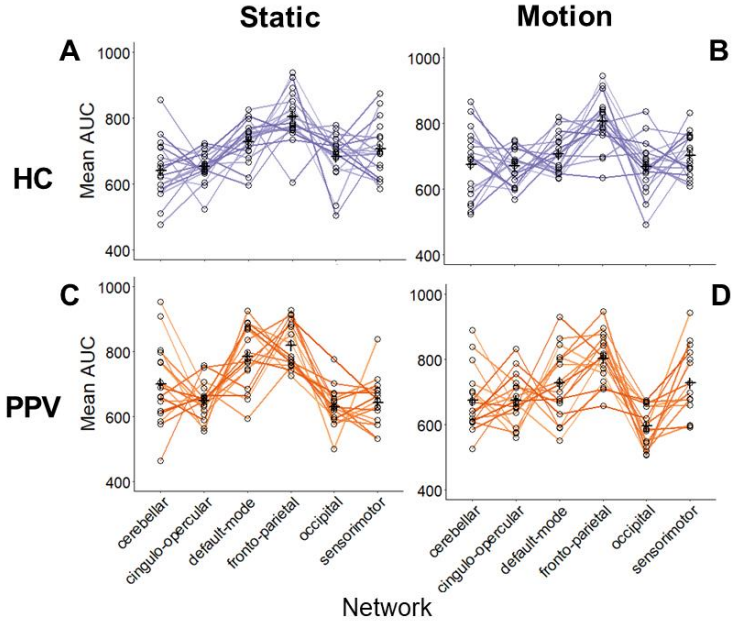

Supplementary Figure A.1 Within-participant changes of degree centrality for six functional networks.
A) Healthy controls (HC) during the static condition B) HC during the motion condition C) Patients (PPV) during the static condition D) PPV during the motion condition

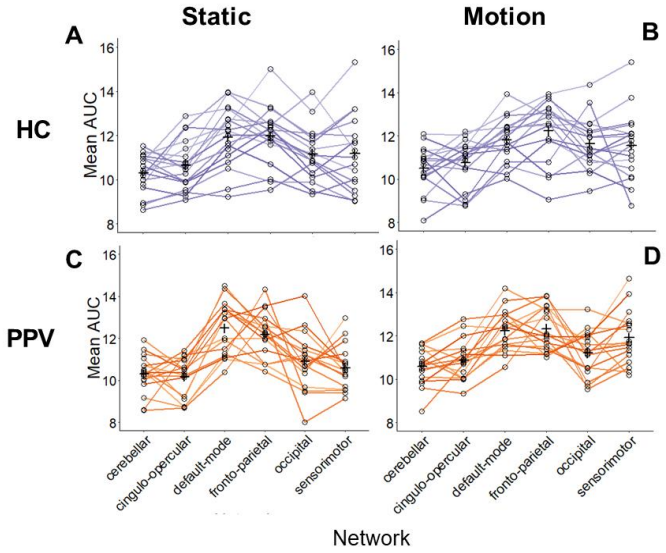

Supplementary Figure A.2 Within-participant changes of clustering coefficient for six functional networks.
A) Healthy controls (HC) during the static condition B) HC during the motion condition C) Patients (PPV) during the static condition d) PPV during the motion condition

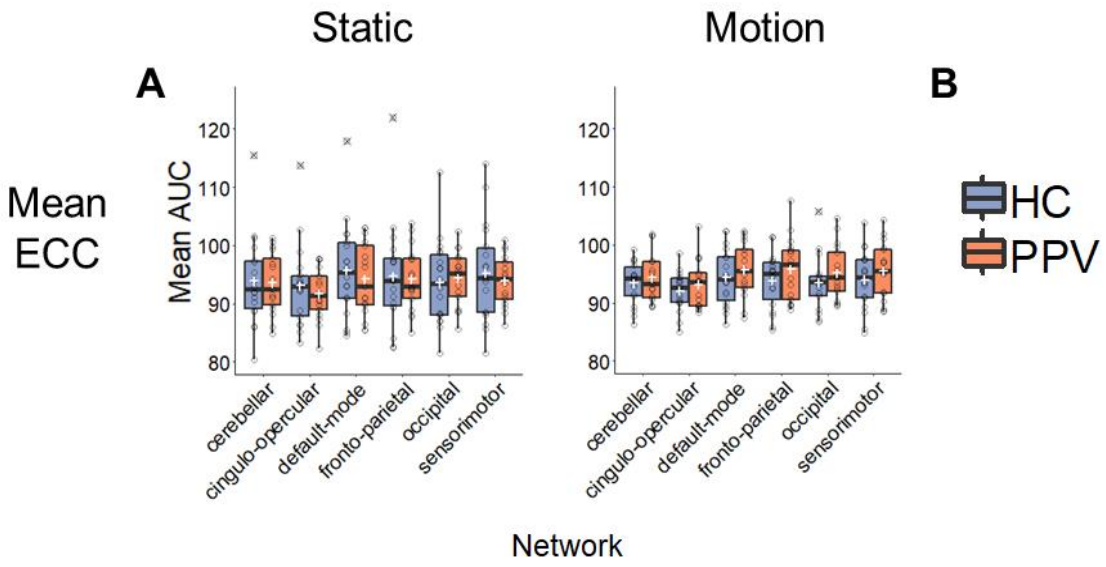

Supplementary Figure A.3 Boxplots comparing mean area under curve (AUC) for eccentricity (ECC) between healthy controls (HC) and patients (PPV) both in static and motion conditions, for each of the six functional brain networks given by Dosenbach (2010). White crosses indicate mean values, outliers are marked with a black cross. A) Mean shortest eccentricity during static conditions B) Eccentricity during motion conditions

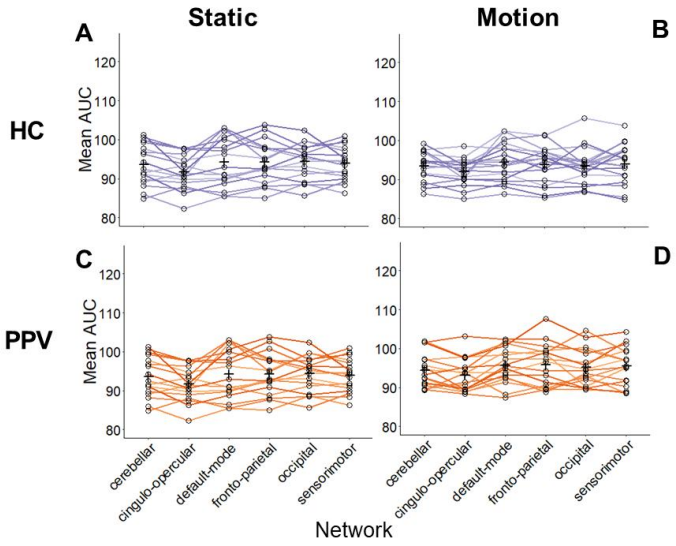

Supplementary Figure A.4. Within-participant changes of eccentricity for six functional networks.
A) Healthy controls (HC) during the static condition B) HC during the motion condition C) Patients (PPV) during the static condition D) PPV during the motion condition

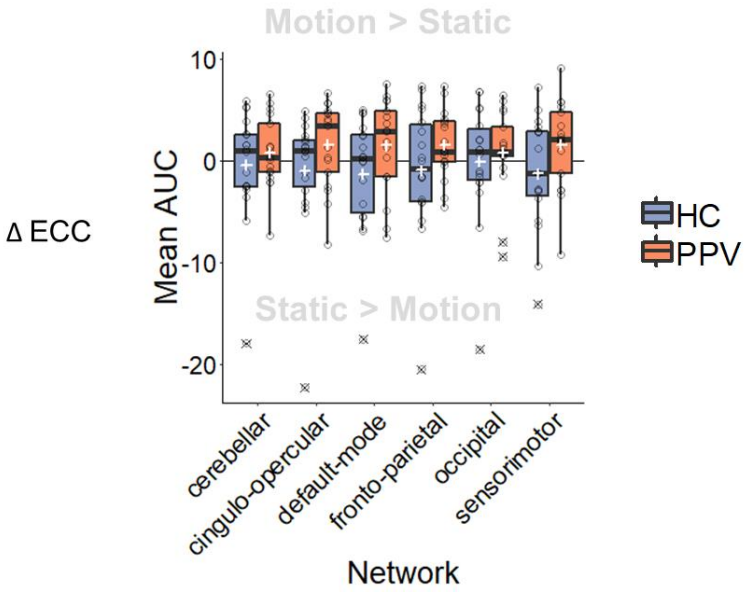

Supplementary Figure A.5 Boxplots showing eccentricity (ΔECC) across tasks (i.e. graph values during the static condition subtracted from motion) for six functional networks of the Dosenbach atlas, healthy controls (HC) and patients (PPV) .
Values above zero indicated nodes in the respective network had a higher AUC during motion on average, whereas values below zero mean nodes in the network had a higher AUC value during the static condition on average. White cross indicates mean values, outliers are marked with a black cross.

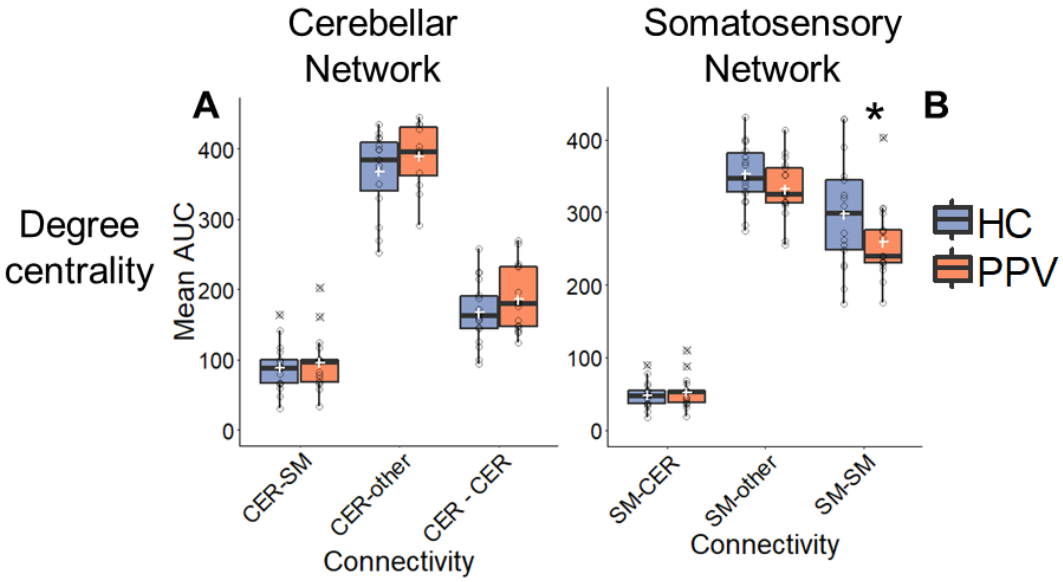

Supplementary Figure A.6 Boxplot showing how degree centrality during the static condition differs between groups (healthy controls (HC) and patients (PPV)) if calculated within the same network (CER-CER or SM-SM), to the other network (CER-SM / SM – CER) or the remaining brain (CER-other or SM-other.
A) degree centrality of cerebellar and B) somatosensory networks. White cross indicates mean values, outliers are marked with a black cross.

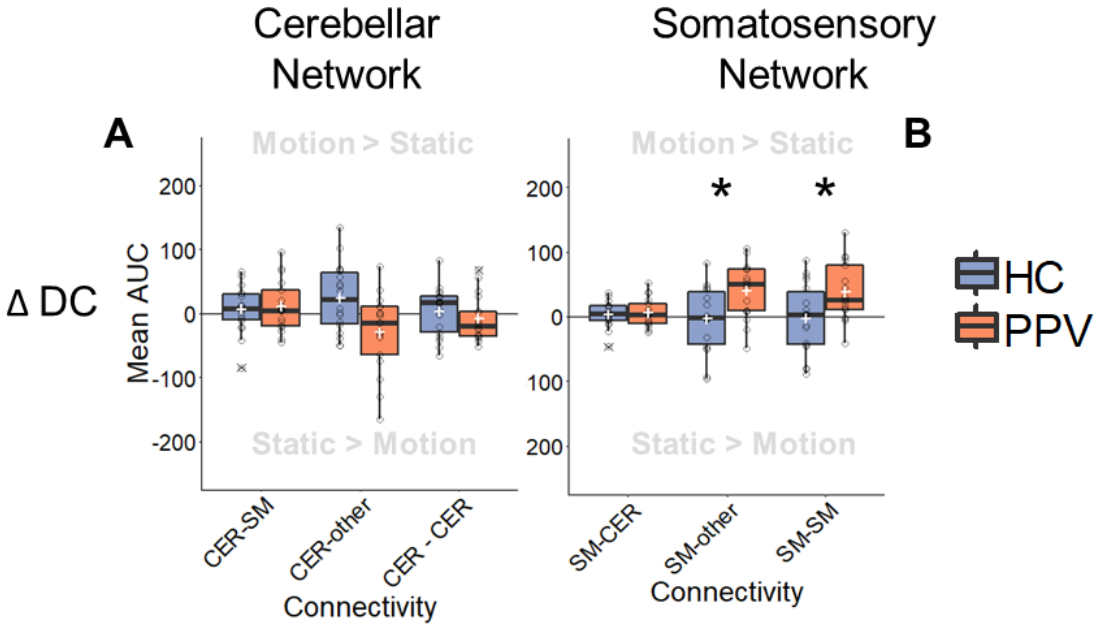

Supplementary Figure A.7 Boxplot showing how degree centrality change (motion-static, ΔDC) differs between groups (healthy controls (HC) and patients (PPV)) if calculated within the same network (CER-CER or SM-SM), to the other network (CER-SM / SM – CER) or the remaining brain (CER-other or SM-other).
A) degree centrality of cerebellar and B) somatosensory networks. White cross indicates mean values, outliers are marked with a black cross.

Appendix B: Supplementary Information

Analysis 1: Correcting for excessive motion

Method: To ensure motion did not influence results, outlier scan identification was performed, as implemented in CONN using a conservative threshold of z-score > 3 and FD > 0.2 mm (with a window size of 2). The frames which exceeded these criteria were included in a subject-specific nuisance regressor for regressing out the signal related to these timepoints. This was preferred over deleting time points to avoid interpolation. Subsequent measures were calculated as described previously. Overall, there was little difference to the results. Only significant main effects and interactions will be reported.

Connectivity group effects during static and motion condition: For the static condition, the interaction between group and network effects was significant again (Pillai's trace=0.204, $F(15,465) = 2.267$, $p=0.004$), as well as the factor networks (Pillai's trace=0.655, $F(15, 465)=8.665$, $p<0.001$). No other interactions and main effects were found. Again, three separate mixed-design ANCOVAs were performed for degree centrality, clustering coefficient and eccentricity during the static condition.

For degree centrality, again a significant interaction ($F_{(5, 160)}$=3.370, p=0.006) as well a significant network effect was found ($F_{(5,160)}$=16.495, p<0.001). Because of the significant interaction, post-hoc t-tests were performed using Tukey's method. Degree centrality of cerebellar network (T(163.3)=-2.215, p=0.028) and default mode network nodes (T(163.3)=-2.060, p=0.041) remained significantly higher in PPV compared to HC. Sensorimotor remained significantly lower in PPV, when compared to HC (F(163.3)=2.640, p=0.009). No significant effect was found in the occipital nodes anymore (F(163.3)=1.737, p=0.084), suggesting that the effect in the occipital network is either not stable and possibly caused by excessive movement (Figure B.1A)

For clustering coefficient, again a significant interaction was found ($F_{(3.41,109.12)}$=3.2046, p=0.021, after adjusting degrees of freedom using Greenhouse Geisser estimates of sphericity (ε=0. 682), since Mauchly's test indicated that the assumption of sphericity was violated ($W_{(14)}$=0.298, p=0.001). The factor of network also remained significant ($F_{(3.41,109.12)}$= 22.492, p<0.001). As in the main analysis, there was a significant effect of age

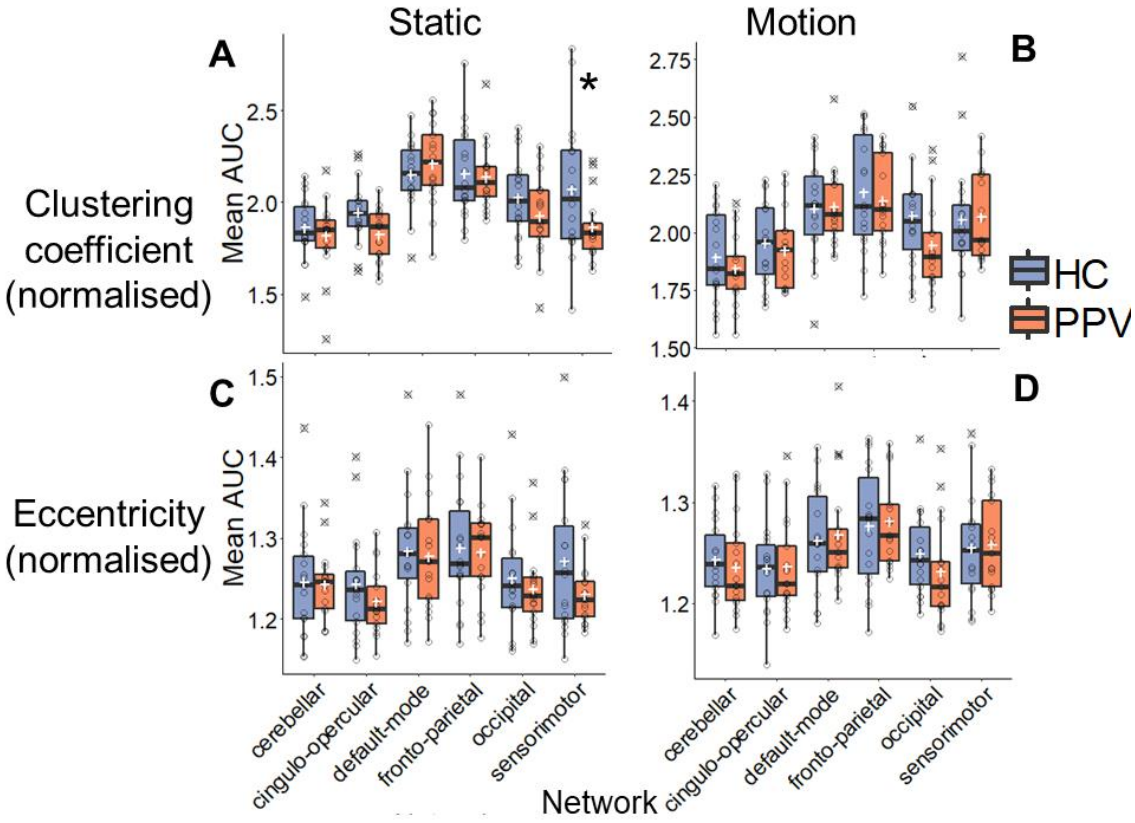

Supplementary Figure B.1 Boxplots comparing degree centrality mean area under the curve (AUC) and clustering coefficient AUC between healthy controls (HC) and patients (PPV) both in static and motion, for each of the six functional brain networks given by Dosenbach (2010) after correcting for excessive motion.
A) Degree centrality during static conditions B) Degree centrality during motion conditions C) Clustering coefficient during static conditions D) Clustering coefficient during visual motion conditions. White crosses indicate means, stars indicate a significant (p<0.05) group effect outliers are marked with a black cross.

($F_{(1,32)}$=4.370, p=0.045). Because of the significant interaction, post-hoc t-tests were performed using Tukey's method to determine in which networks clustering coefficient significantly differed between HC and PPV. Indeed, the only significant effect was again found in the sensorimotor network ($t_{(103.2)}$=3.669, p=0.009), with HC showing higher clustering coefficient in the sensorimotor network (Figure B. 2C)

For eccentricity, again no significant interaction or main group effect was found during the static condition.

During the visual motion condition, only the factor of age was found to be significant using MANCOVA (Pillai's trace = 0.350, F(3,29)= 5.205, p= 0.005). No subsequent ANCOVAs were thus performed (Figure B. 3B, Figure B. 3D)

Change of graph measures between conditions: Again the interaction of network and group was significant (Pillai's trace = 0.189, $F_{(15, 465)}$=2.088, p=0.010). The main effect for group effect also remained significant (Pillai's trace = 0.439, $F_{(3,29)}$ = 7.577, p= 0.001). No other main effects were significant. To determine the specific effects on each graph measures, mixed-design ANCOVAs were performed for ΔDC, ΔCC and ΔECC.

For ΔDC a significant interaction between group and network ($F_{(5,160)}$=4.534, p=0.001) was found again. In terms of main effects, the factor of group ($F_{(1,32)}$ =12.700, p= 0.001) and network remained significant ($F_{(5,160)}$=3.860, p=0.002). Subsequent t-tests using Tukey's method revealed that the difference between groups remained significant for the nodes in the cerebellar network ($t_{(162.89)}$=2.800, p= 0.006) and the nodes in the sensorimotor network ($t_{(162.89)}$=-3.966, p=0.0001). While the cerebellar network displayed significant increased ΔDC in HC, the sensorimotor network displayed significant increased ΔDC in PPV (see Figure B.2A).

For ΔCC, only a significant interaction between group and network ($F_{(5,160)}$=3.969, p= 0.002) was found. Because of the significant interaction, post-hoc t-tests were performed. In the sensorimotor network a significant difference of ΔCC between groups was found ($t_{(171.63)}$=-4.469, p<0.001). The PPV group displayed a significantly increased ΔCC compared to HC (see Figure B.2B).

For ΔECC no significant interaction or main group effect was found.

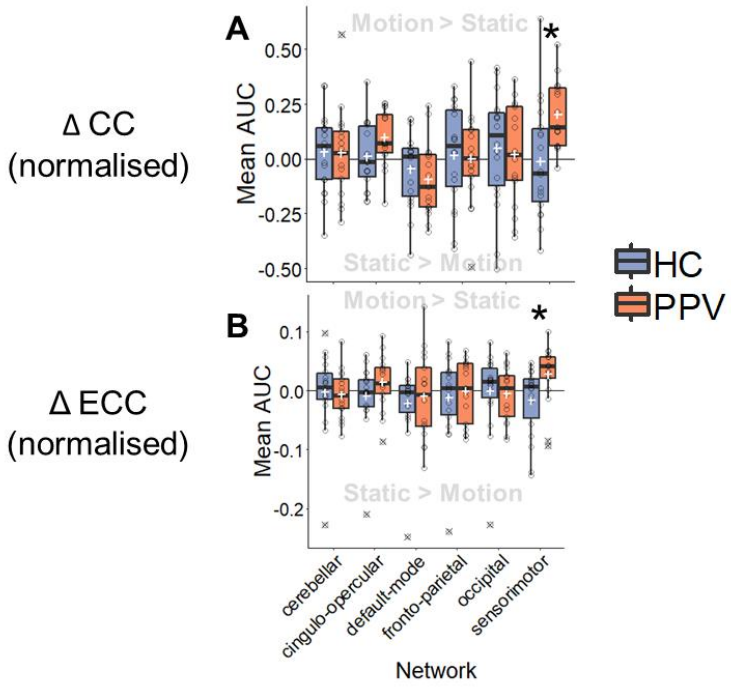

Supplementary Figure B.2 Boxplots showing A) change in degree centrality (ΔDC) and B) clustering coefficient (ΔCC) across tasks (i.e. graph values during static subtracted from motion condition) for six functional networks of the Dosenbach atlas for healthy controls (HC) and patients (PPV) after correcting for excessive motion.
Values above zero indicated nodes in the respective network had an AUC value during motion on average, whereas values below zero mean nodes in the network had a higher AUC value on average during the static condition. White cross indicates mean, stars indicate a significant ($p<0.05$) group effect, outliers are marked with a black cross.

Analysis 2: Normalisation to random networks

Method: For each participant and each threshold, adjacency matrices were randomised using the randmio_und function from the BCT, with a rewiring parameter of 100. Clustering coefficient and eccentricity were calculated for these random matrices, AUC was used to summarise the values. Clustering coefficient and eccentricity were normalised by dividing the AUC values determined from the real data by the AUC values of the randomised matrices. Difference values were calculated by simply subtracting normalised graph measures during the REST condition from the normalised graph measures during the TASK conditions.

ANCOVAS were calculated for clustering coefficient and eccentricity separately. Group of participants and six functional networks were included as independent variables. Age was added as a covariate.

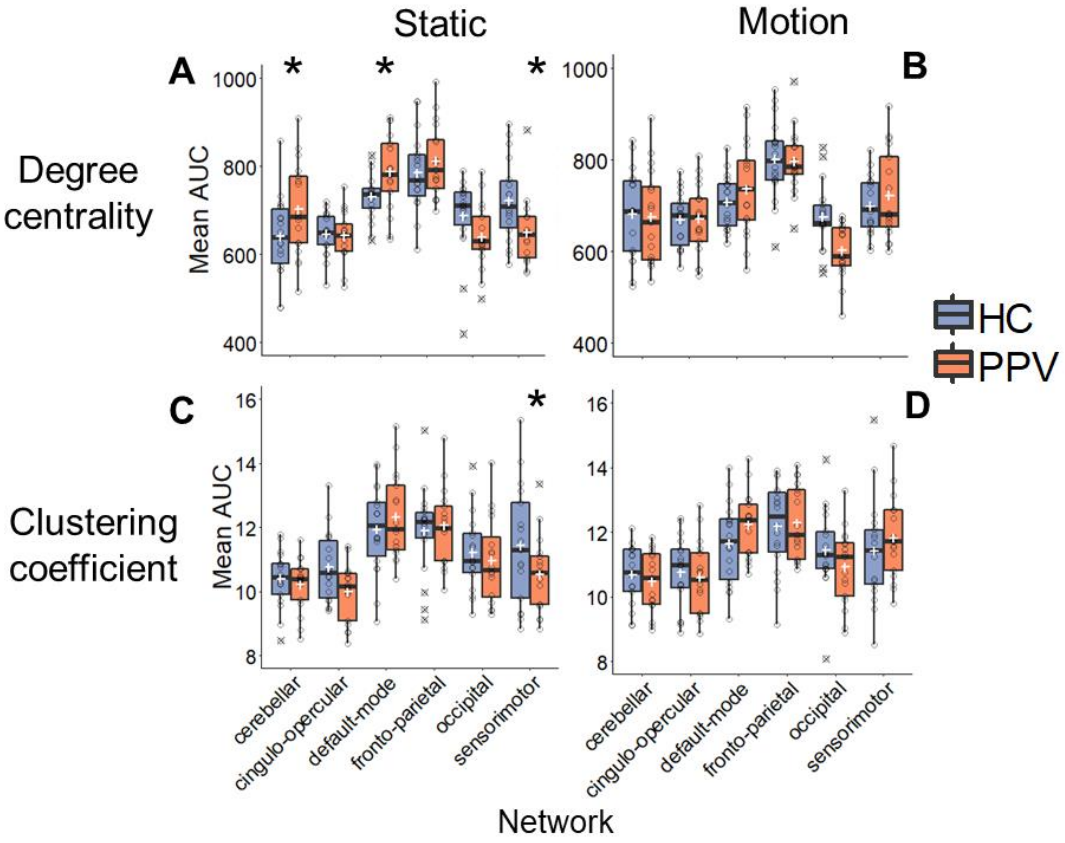

Figure B.3 Boxplots comparing degree centrality mean area under the curve (AUC) and clustering coefficient AUC between healthy controls (HC) and patients (PPV) both in static and motion, for each of the six functional brain networks given by Dosenbach (2010) after normalising to random networks.
White crosses indicate means, stars indicate a significant ($p<0.05$) group effect, outliers are marked with a black cross. A) Clustering coefficient during static conditions B) Clustering coefficient during motion conditions C) Eccentricity during static conditions D) Eccentricity during visual motion conditions.

Connectivity group effects during static and motion condition: During the static condition, for clustering coefficient, a significant interaction of group and network was found ($F_{(3.56,\ 113,76)}=2.6522$, $p=0.043$ after adjusting degrees of freedom using Greenhouse Geisser estimates of sphericity ($\varepsilon=0.711$) due to violations of the assumption of sphericity as determined by Mauchly's test ($W_{(14)}=0.375$, $p=0.009$). A main effect of network ($F_{(3.56,\ 113,76)}=24.7726$, $p<0.001$ after the same adjustments to degrees of freedom) and age ($F_{(1,32)}=4.158$, $p=0.050$) was also found. Due to the significant interaction, post-hoc t-tests were conducted. Indeed, the clustering coefficient of the nodes in the sensorimotor network was significantly lower in the PPV group, when compared to HC ($t_{(105.3)}=2.829$, $p=0.006$) (Figure B.3A).

For eccentricity, only a significant main effect of network was found in the static condition ($F_{(3.375,108)}=16.060$, $p<0.001$ after adjusting degrees of freedom using Greenhouse Geisser estimates of sphericity ($\varepsilon=0.675$) due to violations of the assumption of sphericity as determined by Mauchly's test ($W_{(14)}=0.356$, $p= 0.003$) (see Figure B.3C)

During the motion condition, for the clustering coefficient only main effects of age ($F_{(1,32)}$=10.686, p=0.003) and network were found ($F_{(3.805,121.76)}$=18.4284 p< 0.001 after adjusting degrees of freedom using Greenhouse Geisser estimates of sphericity (ε=0.761) due to violations of the assumption of sphericity as determined by Mauchly's test $W_{(14)}$=0. 392, p= 0.014) (see Figure B.3B).
For eccentricity, only a significant effect of network was found in the motion condition ($F_{(3.96,126.72)}$=18.660, p<0.001 after adjusting degrees of freedom using Greenhouse Geisser estimates of sphericity (ε=0.792) due to violations of the assumption of sphericity as determined by Mauchly's test ($W_{(14)}$=0.452, p= 0.047) (Figure B. 3D)

Change of graph measures between conditions: For ΔCC, a significant interaction of network and group was found ($F_{(5,160)}$= 3.2083, p= 0.009) as well as a significant effect of network ($F_{(5,160)}$=3.930, p=0.002). No other significant main effects or interactions were found. Post-hoc t-tests again revealed a significant difference between groups in the sensorimotor network, with PPV showing significantly increased clustering coefficient compared to the HC group ($t_{(123.38)}$=-3.124, p=0.002) (Figure B. 4A).

In contrast to the previous results, for ΔECC a significant interaction of network and group was found ($F_{(3.59,114,88)}$=2.357, p=0.064 after adjusting degrees of freedom using Greenhouse Geisser estimates of sphericity (ε=0.718) due to violations of the assumption of sphericity as determined by Mauchly's test ($W_{(14)}$=0.356, p= 0.003). No other interactions of main effects were found. Because of the significant interaction, post-hoc t-tests were performed using Tukey's method to determine in which networks eccentricity significantly differed between HC and PPV. A significant difference between groups was only found in the sensorimotor network, with PPV showing significantly increased eccentricity compared to the HC group ($t_{(63.51)}$=-2.217, p=0.030). (Figure B. 4B)

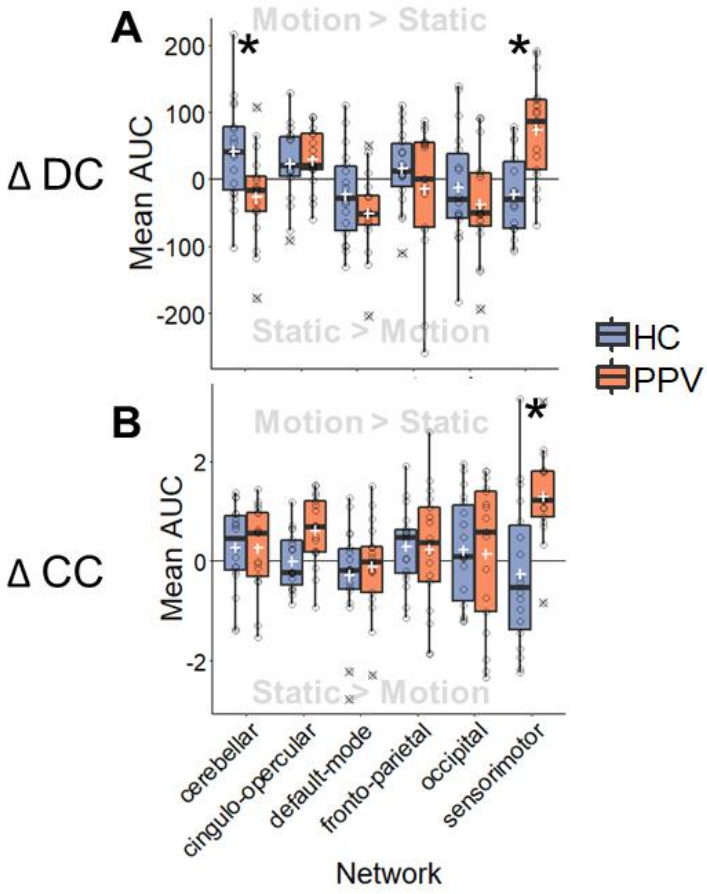

Figure B.4 Boxplots showing A) change in clustering coefficient (ΔCC) and B) eccentricity (ΔECC) across tasks (i.e. graph values during static subtracted from motion condition) for six functional networks of the Dosenbach atlas for healthy controls (HC) and patients (PPV) after normalisation to random networks.
Values above zero indicated nodes in the respective network had an AUC value during motion on average, whereas values below zero mean nodes in the network had a higher AUC value on average during the static condition. White cross indicates mean, stars indicate a significant ($p<0.05$) group effect, outliers are marked with a black cross.

3. The Modulation of Human Brain Networks by Means of Vestibular Stimulation

Judita Huber[1,2], Virginia L. Flanagin[1,2,3,4], Ria Maxine Ruehl[3,4], Peter zu Eulenburg[1,3,4,5]

1 Graduate School of Systemic Neurosciences, LMU Munich; 2 Research Training Grant 2175, LMU Munich; 3 Neurologische Klinik und Poliklinik (Department of Neurology), LMU München; 4 German Center for Vertigo and Balance Disorders, LMU Munich; 5 Munich Cluster of Systems Neurology (SyNergy), LMU Munich

Author Contributions

JH conceived the analysis, preprocessed the data for the functional connectivity analysis, analysed, and interpreted the data, wrote the manuscript, and created the figures. VLF provided support with data analysis, reviewed the manuscript and figures. RMR acquired the data. PzE conceived the experiment and the analysis, preprocessed the data for the task-based analysis, interpreted the data, and reviewed the manuscript and figures.

Acknowledgements

This research was supported by a grant from the German Ministry for Education and Research (http:// www.bmbf.de, Grant number: IFB 01EO1401). It was further funded by the German Research Association (DFG) via the RTG 2175 "Perception in context and its Neural Basis" and the Graduate School of Systemic Neurosciences (GSC 82/1), Munich, Germany. We thank Martijn van der Heuvel and Gabriel Castrillon for methodological input on the network analyses and for providing the scripts for the modularity analysis.

Abstract

Vestibular information is ubiquitous and often processed jointly with visual and proproceptive information. Several cortical brain regions have been associated with human vestibular processing, but to what extent they uniquely contribute to vestibular perception or whether they are mostly related to general somatosensory processing is not clear. Furthermore, it is not known if and how the interaction of the cortical vestibular network changes during vestibular stimulation. In the present study, we therefore aimed to characterise vestibular processing in terms of task activity and functional network architecture. We disentangled vestibular from general somatosensory information processing by analysing data from two experiments, which uniquely differed in their sensory target of stimulation: vestibular (GVS) and nociceptive (GNS) stimulation. Comparing GVS directly with GNS should reveal exclusive vestibular processes or distinct nociceptive processing. In the task-based analysis we confirmed several dedicated regions in vestibular processing, such as the parietal opercular area OP2 and the bilateral cingulate sulcus visual (CSv). In the conjunction analysis for detecting activated regions by both modalities we delineated vestibular regions associated with more general spatial and somatosensory processing, notably the ventral intraparietal area (VIP). We found no distinct regions involved exclusively in cortical nociceptive processing. Surprisingly, we did not find network evidence for a functional cortical reorganisation during vestibular stimulation. Here, we found only network changes during nociceptive stimulation. We hypothesise that vestibular stimulation is not sufficient to change synchronisation of brain regions. This may also be reflected by the fact that vestibular processing mostly occurs subconsciously.

3.1 Introduction

The vestibular system monitors active and passive head movements in all translational and rotational directions while at the same time sensing gravity. The interaction of human brain areas that compute this information from vestibular input is still not fully understood. Several notable aspects about the vestibular sense contribute to the complexity of human vestibular research. Under normal circumstances, vestibular information is accompanied by separate congruent sensory information such as vision or proprioception, and vestibular processing does not seem to involve conscious awareness in healthy subjects. Probing vestibular properties of brain areas whilst controlling for the confounding effects of other sensations therefore represents a hurdle in the efforts to understand the neural underpinnings of the vestibular system. These efforts are additionally complicated by the immobility necessitated by most non-invasive human brain activity measurements, such as functional magnetic resonance imaging. Therefore, our understanding of the vestibular system in humans is still primarily based on single-unit recordings during real movement in non-human primates.

These electrophysiological recordings have implicated a distributed set of cortical brain regions for processing different types of vestibular information. The posterior thalamocortical pathway appears to process self-motion perception (Cullen & Taube, 2017). Vestibular information is transmitted from the posterior thalamic vestibular nuclei to the somatosensory cortex and to the parieto-insular vestibular cortex (PIVC). The PIVC is considered by some to be the primary vestibular cortex because of the large amount of neurons that respond to vestibular input (Guldin & Grüsser, 1998) even in the absence of visual input in darkness (Chen, DeAngelis, & Angelaki, 2010). In the macaque, PIVC is located in the lateral sulcus adjacent to the insula. Another region in the parietal lobe targeted by the posterior thalamocortical vestibular pathway is the ventral intraparietal cortex (VIP). Neurons in this region are important for visual-vestibular integration and representation of object location in near extra-personal space (Bremmer, Schlack, Kaminiarz, & Hoffmann, 2013; Cullen, 2019; A. T. Smith, Greenlee, DeAngelis, & Angelaki, 2017). Neurons the medial superior temporal area (MST) also integrate visual-vestibular information, but with more weight given to the visual input (A. T. Smith, Greenlee, et al., 2017). Human equivalents of these areas have been found using functional magnetic resonance (fMRI) during artificial vestibular stimulation. These include caloric irrigation, in which one ear is irrigated with warm or cold water (Lopez, Blanke, & Mast, 2012), and galvanic vestibular stimulation (GVS), where electrodes are attached to the mastoid and small electrical currents stimulate the primary vestibular afferents (Kwan, Forbes,

Mitchell, Blouin, & Cullen, 2019). Both result in a strong perception of being moved, but GVS is more consistent, bilateral and more feasible experimentally, which has made it a more common stimulation method in human experiments.

The parietal opercular area OP2 was consistently activated in multiple fMRI experiments using vestibular stimulation suggesting that it is the human homologue of PIVC (zu Eulenburg, Caspers, Roski, & Eickhoff, 2012). Studies from human VIP, located along the intraparietal sulcus, have been inconclusive as to the convergence of multisensory and vestibular information in this area, like that seen in the macaque (A. T. Smith, Greenlee, et al., 2017). The VIP responds to visual stimulation consistent with egomotion (Wall & Smith, 2008), but does not respond strongly to GVS (A. T. Smith, Wall, & Thilo, 2012). The human MST located in lateral occipital cortex, is not very selective for egomotion (Wall & Smith, 2008), but is activated by GVS, even when controlling for the somatosensory components of the stimulation (A. T. Smith et al., 2012).

In addition to human vestibular brain regions with non-human primate homologues, a brain region was found to respond to vestibular stimulation in humans. The cingulate sulcus visual area (CSv), located in the posterior part of the mid-cingulate sulcus responds to visual egomotion stimuli (Wall & Smith, 2008) as well as to GVS (A. T. Smith et al., 2012). Evidence from both structural and functional connectivity suggest that it is connected with VIP and the parietal operculum (A. T. Smith, Beer, Furlan, and Mars (2017)). A non-human primate homolog to the human CSv has only recently been suggested to correspond to area 23c in the macaque (Cottereau et al., 2017). A discussion of other cortical and subcortical regions that process aspects of vestibular information in primates can be found in a number of excellent reviews (Cullen, 2019; Hitier, Besnard, & Smith, 2014; A. T. Smith, Greenlee, et al., 2017).

Although galvanic vestibular stimulation is still the most successful and widely used form of artificial vestibular stimulation, it has a few pitfalls that have not always been sufficiently addressed in neuroimaging studies. GVS over the mastoid bone is not an exclusive vestibular stimulation paradigm; it can also result in a tickling sensation underneath the cathode and induce the percept of a metallic taste via arousal of the chorda tympani (Lobel, Kleine, Bihan, Leroy-Willig, & Berthoz, 1998; A. T. Smith et al., 2012; Stephan et al., 2005). Using larger electrodes can reduce the tactile sensation but it does not eliminate it (Lobel et al., 1998). This is particularly lamentable as the regions of interest for vestibular research are per definition multi-sensory and also receive somatosensory input. Another difficulty common to most human neuroimaging studies is the choice of an appropriate baseline. Ambiguous baselines, such as a general “rest period” can reduce or change the

sign of task-based BOLD signal change, due to the cognitive activity during the baseline condition (Stark & Squire, 2001). Alternative comparisons involve performing an additional non-vestibular galvanic stimulation task to control for somatosensory responses (A. T. Smith et al., 2012).

Additional important information can be gained from investigating the coordination of the BOLD signal across the brain during artificial vestibular stimulation. Such task-state functional connectivity provides information about regional interactions during tasks and reconfigurations of functional networks (Gonzalez-Castillo & Bandettini, 2018) and does not depend on the choice of baseline. Hence, the aim of the following study was two-fold: 1) to determine the brain areas uniquely associated with vestibular stimulation, while minimising and accounting for the confounding effect of salient somatosensation from the scalp and 2) to investigate changes in the network architecture using task-state functional connectivity of the entire cortical network during stimulation uniquely associated with vestibular perception.

To achieve this, we compared galvanic vestibular (GVS) to galvanic nociceptive stimulation (GNS) using an identical setup and stimulation protocol in two experiments during functional magnetic resonance imaging (fMRI). We compared task activations and functional network architecture between GVS and GNS. For task activation results, we hypothesized that previously described vestibular regions would be more active during GVS than GNS, and that the insular cortex would show common activity across both experiments. To our knowledge, whole-brain functional network changes during vestibular stimulation were not investigated so far, we thus followed a hypothesis-free approach. Importantly, we corrected the fMRI signal for activation-induced connectivity estimate inflation (Cole et al., 2019). We first investigated all effects within-subject on a group of subjects that participated in both experiments, and then confirmed our results on a larger between-subject cohort analysis.

3.2 Methods

3.2.1 Participants

Participants underwent one or both of two separate GVS fMRI experiments with either bilateral vestibular stimulation (GVS), or with galvanic nociceptive stimulation (GNS). Participants were recruited via campus-based advertisement. The inclusion criteria were general and neuro-otological health for both experiments. Left-handed participants were excluded as defined by a score below +60 for right-sided dominance using the Edinburgh handedness assessment. Participants gave their informed consent and were monetarily compensated for their participation. Ethical approval was given by the local ethical board

of the University Hospital of Ludwig-Maximilians-Universität München in accordance with the 2008 revision of the Declaration of Helsinki.

Overall, 26 (thirteen female, mean age 28.6 years, age range 19-44) participants consented and completed the GNS experiment, 80 participants completed the GVS experiment. For the between-subject analysis, all these participants were preprocessed and analysed. For the within-subject analysis, data from the subset of eighteen participants who completed both experiments was selected. Due to insufficient data quality in either of the two experiments for the quality criteria for functional connectivity analysis (see Section 3.2.5.2) three participants were excluded from all the within-participant data analyses. Hence, 15 participants remained for the final within-subject cohort (eight female, mean age 27.1 years, age range 19-44).

3.2.2 Procedure & Design

For both experiments, carbon electrodes were attached on the mastoid bone of the participants lateral to the hair line before entering the scanner. For the unilateral GNS experiment, one electrode was placed on the mastoid, and one two centimeters inferior to it on the ipsilateral neck. The GNS experiment was repeated in separate sessions for each side of the head. This electrode positioning eliminates vestibular stimulation, while sustaining the galvanic-induced somatosensory sensations. For the GVS experiment, both electrodes were placed on the mastoid. Forty-five Minutes before the GVS experiment, 3g lidocaine creme anaesthetic crème (Emla, Aspen Germany GmbH, Bad Oldesloe, Germany) was applied to the skin above the mastoid process behind each ear. All participants received ear plugs and a gel capsule was attached on their right temple to ensure correct identification of side after preprocessing. During the experiment, participants were lying in the scanner in supine position, the head carefully fixed using an air-based cushion (Crania adult cap from Pearl Technology AG, Schlieren, Switzerland) to minimise head motion during the experiments).

Both experiments included (in the given order) a head scout sequence, a resting-state session with eyes open (roughly 7 minutes), a structural T1-weighed acquisition and the stimulation session(s), each lasting almost 12 minutes (see Section 3.2.4 for the image acquisition parameters). The GVS experiment consisted of one stimulation session, the GNS experiment consisted of two stimulation sessions (GNS on left side and GNS on right side, conditions were pseudo-randomised). The instructions for all participants were the same for both the GVS and the GNS experiment: to passively experience the stimulation, but to keep their eyes opened and to look straight ahead at a white cross on a laminated

black board on the scanner tunnel ceiling. In addition to neuroimaging, high-resolution video-oculography was performed for during the stimulation sessions, and a debriefing immediately following the stimulation sessions with scale pain ratings (reaching from 1 to 10) and a debriefing with respect to the trajectories and body movements during vestibular stimulation.

3.2.3 Stimulation

Stimulation was performed using custom-made stimulator as detailed in Stephan et al. (2005). The stimulation conditions were conducted in a block-design approach and consisted of identical stimulation protocols. Three types of stimulations were delivered for seven seconds: 1) stimulation with a sinusoidal waveform of 0.875 Hz 2) stimulation with a step waveform (1 second upward, 4 second plateau and 2 second down), with the current going from cathode to anode 3) stimulation with a step waveform with the current going from the anode to the cathode, resulting in a sway to the opposite side. The GVS stimulus was delivered with 3mA, the strength of the GNS stimulus was adjusted based upon the participants' individual pain thresholds between 2.5 mA and 4.5 mA (mean stimulation strength across participants and sessions was 4mA). The stimulation strength here was adjusted by stepwise increase of the stimulation according to a pain rating or feedback from participants. The rest period between simulations was variable and lasted between 9.1 and 16.1 seconds.

3.2.4 MR acquisition

Data was collected with a 3 Tesla Siemens Magnetom Skyra scanner using a 64-channel head/neck coil. A T1 structural image was acquired using a MPRAGE Grappa sequence (TR=2060 ms, TE=2.17 ms, FA= 12°, voxel size: 0.8 mm isotropic, 256 slices). The rs-fMRI and stimulation conditions were acquired using a GE-EPI sequence (TR= 700ms, TE=33ms, FA=45°, multi-band factor = 6 with interleaved multi-band slice package order, voxel size = 2.5 mm isotropic, 54 slices, prescan normalised)

3.2.5 Preprocessing

After data quality control assessment via MRIQC (Oscar Esteban et al., 2017) to detect banding artefacts from multi-band imaging and excessive head movements, the functional imaging preprocessing differed for the two types of analyses performed.

3.2.5.1 Task-activation (GLM) preprocessing

Preprocessing for task-activation was performed predominantly in SPM12 (7487). Functional images were field-map corrected for distortions, realigned to the first image of

each session and normalised to MNI-space with DARTEL and geodesic shooting including minimal smoothing (4mm). The first 13 images (10 seconds) of each session were removed to account for T1-equilibration effects that go beyond the initial dummy scans removed by Siemens for fast fMRI protocols.

3.2.5.2 Functional connectivity preprocessing

Preprocessing for functional connectivity analysis was performed using fMRIPprep 1.2.5 (O. Esteban et al., 2019), based on Nipype 1.1.6 (Gorgolewski et al., 2011). T1 images were bias field corrected and skull stripped. Spatial normalisation was performed to the ICBM 152 Nonlinear Asymmetrical template version 2009c (Fonov, Evans, McKinstry, Almli, & Collins, 2009) using nonlinear registration (see specifics in the appendix) and brain tissue was segmented into cerebrospinal fluid, white matter and grey matter. BOLD images were registered to the normalised T1 image . Head motions parameters were estimated with six rotation and translation parameters. No slice timing correction was performed. BOLD times-series were resampled, corrected for head-motion and susceptibility distortions, and normalised to MNI152NLin2009cAsym space. Framewise displacement (FD) and DVARS were calculated and three region-wise global signals were extracted within the CSF, the WM, and the whole-brain masks. For detailed methods, see Appendix.

Fmriprep and MRIQC summary outputs were also used for quality control. Because functional connectivity data are particularly susceptible for motion, we used a strict inclusion criterion of a mean framewise displacement of FD > 0.2 as an output in MRQC in any run performed, or BOLD signal extinction in cortical brain areas after fmriprep preprocessing. In the GVS group, five participants were excluded according to these criteria. In the GNS group, one participant was excluded. For the within-group comparison, this resulted in a dataset of fifteen participants who participated in both experiments.

For further signal extraction and correction, CONN 18.b was used (Whitfield-Gabrieli & Nieto-Castanon, 2012). Extraction was performed separately for the GVS and GNS data, however the same parameters were used. The reoriented and normalised functional data were used for signal extraction from 100 ROIs (7 Network parcellation), as defined by Schaefer et al. (2017). Data were despiked, detrended and filtered with a band-pass filter of 0.008-1 Hz to obtain a signal in the standard frequency range used for resting-state analysis. After filtering, regression was performed. For the stimulation sessions, we used a finite impulse response regressor to control for the influence of the mean event responses on functional connectivity values, as suggested by Cole et al. (2019). Further regressors

(for all sessions) included motion (six dimensions), CSF and WM signal as determined by fmriprep (raw signal as well as first-order derivative). High motion frames were also accounted for by creating a scrubbing regressor, which included all frames (including the directly neighbouring frames) with a framewise displacement above 0.9 mm or BOLD signal changes above five standard deviations. Pearson correlation was calculated for the extracted and denoised signals and adjacency matrices were created for each participant and each condition. This means that each participant contributed to the analysis with five adjacency matrices in total: two from the GVS experiments (resting-state and GVS stimulation) and three from the GNS experiment (resting state, GNS stimulation left and GNS stimulation right). All further analysis steps were based on these correlation matrices.

3.2.6 Analysis

We evaluated the mean activation from both the left and the right GNS experiments so that the activity was not lateralized – for readability, this averaged condition will be referred to as mGNS.

3.2.6.1 General Linear Model (GLM) Analysis

To determine the task effects of GVS and GNS stimulation, SPM12 Version 7487 (https://www.fil.ion.ucl.ac.uk/spm/) and the SPM toolbox TFCE (r201 from 2020-04-21) in Matlab R2018a (9.4.0.949201 Update 6, MathWorks Inc., Natick, Massachusetts) was used to perform the GLM analysis. TFCE was used because it allows greater sensitivity compared to cluster-based thresholding whilst robustly controlling for false positives (S. M. Smith & Nichols, 2009). On the first level, smoothed and normalised data from the stimulation conditions were included. Six motion parameters were included as regressors. Three conditions were modelled: sinus, ramp exciting the left side and ramps exciting the left side. Sinus stimulations were modelled as blocks with a duration of 9.5 TRs, ramps with a duration of 7 TRs. Although both stimulation patterns were modelled, the ramp stimulation led to more consistent activity patterns, so we used the ramp stimulation for the group-level analyses. To analyse differences in activations during ramp stimulations in general, we defined the contrast to including the main effects for ramps left and right.
In the group analyses a one-way Analysis of Variance (ANOVA) was used for the within-participant group-level design (n=15). The contrast images for the ramp stimuli of 1) the GVS, 2) the GNS right and 3) the GNS left conditions were included in the analysis. For the between participant design, a t-test was performed between the averaged contrast images for the GNS conditions (mGNS). In both designs, the contrasts GVS > mGNS and mGNS > GVS were statistically tested. Furthermore, we conducted a conjunction analysis to test for areas significantly activated by both mGSN and GVS. Statistical significance was

determined using TFCE, with the default parameters after 10000 permutations using a threshold of $p<0.05$ corrected for multiple comparisons via false discovery rate (FDR). Regions were determined using the Juelich Histology Atlas, cerebellar atlases or the Harvard-Oxford Cortical Structure Atlas (if others did not show any result), as implemented in FSLeyes (McCarthy, 2020). Visualisations were also made in FSLeyes using the MNI152 template with an isotropic resolution of 1mm.

3.2.6.2 Functional network analysis

We determined general whole brain network changes associated with vestibular stimulation using a within-participant design. For this, we made use of the stimulation sessions (GVS and GNS) that were acquired in each of the experiments as well as the resting-state sessions from the two different experiments. By comparing the resting-state sessions from the different experiments (but from the same participant) we wanted to determine effects merely related to the different experimental sessions. In other words, considering that resting-state sessions were from the same participants, no changes in network architecture were expected there.

We performed two types of functional network analyses. The first analysis was performed using network-based statistics (NBS), which focuses on differences in individual connections within the network. The second analysis was focused on differences in modularity of the network, i.e. whether functionally related regions (i.e. groups of nodes) maintain or change their affiliation during different conditions.

Changes in network connectivity: we first wanted to test whether connectivity changed at the level of graph connections. For this, the NBS toolbox by Zalesky, Fornito, and Bullmore (2010) was used to determine changes at the level of graph connections. In NBS, statistical tests are performed at every connection – only connections surpassing a primary threshold are further used to identify topological clusters. Considering the arbitrary nature of selecting the primary threshold, we used a range of primary thresholds (from 2-3.5 in steps of 0.3). For each component a FWER-corrected p value is determined with permutation testing at 10 000 permutations using the method of Freedman and Lane (1983). We only considered a component to be significant, if the p-value was below 0.1 consistently across all primary thresholds tested. Both component extent and component intensity were investigated (weak effects that include many connections tend to become significant with component extent, whereas testing for component intensity is better for detecting strong, focal connections).

Changes in network modularity: we wanted to determine how nodes differ in terms of their functional network participation during the GVS and the GNS sessions, i.e. whether nodes interacted with the same nodes throughout the conditions or whether they changed in terms of their interactions. For this we conducted a consensus modularity analysis as described in Castrillon et al. (2020); & Dwyer et al. (2014) using custom made Matlab and R scripts (4.0.2 within RStudio 1.3.1056). The analysis was only marginally modified from Castrillon et al. (2020). For each participant in each of the four conditions, classification was performed using the Louvain algorithm with a gamma of 1.3 (i.e. larger than the default value of 1 to detect smaller modules) and no pre-defined module affiliation. The parameter for consensus modularity analysis was left at tau = 0.4 (Castrillon et al., 2020; Lancichinetti & Fortunato, 2012). The result of this analysis was the classification consistency (z) and diversity (h) for each node in each of the four conditions (i.e. both resting-state sessions and both stimulation sessions (GVS and GNS). Classification consistency was based on the within-module degree z-score (a within-module version of degree centrality (Rubinov & Sporns, 2010)), classification diversity was based on participation coefficient, a measure of diversity of intermodular connections of individual nodes. Functions from the Brain Connectivity Toolbox (Bullmore & Sporns, 2009; Rubinov & Sporns, 2010) were used to calculate these graph measures. To determine significant differences in classification consistency and diversity between the four conditions, Kruskal-Wallis tests were performed.

3.3 Results

3.3.1 Behavioural results

The median pain rating given by the participants during the GNS condition was 4 (IQR = 2.25). During the GVS condition; participants expectedly reported egomotion. However, also during GNS eleven out of fifteen participants reported light to modest swinging motion during the sinusoidal stimulation. We therefore decided to focus our analysis on the ramp stimulation only to avoid potential vestibular side effects of the unilateral mastoid stimulation during GNS.

3.3.2 Activity changes related to vestibular stimulation

The main results for task-based activity come from the within-subject GLM analysis and are therefore presented first. The larger between-subject cohort is then presented as a confirmatory analysis. Significant positive blood oxygen level-dependent (BOLD) signal activity was found during GVS compared to mGNS (Figure 3.1, Table 3.1) and in the conjunction analysis (positive activity during GVS & mGNS) (Figure 3.2, Table 3.2). The mGNS conditions did not show any significantly active voxels compared to GVS.

GVS > mGNS: During GVS, the cerebellum showed unique activation patterns in the nodulus (Vermis X). In the primary somatosensory cortex, bilateral BA3b was selectively more active during GVS. Portions of the left secondary somatosensory cortex also showed an increased signal, covering OP1 and OP2, the latter considered as the putative human vestibular cortex. In the parietal lobe, bilateral inferior parietal lobule displayed significantly higher signal than during GNS with peak activation in subregion PF. Left posterior supramarginal gyrus showed significantly stronger signal in the GVS experiment only. A large cluster covering big parts of the occipital cortex was found to have a significant stronger BOLD response during GVS stimulation. This cluster extends over V5 into temporal areas which have been previously suggested to contain motion area MT and MST. In the frontal lobe, bilateral cingulate sulcus visual (CSV) areas (premotor cortex areas BA6) were activated only in the GVS sessions. This region has been shown to be selectively process either visual or vestibular cues of self-motion and may important in guiding locomotion (Caspers et al., 2012). In the inferior frontal gyrus, bilateral Brodmann areas (BA) 44 (pars opercularis) and 45 (pars triangularis) were active in both experiments, with a significant stronger activation during GVS in the left hemisphere. Furthermore, right primary motor cortex BA4p was significantly more active in the GVS session.

Conjunction: GVS and mGNS both activated a bigger extent of the lateral cerebellum, only small portions of the central cerebellum (Vermix IX) showed significant signal increase in both sessions. The right putamen (part of the basal ganglia and involved in motion control) had an increased signal in both sessions. In the primary somatosensory cortex, right BA2 was jointly activated in both GVS and GNS. In the secondary somatosensory cortex, the left parietal operculum OP4 and right parietal operculum OP3 (approximately corresponding to BA43) was activated in both tasks, areas corresponding to the somatosensensory field around ears. Joint activations were detected in the parietal lobules. Left anterior intra-parietal sulcus (subregions hlp1 and hlp3) are notable since they also covered the presumed vestibular region VIP (ventral intraparietal area). Large portions of the right superior parietal lobule and also of the bilateral inferior parietal lobules responded in both experiments, with peaks identified in subregions PFt and PFop, and extending over region PFcm. Increased signal in the bilateral insular cortex regions were only found in the conjunction analysis of GVS and GNS. Regions consisted mostly of dysgranular areas in the midinsular/posterior insular cortex (Kurth et al., 2009), which are thought to process and mediate multisensory information (Benarroch, 2019, Uddin (2015)).

Between-subject analysis: the results were largely confirmed by the larger between-participant analysis. Overall, TFCE clusters were more extensive in the between participant analysis for both comparisons, GVS > GNS (see Supplementary Table 1 for all significant clusters) and the conjunction analysis (see Supplementary Table 2 for all significant clusters). The group analysis did not reveal any meaningful significant clusters during mGNS, when compared to GVS.

The additional clusters of activity found in the between-participant analysis for vestibular stimulation were in the left premotor cortex, with the cluster extending to the inferior frontal gyrus (BA44 and 45) and primary somatosensory area BA3. The left cerebellar cluster was rather located in area VIIIb, and not in Crus I. In the conjunction analysis, portions of the premotor cortex (BA6) were additionally activated, but these were located closer to the cingulate gyrus than in the GVS condition (and not on the lateral portions of the cortex). Small additional clusters in the occipital cortex were found in the between-subject design.

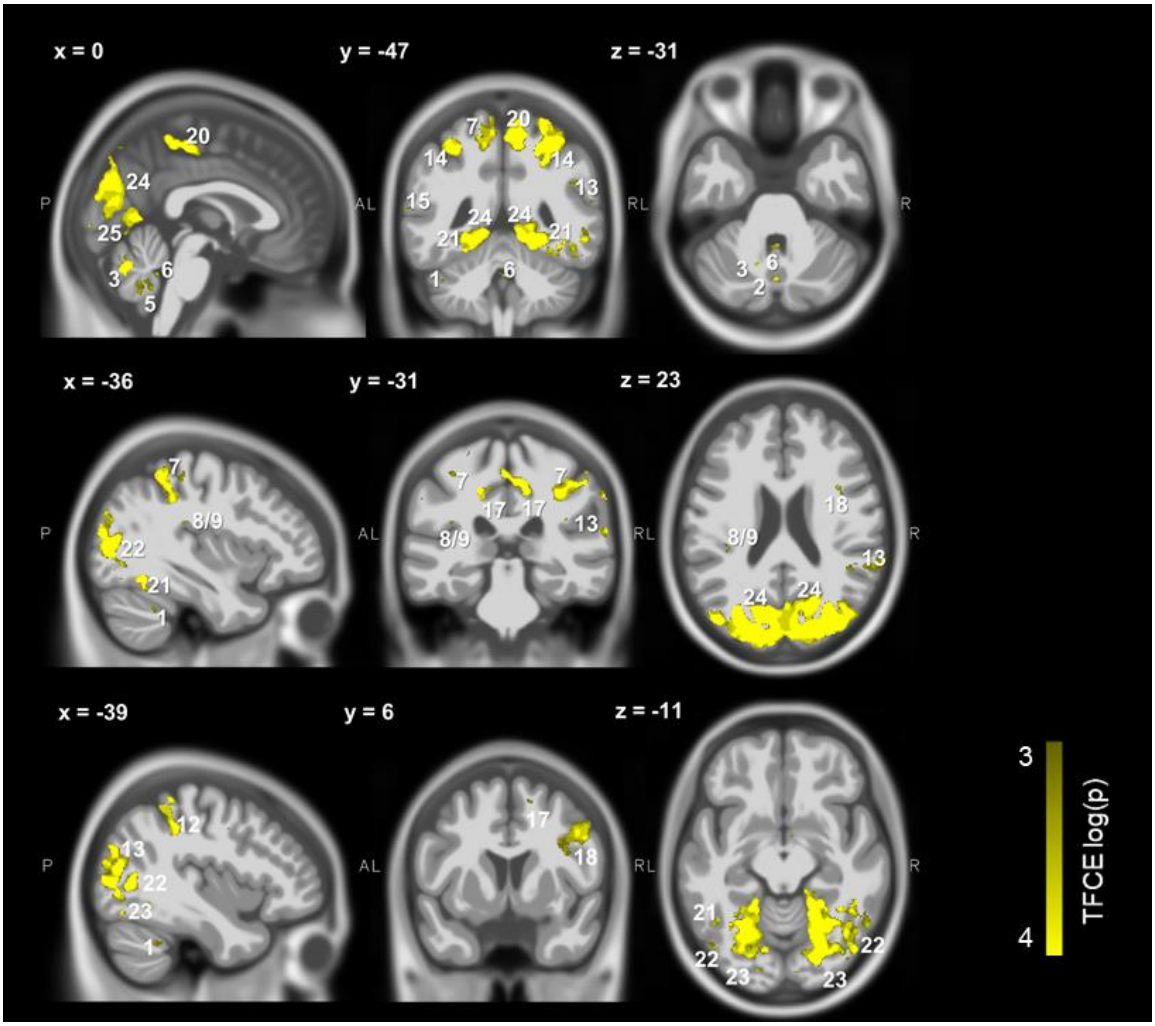

Figure 3.1 Regions with a significantly stronger response to vestibular stimulation (GVS) than to nociceptive stimulation (GNS).
Three slices are depicted in all planes, centered over the cerebellum (top row), the somatosensory cortex (middle row) and insular cortex and ventral visual areas (bottom row). Regions were determined using TFCE with an uncorrected threshold of $p<0.001$. 1:Crus I; 2:Crus II; 3:Vermis VI; 4:Vermis VIIb; 5:Vermis IX; 6:Vermis X; 7:Primary somatosensory cortex Ba3a; 8:Secondary somatosensory cortex OP1; 9:OP2 10:OP3 11:OP4; 12:Anterior intra-parietal sulcus / VIP; 13:Inferior parietal lobule; 14:Superior parietal lobule; 15:Supramarginal gyrus; 16:Insula; 17:Premotor cortex BA6 / CSV; 18:Broca's Area BA44; 19:Broca's area BA45, 20:Motor cortex Ba4a, 21:Temporal occipital fusiform gyrus; 22:MST/ V5, 23:V4; 24:V2; 25:V1

Table 3.1 Peak activations for contrast GVS > mGNS using TFCE. Only clusters in grey matter with a minimum of 10 voxels reported.

Brain region	Cluster size	TFCE	Z	Coordinates			Name of region
				x	y	z	
Cerebellum	110	2216.22	3.16	-39	-52	-35	L Crus I
	39	1758.27	3.35	-1	-49	-31	Vermis X
	317	2632.08	3.24	1	-53	-39	Vermis IX
Primary Somatosensory cortex	941	2827.95	3.19	-23	-36	68	L Primary somatosens. cortex BA3b
		2739.38	3.54	-26	-36	59	L Primary somatosens. cortex BA3b
		2679.88	3.19	-35	-34	53	L Primary somatosens. cortex BA3b
	129	2637.74	3.12	42	-11	48	R Primary somatosens. cortex BA3b
Secondary Somatosensory cortex	22	1584.96	3.16	-36	-31	23	L Secondary somatosens. cortex, Parietal operculum OP1/OP 2
Parietal lobe	204	1643.44	3.12	-62	-45	12	L Supramarginal gyrus, (posterior)
		1555.04	3.16	-51	-43	11	L Supramarginal gyrus (posterior)
	47	2561.32	3.12	56	-39	40	R Inferior parietal lobule PF
		1767.52	3.16	63	-36	43	R Inferior parietal lobule PF
	24	2545.72	3.12	59	-30	32	R Inferior parietal lobule PF
Frontal lobe	2385	3446.58	3.54	41	3	35	R Broca's area ba44
		2888.17	3.54	48	2	46	R Premotor cortex BA6
		2738.81	3.54	36	11	25	R Broca's BA44
	738	3053.85	3.29	25	-9	51	R Premotor cortex BA6
		2792.57	3.29	31	-4	44	R Premotor cortex BA6
		2541.2	3.24	23	0	50	R Premotor cortex BA6
	56	2479.55	3.29	34	-16	40	R Primary motor cortex BA4p
	30	2573.19	3.12	29	-32	64	R Primary motor cortex BA4p
	26	2021.33	3.16	15	4	58	R Premotor cortex BA6
Occipital cortex	140236	12045.23	3.72	-14	-73	26	L Superior lobule 7A
		11409.36	3.72	21	-75	37	R Occipital cortex
		11213.52	3.72	11	-84	27	R Visual cortex v2
	77	2164.35	3.19	-12	-87	-8	L Visual cortex V3V
	17	2342.32	3.35	9	-96	16	R Visual cortex V2
	16	2340.44	3.35	-41	-66	-15	L Occipital fusiform gyrus
	35	2396.4	3.16	42	-40	-22	R Occipital fusiform cortex

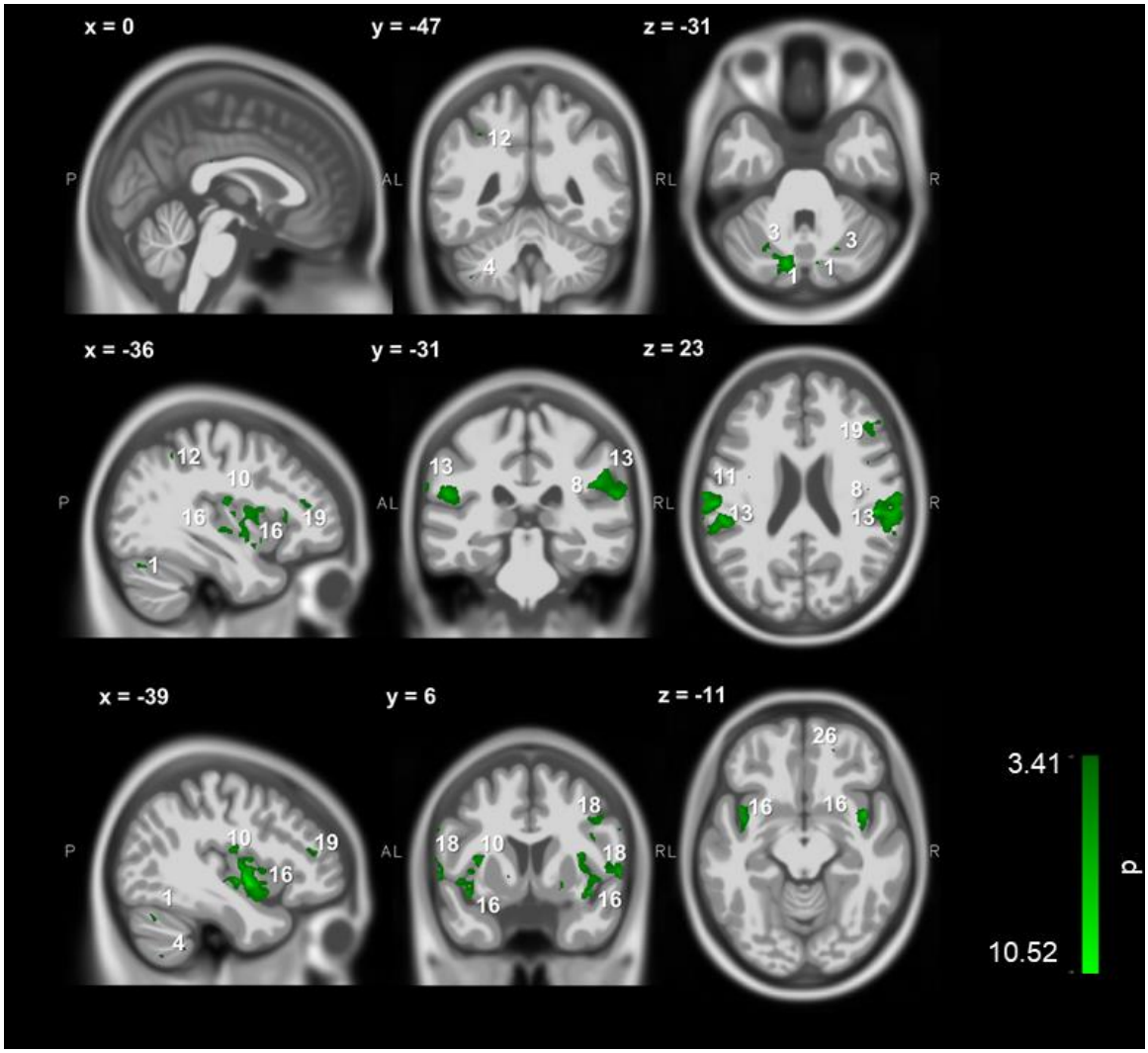

Figure 3.2 Regions responding to both vestibular stimulation (GVS) and nociceptive stimulation (GNS) (within-subject design).
Insular and frontal regions are active during both stimulation conditions. Three slices are depicted in all planes, centered over the cerebellum (top row), the somatosensory cortex (middle row) and insular cortex and ventral visual areas (bottom row) (uncorrected threshold $p<0.001$). 1:Crus I; 2:Crus II; 3:Vermis VI; 4:Vermis VIIb; 5:Vermis IX; 6:Vermis X; 7:Primary somatosensory cortex Ba3a; 8:Secondary somatosensory cortex OP1; 9:OP2 10:OP3 11:OP4; 12:Anterior intra-parietal sulcus / VIP; 13:Inferior parietal lobule; 14:Superior parietal lobule; 15:Supramarginal gyrus; 16:Insula; 17:Premotor cortex BA6/CSV; 18:Broca's Area BA44; 19:Broca's area BA45; 26:frontal pole

Table 3.2 Peak activations for the conjuction analysis GVS & mGNS (p<0.001 uncorrected). Only clusters in grey matter with a minimum of 10 voxels reported.

Brain region	Cluster size	Z	Coordinates			Name of region
			x	y	z	
Cerebellum	6313	5.91	-12	-74	-29	L Crus I
		5.47	-22	-73	-45	L Crus I
		5.32	-13	-73	-50	L Crus I
	84	3.58	-35	-73	-25	L Crus I
		3.25	-39	-66	-29	L Crus I
	11	3.25	-39	-62	-53	L Vermis VIIb
	11	3.32	-38	-46	-48	L Vermis VIIb
	7	3.31	37	-70	-23	R Crus I
	11	3.18	9	-75	-31	R Crus II
	13	3.38	5	-79	-42	R Crus II
	138	3.7	21	-65	-28	R Vermis VI
		3.6	31	-64	-24	R Vermis VI
	1940	4.74	8	-74	-46	R Vermis VIIb
		4.45	23	-66	-47	R Vermis VIIIb
		4.18	18	-74	-50	R Vermis VIIb
	15	3.62	-3	-53	-34	L Vermis IX
Striatum	70	3.84	17	9	0	R Putamen
	26	3.59	22	5	-7	R Putamen
Primary Somatosensory cortices	152	3.8	45	-38	56	R Primary Somatosens. cortex BA2
Secondary Somatosensory Cortices	15263	6.64	42	-2	-4	R Secondary somatosens. cortex / Parietal operculum OP3
		6.06	53	-23	19	R Secondary somatosens. cortex / parietal operculum OP1
		5.79	61	-18	26	R Inferior parietal lobule PFop/PFt
Parietal lobe regions	76	3.35	-36	-51	47	L Anterior intra-parietal sulcus hIP1
	10	3.27	-29	-59	46	L Anterior intra-parietal sulcus hIp3
	36	3.52	-49	-22	36	L Inferior parietal lobule PFt
	12	3.4	58	-25	44	R Inferior parietal lobule PFt
	64	3.6	7	-72	48	R Superior parietal lobule 7M
Insular cortex	12068	6.24	-39	-4	-5	L Insula (Id1)
		5.73	-59	-21	23	L Inferior parietal lobule PFop
		5.67	-56	-10	10	L Secondary somatosens. ctx. / Parietal operculum OP4
	15	3.58	38	-10	-5	R Insula Id1
Temporal cortex	11	3.46	-46	-36	-19	L Inferior temporal gyrus (posterior)
Frontal lobe	239	4.3	-32	24	7	L Broca's area BA45
	61	3.96	-60	8	29	L Premotor cortex BA6
	161	3.83	-53	9	16	L Broca's Area BA44
	141	3.77	-36	35	17	L Broca's Area BA45
	74	3.67	-44	45	15	L Broca's Area BA45
	1152	4.88	43	42	7	R Frontal Pole
	59	4.2	60	8	31	R Broca's area BA44
	413	4.13	45	7	36	R Broca's area BA44
		3.47	41	7	27	R Broca's area BA44
	284	4.09	43	31	23	R Broca's area BA45
	29	3.37	38	30	17	R Broca's Area BA45
	26	3.36	54	11	36	R Broca's Area BA44
	10	3.27	4	25	39	R Paracingulate gyrus
Occipital lobe	20	3.46	15	-78	-20	R V1 / BA17

3.3.3 Functional network changes related to vestibular stimulation

We analysed functional connectivity differences within participants to determine a set of nodes (=*component*) with changes in functional connectivity associated with vestibular stimulation. For this, we made use of the stimulation sessions (GVS and GNS) that were acquired in each of the experiments as well as the resting-state sessions from the two different experiments. By comparing the resting-state sessions from the different experiments (but from the same participant) we could disentangle effects merely related to the different session.

3.3.3.1 Changes in network connectivity

To determine the connections which are associated with the change in experimental condition, the networks during GVS, GNS and rest were tested with network-based statistics. Seven primary thresholds were used for the NBS analysis. We only considered the contrast to be significant if the overall probability value was consistently below 0.1 across all thresholds tested. We tested for differences between the two stimulation datasets, the two rest datasets, and each stimulation dataset with its respective resting-state dataset. In each case, both extent and intensity were examined (see 3.2 Methods). A summary of what comparisons are significant can be found in Table 3.3.

In the comparison between GVS and GNS stimulation, we consistently identified a significant component associated with experimental condition. Specifically, we found that vestibular stimulation was associated with a significant decrease of connectivity in a number of nodes located in regions which were found to be associated with GVS in the task-based analysis (Figure 3.3). Nodes were located both in regions uniquely activated by GVS (also including OP2 and CSV) as well as regions conjointly activated by both GVS and GNS. No other comparison resulted in significantly different components when testing for significant extent. The results were confirmed when testing for intensity instead of extent.

Importantly, there were no differences found between the two rs-fMRI sessions, confirming that the two imaging experiments did not change connections of the network. Session effects were thus ruled out. When testing for significant intensity, additional significant differences were found between GNS and its corresponding resting-state session. As we were not interested in the GNS condition per se, we did not follow up on these differences. Notably, no differences were found between GVS and rest. Overall, this suggests, that changes in individual connections between nodes were driven by nociception and that vestibular stimulation had only a small effect on brain network architecture.

Table 3.3 Overview of significant results from NBS analysis.

Comparison	Significant contrast (extent)	Significant contrast (intensity)
stim-GVS vs. stim-mGNS	GVS<mGNS	GVS < mGNS
rs-GVS vs. rs-GNS	-	-
stim-GVS vs. rs-GVS	-	-
stim-GNS vs. rs-GNS	-	stim-GNS > rs-GNS rs-GNS > stim-GNS

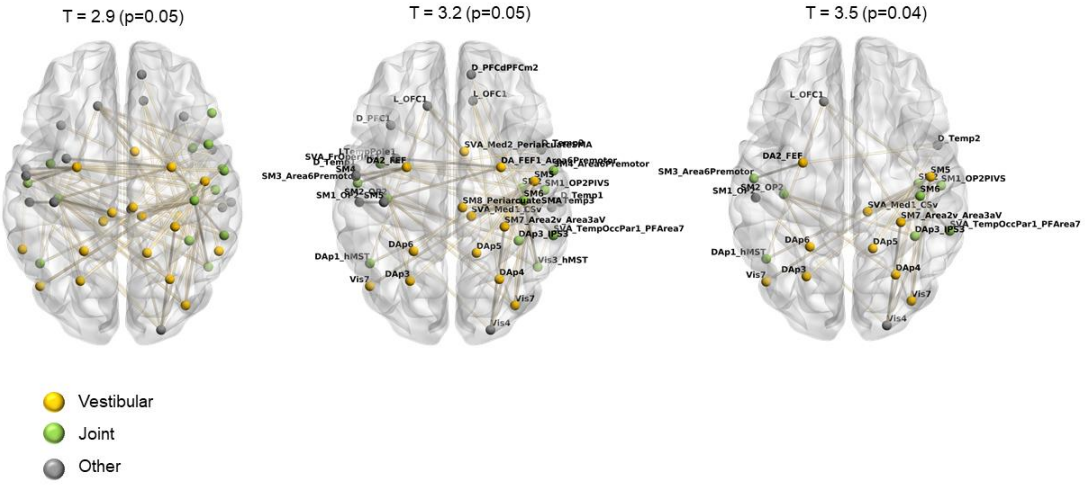

Figure 3.3 Significant component for three incremental primary thresholds of the contrast GNS > GVS (left: T=2.9; middle: T=3.2; right: T.3.5).
Nodes were coloured according to the findings of the task-based analysis, i.e. yellow if nodes within regions which were uniquely activated during GVS and are thus associated with vestibular sensation, green if nodes were located within regions jointly activated by GVS and GSN and grey if they were located in other regions. Labels (only presented in middle and right threshold for readability) are shortened after Schaefer et al. (2017), but names of vestibular regions have been added when appropriate. D=Default, Vis = Visual, DA=Dorsal Attentional, L=Limbic, SM=Somatomotor, SVA=Salience Ventral Attention, Cont = Control. analysis.

3.3.3.2 Changes in network modularity

The NBS analysis showed that sets of connections are affected by the stimulation condition, with regions associated with vestibular processing being significantly less connected during GVS, when compared to GNS. To get a better understanding about the general network changes involved during the stimulation, we performed a modularity analysis (see Methods). Both classification consistency and classification diversity were calculated for each node in each condition. Classification consistency measures the extent of functional specialisation – a high value means that the node is consistently classified as belonging to the same module. Conversely, classification diversity measures the proportion of nodes being classified into different modules and hence indicates that the node is well integrated into the network functionally. Low classification diversity means

that a node is usually classified as belonging to the same module. Connectivity of such nodes is less dispersed across modules, while high classification diversity values suggest high dispersion of connectivity (Dwyer et al., 2014). Across all conditions, a significant difference was only found in classification diversity (Kruskal-Wallis chi-squared = 29.172, df = 3, p-value < .001) but not in classification consistency (Kruskal-Wallis chi-squared = .060, df =3, p-value=.996) (see Figure 3.4A). This suggests that nodes within the brain were classified to variable modules across participants.

To determine the specific differences, Mann-Whitney-Wilcoxon tests were performed between all possible combinations using a Bonferroni correction ($\alpha = 0.5 / 6$, adjusted p-values are reported in the following). Classification diversity was significantly lower during GNS stimulation, when compared to the GVS stimulation (U=6429, p=.003). Similarly, while classification diversity was significantly lower during GNS stimulation (median = 0.463), compared to the resting-state condition in the same scanning session (median = 0.661; U = 6570, p=0.001), no difference was found when comparing the GVS stimulation (median = 0.637) to its corresponding resting-state condition (median=0.606; U=5830 , p=0.256). No session effect was found when comparing the two resting-state datasets from the two experiments (U = 5608, p = 0.828) (see Figure 3.4A). These results suggest that cortical nodes become more selective in their interaction during nociceptive stimulation, whilst no reorganisation occurs during vestibular stimulation. To determine the contribution of different nodes to the differences in the stimulation conditions, we conducted two more post-hoc analyses.

First we split the nodes into three groups, depending on whether they were located in regions that were activated uniquely by vestibular stimulation ("vestibular nodes"), jointly by vestibular and nociceptive stimulation ("joint nodes") and all remaining nodes ("other nodes"). Indeed, both vestibular nodes (W=356, p=.020) and joint nodes (W=231, p=.010 had a higher classification diversity in the GVS condition. The remaining nodes did not differ in terms of their classification diversity (W=478, p=.077) after Bonferroni correction ($\alpha=0.5 / 3$) (see Figure 3.4B). Nodes located in regions associated with the stimulation conditions thus contributed to the changes in classification diversity more than the remaining nodes.

We also used a different categorisation and for this we split the nodes according to their membership of the significant NBS component found in the previous analysis. We thus tested whether the significantly decreased connections of these nodes during GVS (as found using the NBS analysis) is related with an increased classification diversity. For this,

38 nodes from the significant network found in the NBS analysis (using a threshold of T = 3.2, i.e. the nodes seen in the middle panel of Figure 3.3) were included in the 'NBS nodes' groups, the remaining 62 nodes were included in the 'Other' group. As apparent in Figure 3.4C, classification diversity significantly differed between the two stimulation periods but in both NBS nodes (W=463, p=.014) as well as in all remaining nodes (W=1447, p=.035) (adjusted p values after Bonferroni correction with α=0.5/2). In this analysis, nodes thus contributed to the main finding, regardless whether they were part of the NBS component or not.

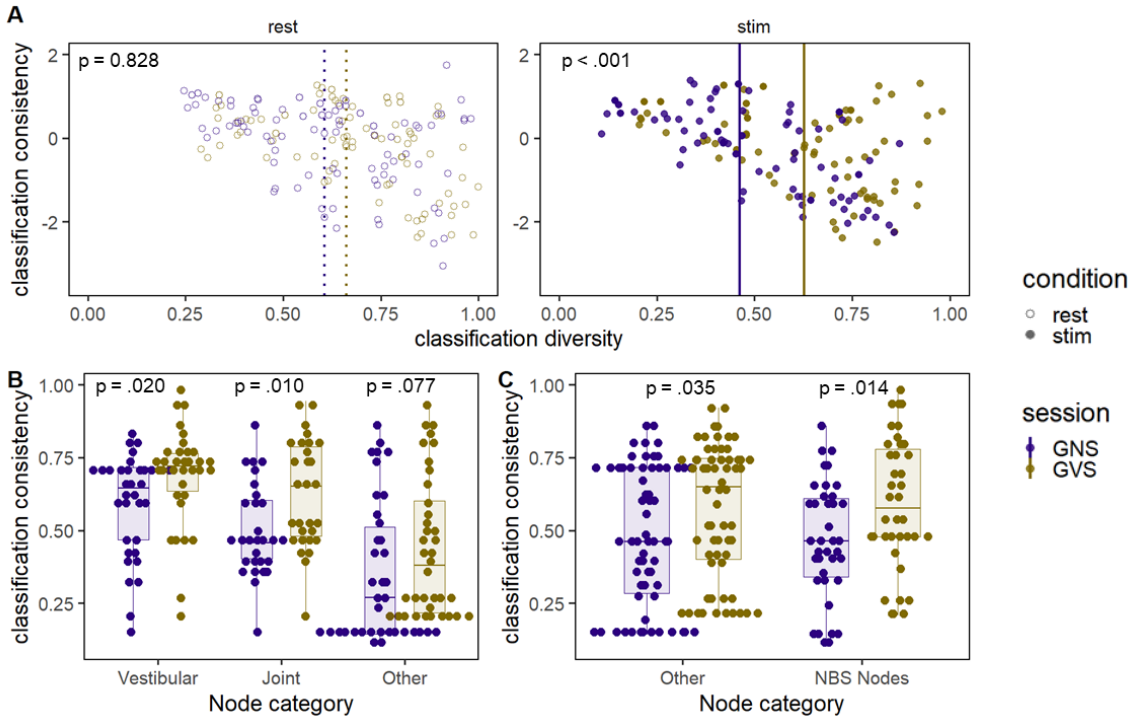

Figure 3.4 Results from modularity analysis
A) Classification diversity and classification consistency for all sessions and conditions B) classification consistency of node categories derived from task-based analysis (Vestibular = nodes in regions significantly stronger activated by GVS, Joint = nodes in regions conjointly active during GVS and GNS, Other = all remaining nodes) C) classification consistency of node categories derived from NBS analysis (NBS Nodes = 38 nodes from the significant network found in the NBS analysis (using a threshold of T = 3.2, Other = remaining 62 nodes)

3.4 Discussion

In the present study, we aimed to characterise vestibular processing in terms of task activity and functional network architecture. Importantly, we wanted to disentangle the processing of vestibular from other somatosensory information. For this, participants underwent two experiments, differing only in the type of stimulation delivered: vestibular (GVS) or nociceptive (GNS) stimulation. The underlying assumption for the comparison of these experiments is that our customised GVS approach using local anaesthesia elicits mostly vestibular and little other somatosensory sensations, whereas GNS induces salient nociceptive arousal in addition to local somatosensory sensations. Comparing GVS directly with GNS should thus reveal uniquely vestibular processes and/or uniquely (salient) nociceptive processing. Joint analysis aimed to reveal the common somatosensory trunk of the two conditions.

3.4.1 Task-based analysis

In the task-based analysis we confirm the existence of distinct regions in vestibular and somatosensory processing. Previously described vestibular processing regions were also found with our experimental design. The, parietal operculum OP2 was more active during GVS than GNS, thus confirming it's central role in vestibular processing as proposed by zu Eulenburg et al. (2012). The cingulate sulcus visual (CSv) area and portions of MST were more strongly active during GVS. Bilateral inferior parietal lobules PF was also found to be involved uniquely during GVS, which may correspond to macaque area 7:

Extensive visual cortex activation was found during the GVS experiment, which was most likely due to the task demands. Participants were asked to fixate a fixation cross, which is not typically done in GVS experiments. Indeed, in paradigms using GVS where participants had their eyes closed, BOLD signal decreases in visual cortex were observed (Bense, Stephan, Yousry, Brandt, & Dieterich, 2001). Vestibular stimulation causes nystagmus that are then supressed during fixation (Curthoys & MacDougall, 2012; Helmchen, Rother, Spliethoff, & Sprenger, 2019). GNS, on the other hand, does not lead to any reflexive eye movements. We therefore believe that the enhanced activity in the visual cortex during GVS reflects the suppression of a torsional nystagmus. Another explanation for activation of visual cortex is the recent finding, that both active and passive head movements in light increase V1 activity in rodents (Bouvier, Senzai, & Scanziani, 2020; Guitchounts, Masís, Wolff, & Cox, 2020). This response persisted even after abolishing eye movements (Bouvier et al., 2020).

Beside cortical activation, parts of the cerebellum were more active during GVS than GNS. Cerebellum receives input from the vestibular nerve and from vestibular nuclei (Goldberg, Wilson, Angelaki, Cullen, & Fukushima, 2012). Notably, the nodulus (i.e. vermis X), whose purkinje cells receive direct input from vestibular afferents (Cullen, 2019; Goldberg et al., 2012; Laurens, Meng, & Angelaki, 2013; Yakusheva, Blazquez, & Angelaki, 2010), was also more active during vestibular stimulation. In contrast to the nodulus, small clusters of the vermis IX were jointly active in both conditions, suggesting that general somatosensation is also processed there.

Although the ventral intraparietal region (VIP) receives vestibular information in non-human primates, we did not see any additional activity in the VIP for vestibular stimulation. Instead, this area was jointly active for both stimulation types, suggesting a role in somatosensory processing. The VIP was previously found to be involved in representing body schema and surrounding space on a multisensory level (Bremmer et al., 2013), which would also explain our results, encoding a type of spatial reference frame function. Thus, our finding also corresponds to the notion that VIP may me more important for general bodily self-consciousness than PIVC and MST, as suggested by Blanke (2012). The parietal operculum OP3 and OP4 (BA43/40) were also jointly active during both stimulation modalities and are likely related to the common somatosensory experience of both stimulations. OP4 is related to attention, stimulus discrimination and sensory-motor integration and OP3 is thought to encode the somatosensory representation of ear (Job et al., 2016; Job, Paucod, O'Beirne, & Delon-Martin, 2011). Large portions of the bilateral inferior frontal gyrus were also found conjointly active. A various set functions have been ascribed to this region ranging from action to cognition related processing and only recently a functional organisation along the posterior-to anterior as well as the dorsal-to ventral axis of the right inferior frontal gyrus was described (Hartwigsen, Neef, Camilleri, Margulies, & Eickhoff, 2019).

Whilst not the initial focus of the study, it is interesting that no unique areas were activated during nociceptive stimulation in the within-participant comparison. The posterior insula and parts of operculum were the only regions active in our study that have previously been found to result in pain upon cortical stimulation (Mazzola, Isnard, Peyron, & Mauguière, 2011). These regions were conjointly activated in both GVS and GNS. Taken together, whilst vestibular stimuli consistently activate dedicated brain regions, our nociceptive stimulation does not result in a specific brain response. It is possible that brain regions previously ascribed to the “pain-matrix” may rather encode processes related to somatosensation, salience or aspects of awareness.

3.4.2 Functional network analysis

Vestibular stimulation does not have a large impact on whole brain functional network connectivity. Despite the clear unique regional activation patterns associated with vestibular stimulation detected using a classic general linear model approach, the opposite was true when examining functional connectivity. We found that vestibular stimulation does not induce a change in cortical network architecture: no significant differences in individual connections was found and modularity remained unchanged, when compared to the resting state. Nociceptive stimulation on the other hand was associated with network changes, and when compared directly to vestibular stimulation, it was associated with increased connectivity of regions which are associated with somatosensory stimulation, as determined in the task-based analysis. This finding corresponds to the proposal by Klingner et al (2016), who suggested that the amount of vestibular information delivered to cortical areas is relatively low compared to other (sensory) information transmitted.

Overall, network organisation and hence synchronisation of the brain regions did not seem to be changed at all by vestibular stimulation. Considering that changes in awareness or arousal seem to be one main underlying factor for modulation of brain synchronisation (Lurie et al., 2019), this finding is remarkable considering that the stimulation induces a strong vestibular sensation and elicits a distinct brain activity pattern. It is particularly noteworthy, that even when comparing classification diversity and consistency of the resting-state condition with the stimulation condition, no differences were found. This stability of brain synchronisation during vestibular sensation possibly reflects that vestibular processing mostly occurs subconsciously and that synchronisation effects during vestibular stimulation may be more subtle compared to nociceptive stimulation.

3.4.3 Limitations and open questions

In the present study we focused on cortical activations and connectivity. In the future it would be interesting to perform a closer investigation of subcortical and cerebellar involvement during vestibular stimulation. Specifically, it would be interesting to investigate the task-related connectivity of different cerebellar regions, with a specific focus on the nodulus. Furthermore, it would be interesting to see whether individual differences influence results.

3.4.4 Conclusion

Overall, we differentiated regions involved in vestibular processing and compared the full brain network during states of vestibular stimulation and nociceptive stimulation. We found distinct activation patterns during vestibular stimulation, which matched with

previous reported areas. Surprisingly, we found that only nociceptive stimulation modulated the functional network, but that vestibular stimulation was seemingly not sufficient for cortical nodes to change their global network properties. These seemingly contradictory results may reflect the unique features of the vestibular system, namely that vestibular processing mostly occurs subconsciously As a next step, the contribution of subcortical regions should be analysed to determine whether the observed lack of network modulation is limited to cortical regions.

3.5 References

Bense, S., Stephan, T., Yousry, T. A., Brandt, T., & Dieterich, M. (2001). Multisensory Cortical Signal Increases and Decreases During Vestibular Galvanic Stimulation (fMRI). *Journal of Neurophysiology, 85*(2), 886-899. doi:10.1152/jn.2001.85.2.886

Blanke, O. (2012). Multisensory brain mechanisms of bodily self-consciousness. *Nature reviews neuroscience, 13*(8), 556-571.

Bouvier, G., Senzai, Y., & Scanziani, M. (2020). Head Movements Control the Activity of Primary Visual Cortex in a Luminance-Dependent Manner. *Neuron*. doi:https://doi.org/10.1016/j.neuron.2020.07.004

Bremmer, F., Schlack, A., Kaminiarz, A., & Hoffmann, K. (2013). Encoding of movement in near extrapersonal space in primate area VIP. *Frontiers in Behavioral Neuroscience, 7*(8). doi:10.3389/fnbeh.2013.00008

Bullmore, E., & Sporns, O. (2009). Complex brain networks: graph theoretical analysis of structural and functional systems. *Nat Rev Neurosci, 10*(3), 186-198. doi:10.1038/nrn2575

Caspers, S., Schleicher, A., Bacha-Trams, M., Palomero-Gallagher, N., Amunts, K., & Zilles, K. (2012). Organization of the Human Inferior Parietal Lobule Based on Receptor Architectonics. *Cerebral Cortex, 23*(3), 615-628. doi:10.1093/cercor/bhs048

Castrillon, G., Sollmann, N., Kurcyus, K., Razi, A., Krieg, S. M., & Riedl, V. (2020). The physiological effects of noninvasive brain stimulation fundamentally differ across the human cortex. *Sci Adv, 6*(5), eaay2739. doi:10.1126/sciadv.aay2739

Chen, A., DeAngelis, G. C., & Angelaki, D. E. (2010). Macaque parieto-insular vestibular cortex: responses to self-motion and optic flow. *Journal of Neuroscience, 30*(8), 3022-3042. Retrieved from https://www.ncbi.nlm.nih.gov/pmc/articles/PMC3108058/pdf/zns3022.pdf

Cole, M. W., Ito, T., Schultz, D., Mill, R., Chen, R., & Cocuzza, C. (2019). Task activations produce spurious but systematic inflation of task functional connectivity estimates. *Neuroimage, 189*, 1-18. doi:10.1016/j.neuroimage.2018.12.054

Cottereau, B. R., Smith, A. T., Rima, S., Fize, D., Héjja-Brichard, Y., Renaud, L., . . . Durand, J.-B. (2017). Processing of Egomotion-Consistent Optic Flow in the Rhesus Macaque Cortex. *Cerebral Cortex, 27*(1), 330-343. doi:10.1093/cercor/bhw412

Cullen, K. E. (2019). Vestibular processing during natural self-motion: implications for perception and action. *Nat Rev Neurosci, 20*(6), 346-363. doi:10.1038/s41583-019-0153-1

Cullen, K. E., & Taube, J. S. (2017). Our sense of direction: progress, controversies and challenges. *Nat Neurosci, 20*(11), 1465-1473. doi:10.1038/nn.4658

Curthoys, I., & MacDougall, H. (2012). What Galvanic Vestibular Stimulation Actually Activates. *Frontiers in Neurology, 3*(117). doi:10.3389/fneur.2012.00117

Dwyer, D. B., Harrison, B. J., Yucel, M., Whittle, S., Zalesky, A., Pantelis, C., . . . Fornito, A. (2014). Large-scale brain network dynamics supporting adolescent cognitive control. *J Neurosci, 34*(42), 14096-14107. doi:10.1523/JNEUROSCI.1634-14.2014

Esteban, O., Birman, D., Schaer, M., Koyejo, O. O., Poldrack, R. A., & Gorgolewski, K. J. (2017). MRIQC: Advancing the automatic prediction of image quality in MRI from unseen sites. *PLoS One, 12*(9), e0184661. doi:10.1371/journal.pone.0184661

Esteban, O., Markiewicz, C. J., Blair, R. W., Moodie, C. A., Isik, A. I., Erramuzpe, A., . . . Gorgolewski, K. J. (2019). fMRIPrep: a robust preprocessing pipeline for functional MRI. *Nat Methods, 16*(1), 111-116. doi:10.1038/s41592-018-0235-4

Fonov, V. S., Evans, A. C., McKinstry, R. C., Almli, C. R., & Collins, D. L. (2009). Unbiased nonlinear average age-appropriate brain templates from birth to adulthood. *Neuroimage, 47*, S102. doi:https://doi.org/10.1016/S1053-8119(09)70884-5

Freedman, D., & Lane, D. (1983). A nonstochastic interpretation of reported significance levels. *Journal of Business & Economic Statistics, 1*(4), 292-298.

Goldberg, J. M., Wilson, V. J., Angelaki, D. E., Cullen, K. E., & Fukushima, K. (2012). *The vestibular system: a sixth sense*: Oxford University Press.

Gonzalez-Castillo, J., & Bandettini, P. A. (2018). Task-based dynamic functional connectivity: Recent findings and open questions. *Neuroimage, 180*(Pt B), 526-533. doi:10.1016/j.neuroimage.2017.08.006

Gorgolewski, K., Burns, C., Madison, C., Clark, D., Halchenko, Y., Waskom, M., & Ghosh, S. (2011). Nipype: A Flexible, Lightweight and Extensible Neuroimaging Data Processing Framework in Python. *Frontiers in Neuroinformatics, 5*, 13. Retrieved from https://www.frontiersin.org/article/10.3389/fninf.2011.00013

Guitchounts, G., Masís, J., Wolff, S. B. E., & Cox, D. (2020). Encoding of 3D Head Orienting Movements in the Primary Visual Cortex. *Neuron*. doi:10.1016/j.neuron.2020.07.014

Guldin, W. O., & Grüsser, O. J. (1998). Is there a vestibular cortex? *Trends in Neurosciences, 21*(6), 254-259. doi:10.1016/S0166-2236(97)01211-3

Hartwigsen, G., Neef, N. E., Camilleri, J. A., Margulies, D. S., & Eickhoff, S. B. (2019). Functional Segregation of the Right Inferior Frontal Gyrus: Evidence From Coactivation-Based Parcellation. *Cereb Cortex, 29*(4), 1532-1546. doi:10.1093/cercor/bhy049

Helmchen, C., Rother, M., Spliethoff, P., & Sprenger, A. (2019). Increased brain responsivity to galvanic vestibular stimulation in bilateral vestibular failure. *NeuroImage. Clinical, 24*, 101942. doi:10.1016/j.nicl.2019.101942

Hitier, M., Besnard, S., & Smith, P. F. (2014). Vestibular pathways involved in cognition. *Front Integr Neurosci, 8*, 59. doi:10.3389/fnint.2014.00059

Job, A., Jacob, R., Pons, Y., Raynal, M., Kossowski, M., Gauthier, J., . . . Delon-Martin, C. (2016). Specific activation of operculum 3 (OP3) brain region during provoked tinnitus-related phantom auditory perceptions in humans. *Brain Struct Funct, 221*(2), 913-922. doi:10.1007/s00429-014-0944-0

Job, A., Paucod, J., O'Beirne, G. A., & Delon-Martin, C. (2011). Cortical representation of tympanic membrane movements due to pressure variation: An fMRI study. *Human Brain Mapping, 32*(5), 744-749. doi:10.1002/hbm.21063

Klingner, C. M., Axer, H., Brodoehl, S., & Witte, O. W. (2016). Vertigo and the processing of vestibular information: a review in the context of predictive coding. *Neuroscience & Biobehavioral Reviews, 71*, 379-387.

Kwan, A., Forbes, P. A., Mitchell, D. E., Blouin, J. S., & Cullen, K. E. (2019). Neural substrates, dynamics and thresholds of galvanic vestibular stimulation in the behaving primate. *Nat Commun, 10*(1), 1904. doi:10.1038/s41467-019-09738-1

Lancichinetti, A., & Fortunato, S. (2012). Consensus clustering in complex networks. *Scientific Reports, 2*(1), 336. doi:10.1038/srep00336

Laurens, J., Meng, H., & Angelaki, Dora E. (2013). Neural Representation of Orientation Relative to Gravity in the Macaque Cerebellum. *Neuron, 80*(6), 1508-1518. doi:https://doi.org/10.1016/j.neuron.2013.09.029

Lobel, E., Kleine, J. F., Bihan, D. L., Leroy-Willig, A., & Berthoz, A. (1998). Functional MRI of galvanic vestibular stimulation. *J Neurophysiol, 80*(5), 2699-2709. doi:10.1152/jn.1998.80.5.2699

Lopez, C., Blanke, O., & Mast, F. W. (2012). The human vestibular cortex revealed by coordinate-based activation likelihood estimation meta-analysis. *Neuroscience, 212*, 159-179. doi:10.1016/j.neuroscience.2012.03.028

Lurie, D. J., Kessler, D., Bassett, D. S., Betzel, R. F., Breakspear, M., Kheilholz, S., . . . Calhoun, V. D. (2019). Questions and controversies in the study of time-varying functional connectivity in resting fMRI. *Network Neuroscience, 4*(1), 30-69. doi:10.1162/netn_a_00116

Mazzola, L., Isnard, J., Peyron, R., & Mauguière, F. (2011). Stimulation of the human cortex and the experience of pain: Wilder Penfield's observations revisited. *Brain, 135*(2), 631-640. doi:10.1093/brain/awr265

McCarthy, P. (2020). FSLeyes. *Zenodo*. doi:http://doi.org/10.5281/zenodo.3937147

Rubinov, M., & Sporns, O. (2010). Complex network measures of brain connectivity: uses and interpretations. *Neuroimage, 52*(3), 1059-1069. doi:10.1016/j.neuroimage.2009.10.003

Schaefer, A., Kong, R., Gordon, E. M., Laumann, T. O., Zuo, X.-N., Holmes, A. J., . . . Yeo, B. T. T. (2017). Local-Global Parcellation of the Human Cerebral Cortex from Intrinsic Functional Connectivity MRI. *Cerebral Cortex, 28*(9), 3095-3114. doi:10.1093/cercor/bhx179

Smith, A. T., Beer, A. L., Furlan, M., & Mars, R. B. (2017). Connectivity of the Cingulate Sulcus Visual Area (CSv) in the Human Cerebral Cortex. *Cerebral Cortex, 28*(2), 713-725. doi:10.1093/cercor/bhx002

Smith, A. T., Greenlee, M. W., DeAngelis, G. C., & Angelaki, D. E. (2017). Distributed Visual–Vestibular Processing in the Cerebral Cortex of Man and Macaque. *Multisensory Research, 30*(2), 91-120. doi:10.1163/22134808-00002568

Smith, A. T., Wall, M. B., & Thilo, K. V. (2012). Vestibular inputs to human motion-sensitive visual cortex. *Cereb Cortex, 22*(5), 1068-1077. doi:10.1093/cercor/bhr179

Smith, S. M., & Nichols, T. E. (2009). Threshold-free cluster enhancement: Addressing problems of smoothing, threshold dependence and localisation in cluster inference. *Neuroimage, 44*(1), 83-98. doi:https://doi.org/10.1016/j.neuroimage.2008.03.061

Stark, C. E., & Squire, L. R. (2001). When zero is not zero: the problem of ambiguous baseline conditions in fMRI. *Proc Natl Acad Sci U S A, 98*(22), 12760-12766. doi:10.1073/pnas.221462998

Stephan, T., Deutschländer, A., Nolte, A., Schneider, E., Wiesmann, M., Brandt, T., & Dieterich, M. (2005). Functional MRI of galvanic vestibular stimulation with alternating currents at different frequencies. *Neuroimage, 26*(3), 721-732. doi:10.1016/j.neuroimage.2005.02.049

Uddin, L. Q. (2015). Salience processing and insular cortical function and dysfunction. *Nature reviews neuroscience, 16*(1), 55-61. doi:10.1038/nrn3857

Wall, M. B., & Smith, A. T. (2008). The Representation of Egomotion in the Human Brain. *Current Biology, 18*(3), 191-194. doi:https://doi.org/10.1016/j.cub.2007.12.053

Whitfield-Gabrieli, S., & Nieto-Castanon, A. (2012). CONN: a functional connectivity toolbox for correlated and anticorrelated brain networks. *Brain Connectivity, 2*, 125-141. doi:10.1089/brain.2012.0073

Yakusheva, T., Blazquez, P. M., & Angelaki, D. E. (2010). Relationship between complex and simple spike activity in macaque caudal vermis during three-dimensional vestibular stimulation. *Journal of Neuroscience, 30*(24), 8111-8126.

Zalesky, A., Fornito, A., & Bullmore, E. T. (2010). Network-based statistic: identifying differences in brain networks. *Neuroimage, 53*(4), 1197-1207. doi:10.1016/j.neuroimage.2010.06.041

zu Eulenburg, P., Caspers, S., Roski, C., & Eickhoff, S. B. (2012). Meta-analytical definition and functional connectivity of the human vestibular cortex. *Neuroimage, 60*(1), 162-169. doi:10.1016/j.neuroimage.2011.12.032

Appendices

Appendix A: Supplementary Methods

For anatomical data preprocessing, the T1-weighted (T1w) image was corrected for intensity non-uniformity (INU) using N4BiasFieldCorrection (Tustison et al. 2010, ANTs 2.2.0), and used as T1w-reference throughout the workflow. The T1w-reference was then skull-stripped using antsBrainExtraction.sh (ANTs 2.2.0), using OASIS as target template. Brain surfaces were reconstructed using recon-all (FreeSurfer 6.0.1, RRID:SCR_001847, Dale, Fischl, and Sereno 1999), and the brain mask estimated previously was refined with a custom variation of the method to reconcile ANTs-derived and FreeSurfer-derived segmentations of the cortical gray-matter of Mindboggle (RRID:SCR_002438, Klein et al. 2017). Spatial normalization to the ICBM 152 Nonlinear Asymmetrical template version 2009c (Fonov et al. 2009, RRID:SCR_008796) was performed through nonlinear registration with antsRegistration (ANTs 2.2.0, RRID:SCR_004757, Avants et al. 2008), using brain-extracted versions of both T1w volume and template. Brain tissue segmentation of cerebrospinal fluid (CSF), white-matter (WM) and gray-matter (GM) was performed on the brain-extracted T1w using fast (FSL 5.0.9, RRID:SCR_002823, Zhang, Brady, and Smith 2001).

For each of the BOLD runs found per subject (across all tasks and sessions), the following functional preprocessing was performed. First, a reference volume and its skull-stripped version were generated using a custom methodology of fMRIPrep. A deformation field to correct for susceptibility distortions was estimated based on fMRIPrep's 2019s fieldmap-less approach. The deformation field is that resulting from co-registering the BOLD reference to the same-subject T1w-reference with its intensity inverted (Wang et al. 2017; Huntenburg 2014). Registration is performed with antsRegistration (ANTs 2.2.0), and the process regularized by constraining deformation to be nonzero only along the phase-encoding direction, and modulated with an average fieldmap template (Treiber et al. 2016). Based on the estimated susceptibility distortion, an unwarped BOLD reference was calculated for a more accurate co-registration with the anatomical reference. The BOLD reference was then co-registered to the T1w reference using bbregister (FreeSurfer) which implements boundary-based registration (Greve and Fischl 2009). Co-registration was configured with nine degrees of freedom to account for distortions remaining in the BOLD reference. Head-motion parameters with respect to the BOLD reference (transformation matrices, and six corresponding rotation and translation parameters) are estimated before any spatiotemporal filtering using mcflirt (FSL 5.0.9, Jenkinson et al. 2002). The BOLD time-series, were resampled to surfaces on the following spaces: fsaverage. The BOLD

time-series were resampled onto their original, native space by applying a single, composite transform to correct for head-motion and susceptibility distortions. These resampled BOLD time-series will be referred to as preprocessed BOLD in original space, or just preprocessed BOLD. The BOLD time-series were resampled to MNI152NLin2009cAsym standard space, generating a preprocessed BOLD run in MNI152NLin2009cAsym space. First, a reference volume and its skull-stripped version were generated using a custom methodology of fMRIPrep. Several confounding time-series were calculated based on the preprocessed BOLD: framewise displacement (FD), DVARS and three region-wise global signals. FD and DVARS are calculated for each functional run, both using their implementations in Nipype (following the definitions by Power et al. 2014). The three global signals are extracted within the CSF, the WM, and the whole-brain masks. Additionally, a set of physiological regressors were extracted to allow for component-based noise correction (CompCor, Behzadi et al. 2007). Principal components are estimated after high-pass filtering the preprocessed BOLD time-series (using a discrete cosine filter with 128s cut-off) for the two CompCor variants: temporal (tCompCor) and anatomical (aCompCor). Six tCompCor components are then calculated from the top 5% variable voxels within a mask covering the subcortical regions. This subcortical mask is obtained by heavily eroding the brain mask, which ensures it does not include cortical GM regions. For aCompCor, six components are calculated within the intersection of the aforementioned mask and the union of CSF and WM masks calculated in T1w space, after their projection to the native space of each functional run (using the inverse BOLD-to-T1w transformation). The head-motion estimates calculated in the correction step were also placed within the corresponding confounds file. All resamplings can be performed with a single interpolation step by composing all the pertinent transformations (i.e. head-motion transform matrices, susceptibility distortion correction when available, and co-registrations to anatomical and template spaces). Gridded (volumetric) resamplings were performed using antsApplyTransforms (ANTs), configured with Lanczos interpolation to minimize the smoothing effects of other kernels (Lanczos 1964). Non-gridded (surface) resamplings were performed using mri_vol2surf (FreeSurfer).

Many internal operations of fMRIPrep use Nilearn 0.5.0 (Abraham et al. 2014, RRID:SCR_001362), mostly within the functional processing workflow. For more details of the pipeline, see the section corresponding to workflows in fMRIPrep\u2019s documentation.

Appendix B: Supplementary Results

Supplementary Table B.1 Peak activations for contrast GVS > GNS (TFCE, p< 0.001 unc.) for between-group comparison (n=108). Only clusters in grey matter with a minimum of 10 voxels reported.

Brain region	Cluster size	T	Z	Coordinates			Name of region
				x	y	z	
Cerebellum	12261	8.48	7.39	-13	-71	-47	L Vermis VIIb
		7.24	6.51	-28	-68	-22	L Vermis VI
		6.12	5.65	-10	-76	-32	L Vermis Crus II
	489	4.6	4.38	-36	-48	-47	L Vermis VIIb
	22	3.79	3.66	-26	-57	-43	L Vermis VIIIa
	37	3.53	3.42	-31	-63	-46	L Vermis VIIb
	14	3.35	3.26	-33	-43	-36	L Vermis VI
	18	3.56	3.45	-24	-44	-48	L Vermis VIIIb
	3722	5.72	5.33	23	-69	-22	R Vermis VI
		5.3	4.98	15	-72	-18	R Vermis VI
		5.29	4.97	31	-60	-24	R Vermis VI
	3052	10.01	Inf	18	-70	-46	R Vermis VIIb
		5.38	5.04	24	-64	-49	R Vermis VIIIa
		4.97	4.7	6	-77	-31	R Crus II
	190	4.29	4.11	3	-53	-32	R Vermis IX
	18	3.67	3.55	37	-48	-29	R Vermis VI
	33	3.53	3.42	6	-70	-24	R Vermis VI
	39	3.51	3.41	50	-59	-29	R Crus I
	10	3.38	3.29	0	-70	-13	Vermis VI
Limbic System	209	4.87	4.61	-23	2	-13	L Amygdala
	18	3.43	3.33	-11	-18	-3	L Thalamus
Primary Somato-sensory cortex	164	3.7	3.58	-51	-35	53	L Primary somatosens. cortex BA2
	34	3.55	3.44	-25	-34	61	L Primary somatosens. cortex BA3b
	74	3.56	3.45	59	-24	49	R Primary somatosens. cortex BA2
	335	4.27	4.1	24	-33	61	R Primary somatosens. cortex BA3b (VA = Area 3aV)
Secondary Somato-sensory cortex	46667	12.32	Inf	38	2	-11	R Insular cortex
		12.03	Inf	40	-2	-2	R Secondary somatosens. cortex . OP3
		11.5	Inf	52	-1	7	R Secondary somatosens. cortex / Parietal operculum OP4
	46667	12.32	Inf	38	2	-11	R Insular cortex
		12.03	Inf	40	-2	-2	R Secondary somatosens. cortex OP3
		11.5	Inf	52	-1	7	R Secondary somatosens. cortex / Parietal operculum OP4
	15	3.64	3.52	-40	-21	28	L Secondary somatosens. cortex OP1
Insular cortex	30917	12.57	Inf	-40	-2	-4	L Insular cortex
		9.6	Inf	-57	-1	6	L Secondary Somatosens. cortex OP 4
		9.6	Inf	-33	2	13	L Insular cortex
Parietal lobe	248	4.18	4.01	-6	-72	36	L superior parietal lobule 7P
		3.48	3.38	-7	-73	44	L superior parietal lobule 7P
	452	3.89	3.75	-33	-50	44	L Anterior intra-parietal sulcus hIP3
	30	3.64	3.52	-28	-62	48	L Anterior intra-parietal sulcus hIP3
	623	4.6	4.38	36	-48	43	R Anterior intra-parietal sulcus hIP3
		3.47	3.37	40	-51	51	R Anterior intra-parietal sulcus hIP3
	288	4.33	4.14	2	10	60	R premotor cortex BA6
Frontal lobe	1017	4.38	4.19	-41	38	12	L broca's area BA45
		4.07	3.92	-47	34	18	L broca's area BA45
	103	3.89	3.75	-41	7	30	L Broca's Area BA44
	52	3.83	3.7	55	3	37	R Premotor cortex BA6 (VA = area 6)
	13	3.57	3.46	24	42	-10	R Frontal pole

Supplementary Table 1 Peak activations for conjunction analysis GVS & mGNS using between-participants design (n=108) (p<0.001 uncorrected). Only clusters in grey matter with a minimum of 10 voxels reported.

Brain region	Cluster size	TFCE	Z	Coordinates			Name of region
				x	y	z	
Cerebellum	1787	4070.92	3.72	0	-53	-39	Vermis IX
		2249.14	3.35	0	-50	-31	Vermis IX/ Vermis X
	156	2024.81	3.16	-15	-56	-47	L Vermis VIIIb
		1977.98	3.16	-17	-47	-48	L Vermis VIIIb
Parietal lobe	320	2173.42	3.24	55	-32	42	R Inferior parietal lobule PFt_
		2106.35	3.16	55	-24	41	R Inferior parietal lobule PFt_
Frontal lobe	16357	3781.26	3.72	-34	-16	41	L Primary motor cortex BA4p
		3770.46	3.72	-42	-10	48	L Premotor cortex BA6
		3680.02	3.72	-40	-2	46	L Premotor cortex BA6
	527	2308.86	3.43	-10	4	55	L Premotor Cortex BA6
		2210.66	3.16	-9	8	47	L Premotor Cortex BA6
		2097.29	3.12	-4	4	62	L Premotor Cortex BA6
	33	1900.86	3.12	-15	-23	70	L Premotor Cortex BA6
	10	1531.61	3.12	-12	14	42	L Premotor cortex BA6
	16	2098.5	3.16	2	4	57	R Premotor cortex BA6
Occipital cortex	225997	15622.65	3.72	21	-82	27	R Lateral occipital cortex
		15457.06	3.72	23	-82	35	R Lateral occipital cortex
		15356.51	3.72	27	-76	21	WM
	90	2189.24	3.19	25	-88	-16	R Visual cortex V3V
	1992	5	4.72	3	13	34	WM
		4.29	4.11	0	-3	39	WM
		4.25	4.07	2	7	42	R Premotor cortex BA6
Occipital lobe	24	3.68	3.57	24	-83	-1	R Visual cortex V2 BA18
	27	3.67	3.55	-23	-88	-3	L Visual cortex V2V
	35	3.59	3.48	-25	-85	-9	L visual cortex V4
	41	4.49	4.29	-34	-79	-4	L Visual cortex V4

Appendix C: Supplementary References

Abraham, Alexandre, Fabian Pedregosa, Michael Eickenberg, Philippe Gervais, Andreas Mueller, Jean Kossaifi, Alexandre Gramfort, Bertrand Thirion, and Gael Varoquaux. 2014. "Machine Learning for Neuroimaging with Scikit-Learn." Frontiers in Neuroinformatics 8. https://doi.org/10.3389/fninf.2014.00014.

Avants, B.B., C.L. Epstein, M. Grossman, and J.C. Gee. 2008. "Symmetric Diffeomorphic Image Registration with Cross-Correlation: Evaluating Automated Labeling of Elderly and Neurodegenerative Brain." Medical Image Analysis 12 (1): 26–41. https://doi.org/10.1016/j.media.2007.06.004.

Behzadi, Yashar, Khaled Restom, Joy Liau, and Thomas T. Liu. 2007. "A Component Based Noise Correction Method (CompCor) for BOLD and Perfusion Based fMRI." NeuroImage 37 (1): 90–101. https://doi.org/10.1016/j.neuroimage.2007.04.042.

Dale, Anders M., Bruce Fischl, and Martin I. Sereno. 1999. "Cortical Surface-Based Analysis: I. Segmentation and Surface Reconstruction." NeuroImage 9 (2): 179–94. https://doi.org/10.1006/nimg.1998.0395.

Esteban, Oscar, Ross Blair, Christopher J. Markiewicz, Shoshana L. Berleant, Craig Moodie, Feilong Ma, Ayse Ilkay Isik, et al. 2018. "FMRIPrep 1.2.5." Software. Zenodo. https://doi.org/10.5281/zenodo.852659.

Esteban, Oscar, Christopher Markiewicz, Ross W Blair, Craig Moodie, Ayse Ilkay Isik, Asier Erramuzpe Aliaga, James Kent, et al. 2018. "FMRIPrep: A Robust Preprocessing Pipeline for Functional MRI." bioRxiv. https://doi.org/10.1101/306951.

Fonov, VS, AC Evans, RC McKinstry, CR Almli, and DL Collins. 2009. "Unbiased Nonlinear Average Age-Appropriate Brain Templates from Birth to Adulthood." NeuroImage, Organization for human brain mapping 2009 annual meeting, 47, Supplement 1: S102. https://doi.org/10.1016/S1053-8119(09)70884-5.

Gorgolewski, K., C. D. Burns, C. Madison, D. Clark, Y. O. Halchenko, M. L. Waskom, and S. Ghosh. 2011. "Nipype: A Flexible, Lightweight and Extensible Neuroimaging Data Processing Framework in Python." Frontiers in Neuroinformatics 5: 13. https://doi.org/10.3389/fninf.2011.00013.

Gorgolewski, Krzysztof J., Oscar Esteban, Christopher J. Markiewicz, Erik Ziegler, David Gage Ellis, Michael Philipp Notter, Dorota Jarecka, et al. 2018. "Nipype." Software. Zenodo. https://doi.org/10.5281/zenodo.596855.

Greve, Douglas N, and Bruce Fischl. 2009. "Accurate and Robust Brain Image Alignment Using Boundary-Based Registration." NeuroImage 48 (1): 63–72. https://doi.org/10.1016/j.neuroimage.2009.06.060.

Huntenburg, Julia M. 2014. "Evaluating Nonlinear Coregistration of BOLD EPI and T1w Images." Master's Thesis, Berlin: Freie Universität. http://hdl.handle.net/11858/00-001M-0000-002B-1CB5-A.

Jenkinson, Mark, Peter Bannister, Michael Brady, and Stephen Smith. 2002. "Improved Optimization for the Robust and Accurate Linear Registration and Motion Correction of Brain Images." NeuroImage 17 (2): 825–41. https://doi.org/10.1006/nimg.2002.1132.

Klein, Arno, Satrajit S. Ghosh, Forrest S. Bao, Joachim Giard, Yrjö Häme, Eliezer Stavsky, Noah Lee, et al. 2017. "Mindboggling Morphometry of Human Brains." PLOS Computational Biology 13 (2): e1005350. https://doi.org/10.1371/journal.pcbi.1005350.

Lanczos, C. 1964. "Evaluation of Noisy Data." Journal of the Society for Industrial and Applied Mathematics Series B Numerical Analysis 1 (1): 76–85. https://doi.org/10.1137/0701007.

Power, Jonathan D., Anish Mitra, Timothy O. Laumann, Abraham Z. Snyder, Bradley L. Schlaggar, and Steven E. Petersen. 2014. "Methods to Detect, Characterize, and

Remove Motion Artifact in Resting State fMRI." NeuroImage 84 (Supplement C): 320–41. https://doi.org/10.1016/j.neuroimage.2013.08.048.

Treiber, Jeffrey Mark, Nathan S. White, Tyler Christian Steed, Hauke Bartsch, Dominic Holland, Nikdokht Farid, Carrie R. McDonald, Bob S. Carter, Anders Martin Dale, and Clark C. Chen. 2016. "Characterization and Correction of Geometric Distortions in 814 Diffusion Weighted Images." PLOS ONE 11 (3): e0152472. https://doi.org/10.1371/journal.pone.0152472.

Tustison, N. J., B. B. Avants, P. A. Cook, Y. Zheng, A. Egan, P. A. Yushkevich, and J. C. Gee. 2010. "N4ITK: Improved N3 Bias Correction." IEEE Transactions on Medical Imaging 29 (6): 1310–20. https://doi.org/10.1109/TMI.2010.2046908.

Wang, Sijia, Daniel J. Peterson, J. C. Gatenby, Wenbin Li, Thomas J. Grabowski, and Tara M. Madhyastha. 2017. "Evaluation of Field Map and Nonlinear Registration Methods for Correction of Susceptibility Artifacts in Diffusion MRI." Frontiers in Neuroinformatics 11. https://doi.org/10.3389/fninf.2017.00017.

Zhang, Y., M. Brady, and S. Smith. 2001. "Segmentation of Brain MR Images Through a Hidden Markov Random Field Model and the Expectation-Maximization Algorithm." IEEE Transactions on Medical Imaging 20 (1): 45–57. https://doi.org/10.1109/42.906424.

4. Quantitative Analysis of Perivascular Spaces in Long-Duration Space Flyers

Judita Huber[1, 2], Steven Jillings[3], Ben Jeurissen[4], Elena Tomilovskaya[5], Alena Rumshiskaya[6], Liudmila Litvinova[6], Inna Nosikova[5], Ekaterina Pechenkova[7], Inessa B. Kozlovskaya[5], Viktor Petrovichev[6], Ilya Rukavishnikov[5], Stefan Sunaert[8], Paul M. Parizel[9], Valentin Sinitsyn[10], Jan Sijbers[4], Jitka Annen[11,12], Steven Laureys[11,12], Angelique Van Ombergen[13*], Floris L. Wuyts[3] and Peter zu Eulenburg[1,14,15]

1. Ludwig-Maximilians-Universität München, Graduate School of Systemic Neurosciences, Germany; 2. Ludwig-Maximilians-Universität München, Research Training Grant 2175, Germany; 3. Lab for Equilibrium Investigations and Aerospace, University of Antwerp, Antwerp, Belgium; 4. Imec/Vision Lab, University of Antwerp, Antwerp, Belgium; 5. SSC RF – Institute of Biomedical Problems, Russian Academy of Sciences, Moscow, Russia; 6. Radiology Department, Federal Center of Treatment and Rehabilitation, Moscow, Russia; 7. Laboratory for Cognitive Research, National Research University, Higher School of Economics, Moscow, Russia; 8. Translational MRI, Department of Imaging & Pathology, KU Leuven, Leuven, Belgium; 9.Radiology Department, Antwerp University Hospital & University of Antwerp, Antwerp, Belgium; 10. Faculty of Fundamental Medicine, Lomonosov Moscow State University, Moscow, Russia; 11. Coma Science Group, GIGA-Consciousness, University of Liège, Liège, Belgium; 12. Centre du Cerveau², University Hospital of Liège, Liège, Belgium ; 13. Department of Translational Neurosciences – ENT, University of Antwerp, Antwerp, Belgium; 14. Institute for Neuroradiology, Faculty of Medicine, Ludwig-Maximilians-University Munich, Munich, Germany; 15. German Center for Vertigo and Balance Disorders, Ludwig-Maximilians-University Munich, Munich, Germany

Author contributions

F.W. conceived the experiment and acquired funding together with SL, VS, IK, PP, and SS. BJ, PP, FW, VS, SS, and JS designed the experiment. SJ, AVO, FW, ET, AR, LL, IN, EP, and IK collected the data. JH analysed and interpreted the data, wrote the manuscript, and created the figures. PzE conceived the analysis, preprocessed the data, interpreted the data, and reviewed the manuscript and figures.

Acknowledgements

The authors would like to thank the Russian cosmonauts, the European astronauts, and all volunteers for their participation. We also want to thank Seyed-Ahmad Ahmadi for methodological support concerning the labelling of structural images. This work was supported by the European Space Agency (ISLRA 2009-1062), Russian Academy of Sciences (grant 63.1), Belgian Science Policy (BELSPO), the Research Foundation Flanders (Belgium, FWO Vlaanderen), the French Speaking Community Concerted Research Action (ARC-06/11-340) and Zonta International (Amelia Earhart fellowship 2016-2017 to AVO). SL is research director at FRS-FNRS. BJ is a Postdoctoral Fellow for FWO Vlaanderen. It was further funded by the German Research Association (DFG) via the RTG 2175 "Perception in context and its Neural Basis" and the Graduate School of Systemic Neurosciences (GSC 82/1), Munich, Germany.

Abstract

Perivascular spaces (PVS) are the spaces surrounding blood vessels which function as flow pathways for cerebrospinal (CSF) and interstitial fluid (ISF). Enlarged PVS indicate impaired brain fluid clearance (Wardlaw et al., 2020). Since spending prolonged time in microgravity causes brain changes related to the perturbation of the cephalic fluid movement (Jillings et al., 2020; Van Ombergen et al., 2019), we wanted to characterise PVS load in space travellers before and after they travelled to space and hypothesised increased PVS volume in this population. By developing a semi-automatic detection pipeline using the open source software Slicer (Fedorov et al., 2012), we were able to determine PVS volume across the full brain using only T1 weighted images acquired by means of magnetic resonance imaging. We compared PVS volume from 12 Russian cosmonauts and 4 European astronauts before going to space with age-matched controls. We also evaluated changes in PVS shortly after space flight as well as half a year after the mission. Overall, we found that PVS volume were significantly increased in space travellers at baseline when compared to controls and was further affected by exposure to microgravity. We speculate that astronaut training in combination with actual long-duration space flight contribute to the high load of PVS observed in our conservative approach.

4.1 Introduction

Spending prolonged time in microgravity causes physiological changes in humans, including brain changes such as increased ventricles and CSF volume (Van Ombergen et al., 2019), increased mean brain volumes and pituitary gland deformations (Kramer et al., 2020). These changes were suggested to arise from a circulatory perturbation (or cephalic fluid shift) induced by microgravity.

The mechanisms by which fluid movement allows waste clearance from the brain has been recently described as the glia-lymphatic (or glymphatic) pathway. In this pathway, brain fluids move along vessels through perivascular spaces (PVS, also known as Virchow-Robin spaces) (Abbott, Pizzo, Preston, Janigro, & Thorne, 2018; Wardlaw et al., 2020). Specifically, cerebrospinal fluid (CSF) is driven into arterial PVS, from where it further flows into the brain parenchyma. Here, CSF mixes with interstitial fluid (ISF) and dissipates through the venous PVS and perineural spaces, finally exiting through one of several drainage routes (Rasmussen, Mestre, & Nedergaard, 2018). Body posture, but also sleep-wake cycles were found to influence CSF-ISF exchange (Lee et al., 2015; Xie et al., 2013). Considering the impact of microgravity on lowering cephalic fluid circulation, we wanted to investigate whether related brain changes in the form of enlargement of PVS occurs in after travelling to space.

PVS have been found visible in a high number of healthy participants by means of high-resolution MR imaging techniques (Groeschel, Chong, Surtees, & Hanefeld, 2006). They appear as well defined, symmetrical shapes and are tubular when parallel with image plane and round when perpendicular with the image plane (Benjamin et al., 2018; Wardlaw et al., 2020). Evidence is mixed as to whether a higher visibility or enlarged perivascular spaces are associated with neurological conditions such as stroke and dementia, but they seem to be associated with risk factors such as age and hypertension (Wardlaw et al., 2020). In general, enlarged PVS are suspected to be caused by a decrease in perivascular fluid circulation (Abbott et al., 2018; Mestre, Kostrikov, Mehta, & Nedergaard, 2017).

Qualitative rating scores have been mostly used to estimate PVS in humans, typically using T2-weighted MR images (Laveskog, Wang, Bronge, Wahlund, & Qiu, 2018; Potter, Chappell, Morris, & Wardlaw, 2015). The advantage of these rating methods is that they are reasonably fast and robust. However, whilst these methods are good in indicating the approximate amount of enlarged PVS, it does not allow for an observer-independent quantification of PVS volume (such as volume, size, etc.). More advanced automatic

quantification methods have been developed using computational methods, these usually require more than one image modality though (e.g. both T1 and T2) (Ballerini et al., 2018).

For this endeavour, astronaut and cosmonaut MRI data from a single modality (T1-weighted images) were available, requiring manual segmentation of PVS. In order to compare changes in PVS in space travellers before and after their mission to space, we decided to manually label PVS within a white matter segmentation mask and applied stringent, predefined segmentation criteria for selecting elongated, non-round structures. We were interested, if space travellers display increased PVS volume compared to control participants in general, and if they display changes in PVS volume at dedicated timepoints before, after and during follow-up of a space mission. Specifically, we hypothesised that astronauts will display increased PVS volume after the space mission.

4.2 Methods

4.2.1 Participants

Overall, data from 12 male ROSCOSMOS cosmonauts and four ESA astronauts were imaged for this study (average age 42.3 ±4.9 years). 16 male controls (average age 41.6 ±6.2 years) matched in terms of age, gender, and education level also participated in the same imaging protocol. These control participants did not undergo any astronaut training.

4.2.2 Acquisition

Space travellers were scanned with a repeated T1w sequence in two different sessions on three different timepoints: once prior to launch ('preflight', n=15), once shortly after re-entry ('postflight', n=16) and once at long-term follow-up ('follow-up', n=12). The ROSCOSMOS cosmonauts (average age 45.45 ±4.9 years) and their respective control subjects (n=12, average age 43 ±5.8 years) were assessed on a clinical scanner 3T MRI (Discovery 750; GE Healthcare, USA) located at the Federal Center for Treatment and Rehabilitation in Moscow, Russia, using a 16-channel head and neck array coil. For each time point, two high-resolution sagittal T1-weighted 3D fast spoiled gradient echo (FSPGR) images were acquired approximately one hour apart (time of repetition (TR) 7.90 ms; echo time (TE) 3.06 ms; inversion time (TI) 450 ms; voxel size 1×1×1 mm; flip angle 12°; field of view (FOV) 240 mm, 180 slices; bandwidth 31.25 Hz/px). Four ESA astronauts (average age = 40.8±2.1 years) and their respective control subjects (n=4, average age = 33.5 years ±1.6) were assessed on a dedicated research scanner 3T MRI (Siemens Biograph, Erlangen, Germany) located at the ENVIHAB facility in Cologne, Germany using a 20-channel head and neck array coil. For each time point, two high-resolution sagittal

T1-weighted 3D magnetization prepared rapid gradient echo (MPRAGE) images were acquired approximately one hour apart (TR 1900 ms; TE 2.43 ms; TI 900 ms; voxel size 1×1×1 mm; flip angle 9°; field of view (FOV) 256 mm, 176 slices; bandwidth 180 Hz/Px).For the subsequent analysis, T1 data from only one session were used in the space traveller group. Only the baseline time-point was used for the control group.

4.2.3 Processing

T1-weighted images were used to create a tissue probability map in native space via segmentation using the CAT 12 toolbox (Gaser & Dahnke, 2016). The original T1 images were bias field corrected and denoised using a spatial adaptive non-local means (SANLM) denoising filter, as implemented in the CAT 12 toolbox.

4.2.4 Labelling

Identification and labelling of PVS was performed by one author (J.H.) who was blinded regarding time point acquired of astronauts and cosmonauts. Slicer 4.11.0 (Fedorov et al., 2012) was used for identifying and labelling PVS. PVS were defined as elongated hypointensities surrounded by white matter. Hence, for labelling, first a white matter mask was created for each participant. The white matter mask was determined from the tissue probability map by thresholding to a relatively conservative range of 2.7 – 3 (i.e. 70% probability of white matter). Using the three-dimensional 'sphere brush' tool in the Segment Editor module, suspected PVS were labelled in regions not covered by the white matter mask. Care was taken not to label regions, where sulci were just about to form (thus causing similar hypointensities in some sections). Furthermore, hypointensities were not labelled if they were not surrounded by white matter. See Figure 4.1 for a flow diagram of the PVS labelling method. See Figure 4.2A for examples of PVS.

After labelling all putative PVS regions, only segments with a minimum size of 5 voxels were selected. Parameters were extracted using the module Segment Statistics using the T1 image as scalar volume. The following segment parameters were used, as calculated via the software: volume (mm3), roundness (ratio of the area of the hypersphere by the actual area), elongation (square root of the ratio of the second largest principal moment by the second smallest). These criteria were chosen due to previously described visual characteristics of PVS, i.e structures along perforating vessels appearing tubular when parallel with image plane and round when perpendicular with the image plane.

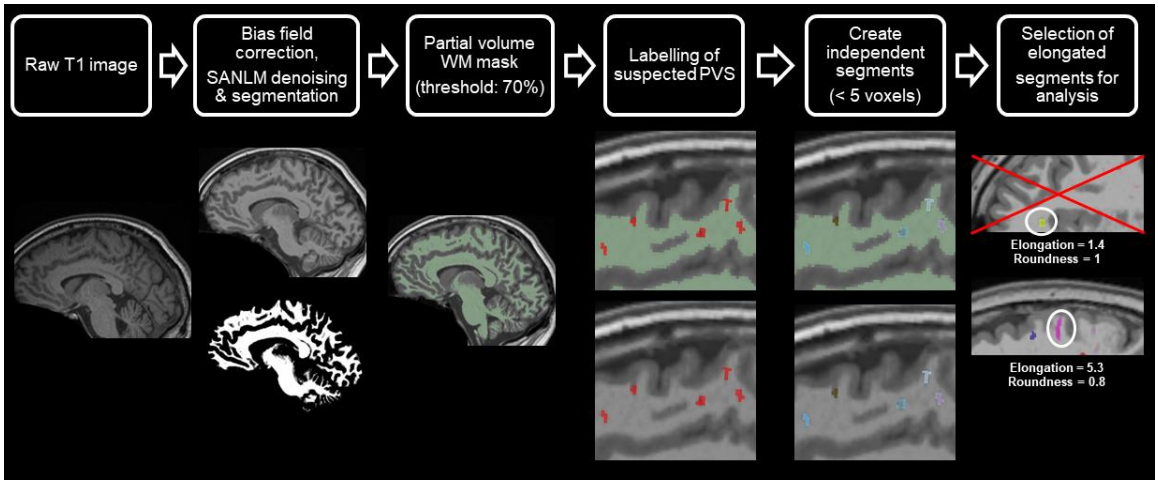

Figure 4.1 Image processing flow and perivascular space (PVS) labelling.
Raw T1 images were bias corrected and a partial tissue probability map was created which was used to create a partial volume white matter (WM) mask (shown here in green). Only large, elongated segments were used for subsequent analysis.

2.1.1 Analysis procedure

For analysis, only marked segments were selected which had an elongation value below 1.5 and a roundness value below 0.9 or above 1.1. The total PVS volume was calculated for each brain volume using a custom-made MATLAB (R2019b) script (The MathWorks, Inc., United States). For statistical analysis, R 3.6.1 was used with the packages afex_0.25-1, dplyr_0.8.3 and rstatix_0.4.0.

4.3 Results

4.3.1 Included Data

Total PVS volume was calculated for each T1 scan. We pooled data of four European and twelve Russian astronauts for three timepoints: *pre-flight*, shortly after return (*post-flight*, average 8.7 ±3.2 days) and approximately half a year after return to earth (*follow-up*, average 210.4 ± 39.7 days). Outlier detection was performed for each time point of astronauts and for the control group. Outliers were defined as values below/above the first/third quartile +/- 3x inter-quartile range (IQR). One extreme value within the control group was excluded according to these criteria (PVS = 1444.92 µl). No other values had to be excluded (see Table 4.1 for descriptive statistics). Since we had a directed hypothesis and hypothesised that PVS volume will be increased in astronauts, for all subsequent analyses we considered p-values below as 0.1 as significant.

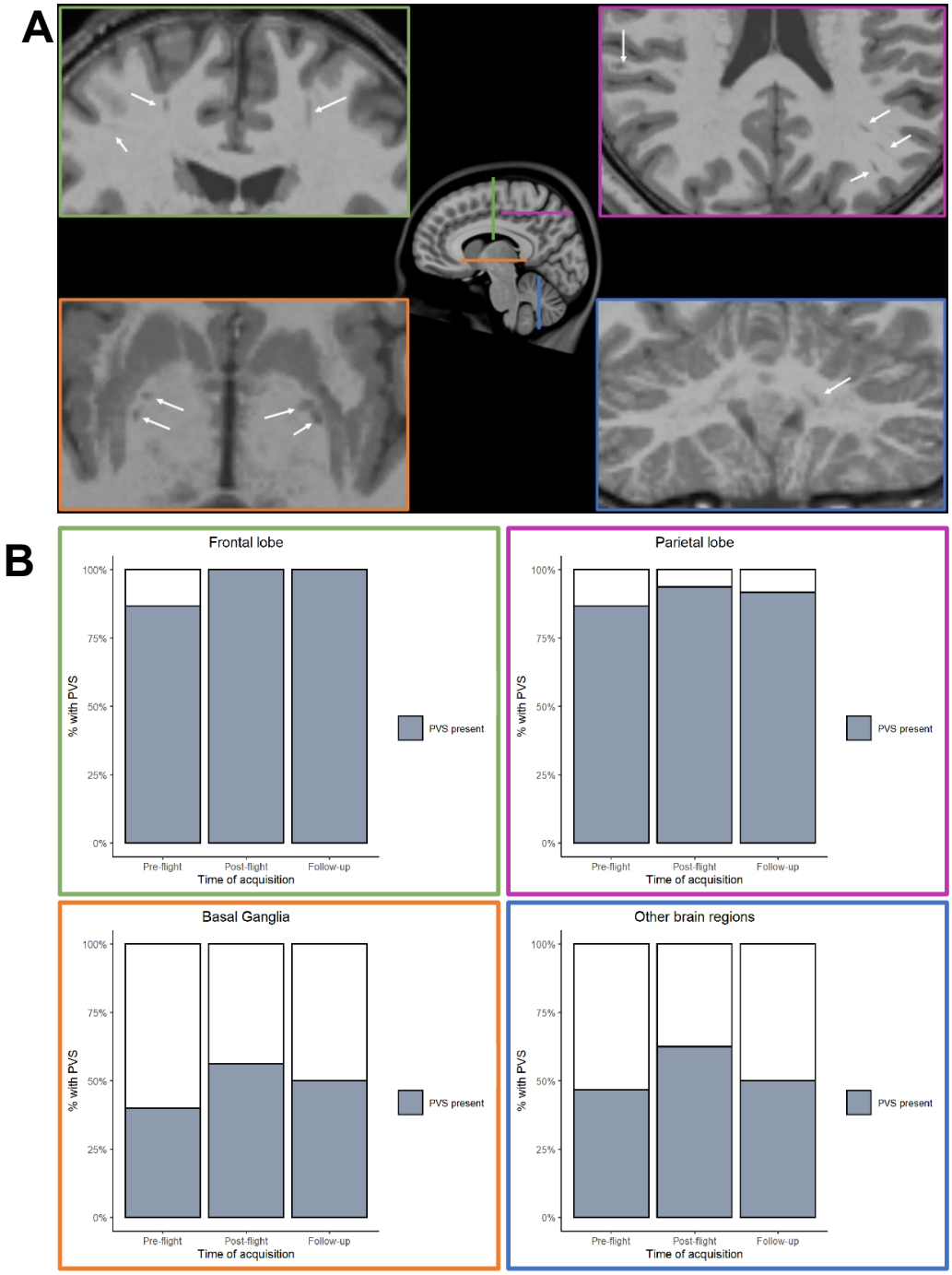

Figure 4.2 Perivascular spaces found in space travellers.
A) Examples of PVS in different regions of the brain B) Proportion of astronauts & cosmonauts with PVS found before (pre-flight), shortly after return to earth (post-flight) and 180 days after return to earth (follow-up) for different regions of the brain (green/top left border = frontal lobe, purple/top right border = parietal lobe, orange/bottom left = basal ganglia, blue/bottom left = other brain regions, including the cerebellum)

Table 4.1 Summary table for all astronaut & cosmonauts and control participants.

Group	n	Days in space (previous missions)		Days in space (current mission)		Total PVS (µl)		Shapiro Wilk		Shapiro Wilk (transf. data)	
		Mean (SD)	*Med. (IQR)*	*Mean (SD)*	*Med. (IQR)*	*Mean (SD)*	*Med. (IQR)*	*W*	*p*	*W.*	*p*
Controls	15	0	0	0	0	84.24 (57.04)	80 (76.85)	.97	.78	-	-
Pre-flight	15	147.47 (188.17)	159 (165)	176.8 (65.84)	173 (27.5)	214.34 (193.14)	154.69 (263.51)	.90	.08	.91	.15
Post-flight	16	148.63 (181.85)	162 (165.25)	174.44 (64.31)	173 (28)	234.43 (189.57)	174.02 (263.41)	.88	.03	.97	.79
Follow-up	12	171.17 (201.22)	165 (168.25)	193.32 (49.67)	184 (27.25)	204.25 (181.99)	154.55 (197.70)	.87	.06	.97	.86

4.3.2 Comparison of pooled dataset (pre-flight) with controls

In general, PVS were found in almost all space travellers in frontal and parietal cortices. In some, PVS were also found in basal ganglia, cerebellum and parietal lobes (see Figure 4.2B for distribution of PVS). We determined if controls differed in terms of their total PVS volume compared to all astronauts and cosmonauts before going to space. Using a t-test, we found that that PVS volume of the pooled data set pre-flight was indeed higher on average when compared to controls ($t_{(16.43)}$=2.50, p=0.02). The effect was large, as suggested using Cohen' D with Hedges correction for small samples (r = 0.89) (Figure 4.3A).The non-parametric equivalent (Wilcoxon rank sum test) resulted in W=159, p=0.056. No obvious relationship between previous experience in space and PVS volume was found upon visual exploration of data (raw data not shown to protect the identity of astronauts and cosmonauts).

4.3.3 Short term and long term effects of microgravity

Based on previous research, we hypothesised that microgravity will increase PVS volume, when compared to the baseline value before flight. To test this hypothesis, a linear model was calculated with scanning time-point as a fixed factor (three levels: (pre-flight, post-flight, follow-up) and included random effect intercepts for each participant (*PVS volume ~ scan time-point + (1|participant ID)*). Since PVS volume data were not normally distributed at each timepoint, a logarithmic transformation was performed (see Table 4.1 for for Shapiro-Wilk normality test statistics).

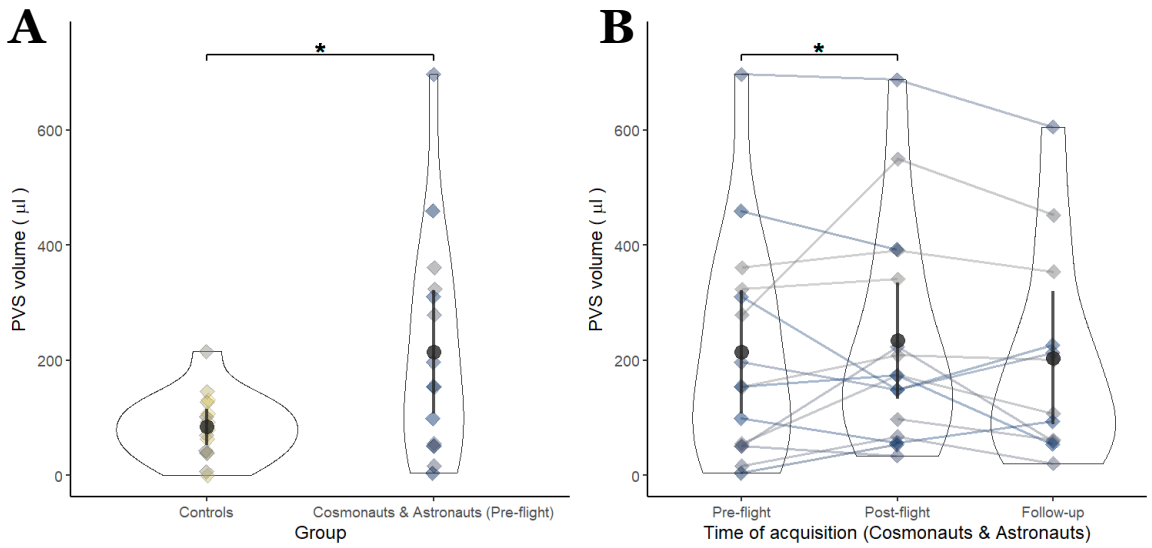

Figure 4.3 Comparison of perivascular spaces (PVS) in space travellers and controls.
A) PVS volume in controls and merged astronaut and cosmonaut data set (before their mission) B) PVS volume before (pre-flight), shortly after return to earth (post-flight) and approximately 180 days after return to earth (follow-up). Sample means and 95% confidence intervals shown in black.

The levels of the fixed effects were significant for the condition pre vs. post1, with an estimate of b=0.37 ($t_{(24.88)}$=1.97, p=0.06), corresponding to an average increase of 1.45 µl (after taking the exponential e0.37), or an average 0.6% increase from the mean baseline PVS volume pre-flight. PVS volume did not significantly increase when compared to the followup session ($t_{(25.35)}$=0.25, p = 0.81, b= 0.19), suggesting a 'normalisation' of PVS volume back to baseline (i.e. to pre-flight) (Figure 4.3B). Probability values were estimated via t-tests using the Satterthwaite approximations to degrees of freedom.

4.3.4 Pituitary gland deformations

Similarly to Kramer et al. (2020) we observed a flattening of the pituitary gland dome in cosmonauts and astronauts after return to earth (see Figure 4.4 for examples)

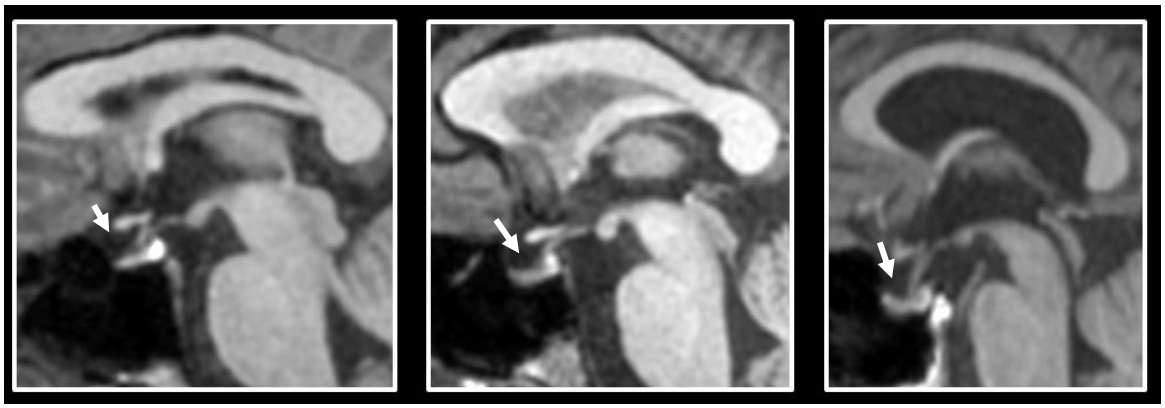

Figure 4.4 Examples of pituitary gland flattening in cosmonauts.

4.4 Discussion

In the present study we were interested in characterising PVS in astronauts and cosmonauts before and after they travelled to space. For this we established a semi-automatic procedure to determine PVS volume from T1 images using the openly accessible software Slicer. We compared PVS volume of T1 images from individuals before going to space to age-matched controls, to evaluate a general effect of microgravity and/or training. We additionally evaluated whether PVS volume increases after space flight and whether these effects are detectable in the short- or long term. Overall we found a higher PVS volume in space travellers before their mission, when compared to controls and only found a small influence of microgravity on PVS volume. We suggest that inter-individual differences, scanner effects and biological preflight status may affect initial PVS load considerably.

Our findings suggest that PVS are larger in astronauts & cosmonauts on average, when compared to controls. Only a very small (but significant) short-term effect of average PVS volume increase was also found in space travellers. It is noteworthy, that PVS volume varied substantially across astronauts and cosmonauts. Upon exploration of the data, this variation could not be explained by previous experience in space. We hypothesise that individual factors during cosmonaut training or previous missions may contribute to this variance. One possible factor could be the individual sleep architecture: Barger et al. (2014) have shown that crew members obtain significantly less sleep per night before and during spaceflight, when compared to sleep shortly after their mission. Sleep disturbances have been further found to be related to an increase in PVS: in sleep apnea, PVS load is increased (Song et al., 2017) and poor sleep quality was found to be related to increased PVS in the basal ganglia (other regions were not considered) in a study by Del Brutto, Mera, Del Brutto, and Castillo (2019). In future it would be interesting to further evaluate the effect of inter-individual factors (such as amount of sleep) on MRI-visible PVS. Furthermore, amount of sleep may be an important factor to consider when selecting participants for the control group in future studies.

It is important to mention that due to our very cautious and conservative analysis we likely underestimated the actual volume of PVS detected. This is because firstly, detecting PVS from T1 contrast is less straightforward than from detecting them from T2 contrasts, where PVS appear as hyperintensities. Secondly, we decided to only label PVS with the help of a white matter mask with a conservative threshold, meaning that some PVS may have been misidentified as white matter. Furthermore, hypointensities lying outside of white matter

were not considered in the analysis at all, thus likely explaining the low number of PVS determined in the basal ganglia.

We made the notable observation of a flattened pituitary glands (i.e. an increase in concavity and volume) in some of the individuals who have been subjected to microgravity. This observation was just previously also published in astronauts (Kramer et al., 2020) and in individuals with idiopathic intracranial hypertension (Hoffmann et al., 2013; Yuh et al., 2000), a condition characterised by elevated intracranial pressure. Indeed, it was suggested previously that expansion of CSF may result in increased intracranial pressure (Kramer et al., 2020; Van Ombergen et al., 2019) which in turn would cause the observed changes in pituitary gland morphology. We also made the observation of perivascular spaces in cerebellum, a phenomenon which, to our knowledge, has not been reported yet to co-occur in combination with the increased intracranial pressure.

Overall, we believe it is important to further evaluate the effect of microgravity and astronaut training on PVS and the glymphatic system in general. Disturbances have been found to be related to several a number of neurological conditions (Rasmussen et al., 2018; Wardlaw et al., 2020), it is thus important to understand the extent and longevity of brain changes occurring during microgravity. A better understanding will not only allow for appropriate interventions, but will also help towards a better understanding of the principles of glymphatic system in general. We suggest to that particularly the interaction of sleep and microgravity on perivascular space volume should be investigated.

4.5 References

Abbott, N. J., Pizzo, M. E., Preston, J. E., Janigro, D., & Thorne, R. G. (2018). The role of brain barriers in fluid movement in the CNS: is there a 'glymphatic' system? *Acta Neuropathol, 135*(3), 387-407. doi:10.1007/s00401-018-1812-4

Ballerini, L., Lovreglio, R., Valdes Hernandez, M. D. C., Ramirez, J., MacIntosh, B. J., Black, S. E., & Wardlaw, J. M. (2018). Perivascular Spaces Segmentation in Brain MRI Using Optimal 3D Filtering. *Sci Rep, 8*(1), 2132. doi:10.1038/s41598-018-19781-5

Barger, L. K., Flynn-Evans, E. E., Kubey, A., Walsh, L., Ronda, J. M., Wang, W., . . . Czeisler, C. A. (2014). Prevalence of sleep deficiency and use of hypnotic drugs in astronauts before, during, and after spaceflight: an observational study. *The Lancet Neurology, 13*(9), 904-912. doi:10.1016/s1474-4422(14)70122-x

Benjamin, P., Trippier, S., Lawrence, A. J., Lambert, C., Zeestraten, E., Williams, O. A., . . . Markus, H. S. (2018). Lacunar Infarcts, but Not Perivascular Spaces, Are Predictors of Cognitive Decline in Cerebral Small-Vessel Disease. *Stroke, 49*(3), 586-593. doi:10.1161/STROKEAHA.117.017526

Del Brutto, O. H., Mera, R. M., Del Brutto, V. J., & Castillo, P. R. (2019). Enlarged basal ganglia perivascular spaces and sleep parameters. A population-based study. *Clinical Neurology and Neurosurgery, 182*, 53-57. doi:https://doi.org/10.1016/j.clineuro.2019.05.002

Fedorov, A., Beichel, R., Kalpathy-Cramer, J., Finet, J., Fillion-Robin, J. C., Pujol, S., . . . Kikinis, R. (2012). 3D Slicer as an image computing platform for the Quantitative Imaging Network. *Magn Reson Imaging, 30*(9), 1323-1341. doi:10.1016/j.mri.2012.05.001

Gaser, C., & Dahnke, R. (2016). CAT-a computational anatomy toolbox for the analysis of structural MRI data. *HBM, 2016*, 336-348.

Groeschel, S., Chong, W. K., Surtees, R., & Hanefeld, F. (2006). Virchow-Robin spaces on magnetic resonance images: normative data, their dilatation, and a review of the literature. *Neuroradiology, 48*(10), 745-754. doi:10.1007/s00234-006-0112-1

Hoffmann, J., Huppertz, H. J., Schmidt, C., Kunte, H., Harms, L., Klingebiel, R., & Wiener, E. (2013). Morphometric and volumetric MRI changes in idiopathic intracranial hypertension. *Cephalalgia, 33*(13), 1075-1084. doi:10.1177/0333102413484095

Jillings, S., Van Ombergen, A., Tomilovskaya, E., Rumshiskaya, A., Litvinova, L., Nosikova, I., . . . Jeurissen, B. (2020). Macro- and microstructural changes in

cosmonauts' brains after long-duration spaceflight. *Science Advances, 6*(36), eaaz9488. doi:10.1126/sciadv.aaz9488

Kramer, L. A., Hasan, K. M., Stenger, M. B., Sargsyan, A., Laurie, S. S., Otto, C., . . . Macias, B. R. (2020). Intracranial Effects of Microgravity: A Prospective Longitudinal MRI Study. *Radiology*, 191413.

Laveskog, A., Wang, R., Bronge, L., Wahlund, L. O., & Qiu, C. (2018). Perivascular Spaces in Old Age: Assessment, Distribution, and Correlation with White Matter Hyperintensities. *AJNR Am J Neuroradiol, 39*(1), 70-76. doi:10.3174/ajnr.A5455

Lee, H., Xie, L., Yu, M., Kang, H., Feng, T., Deane, R., . . . Benveniste, H. (2015). The Effect of Body Posture on Brain Glymphatic Transport. *The Journal of neuroscience : the official journal of the Society for Neuroscience, 35*(31), 11034-11044. doi:10.1523/JNEUROSCI.1625-15.2015

Mestre, H., Kostrikov, S., Mehta, R. I., & Nedergaard, M. (2017). Perivascular spaces, glymphatic dysfunction, and small vessel disease. *Clin Sci (Lond), 131*(17), 2257-2274. doi:10.1042/CS20160381

Potter, G. M., Chappell, F. M., Morris, Z., & Wardlaw, J. M. (2015). Cerebral perivascular spaces visible on magnetic resonance imaging: development of a qualitative rating scale and its observer reliability. *Cerebrovasc Dis, 39*(3-4), 224-231. doi:10.1159/000375153

Rasmussen, M. K., Mestre, H., & Nedergaard, M. (2018). The glymphatic pathway in neurological disorders. *The Lancet Neurology, 17*(11), 1016-1024. doi:10.1016/s1474-4422(18)30318-1

Song, T.-J., Park, J.-H., Choi, K. H., Chang, Y., Moon, J., Kim, J.-H., . . . Lee, H. W. (2017). Moderate-to-severe obstructive sleep apnea is associated with cerebral small vessel disease. *Sleep Medicine, 30*, 36-42. doi:https://doi.org/10.1016/j.sleep.2016.03.006

Van Ombergen, A., Jillings, S., Jeurissen, B., Tomilovskaya, E., Rumshiskaya, A., Litvinova, L., . . . Wuyts, F. L. (2019). Brain ventricular volume changes induced by long-duration spaceflight. *Proc Natl Acad Sci U S A, 116*(21), 10531-10536. doi:10.1073/pnas.1820354116

Wardlaw, J. M., Benveniste, H., Nedergaard, M., Zlokovic, B. V., Mestre, H., Lee, H., . . . colleagues from the Fondation Leducq Transatlantic Network of Excellence on the Role of the Perivascular Space in Cerebral Small Vessel, D. (2020). Perivascular spaces in the brain: anatomy, physiology and pathology. *Nat Rev Neurol, 16*(3), 137-153. doi:10.1038/s41582-020-0312-z

Xie, L., Kang, H., Xu, Q., Chen, M. J., Liao, Y., Thiyagarajan, M., . . . Nedergaard, M. (2013). Sleep Drives Metabolite Clearance from the Adult Brain. *Science, 342*(6156), 373. doi:10.1126/science.1241224

Yuh, W. T., Zhu, M., Taoka, T., Quets, J. P., Maley, J. E., Muhonen, M. G., . . . Kardon, R. H. (2000). MR imaging of pituitary morphology in idiopathic intracranial hypertension. *J Magn Reson Imaging, 12*(6), 808-813. doi:10.1002/1522-2586(200012)12:6<808::aid-jmri3>3.0.co;2-n

5. General Discussion

5.1 Summary

By studying the effect of vestibular modulations on whole brain structure and function, I have shown new perspectives to vestibular system research in health and disease. In summary, in Chapter 2 I described altered sensory and cerebellar network connectivity in individuals suffering from functional dizziness, in Chapter 3 I characterised whole brain activity patterns and network changes occurring during artificial stimulation and in Chapter 4 I determined the impact of microgravity on the occurrence of enlarged perivascular spaces across the brain. In the following, I will put my results into context with previous research, highlight open questions and possible future approaches. I will first discuss clinical relevance of the findings, subsequently I will evaluate the methodology used and review the role of the cerebellum. After that, I will critically evaluate technological approaches for studying vestibular perception.

5.2 Clinical Relevance

A thorough understanding of neural underpinnings of vestibular information processing in both health and disease is relevant for clinical practice, both in terms of improving therapy as well as for developing appropriate preventive measures. In the case of somatoform or functional dizziness such as phobic postural vertigo (PPV), the functional network changes found in Chapter 2 may be related to previously reported experimental evidence that sensory expectation does not fit with the sensory input in these patients (Lehnen et al., 2019). Indeed, one resting state fMRI study in individuals suffering from other types of somatic symptoms also revealed a change in sensorimotor networks (Kim, Hong, Min, & Han, 2019). In the future we should determine whether functional network changes are related to symptoms of perceived dizziness, or whether the observed network changes are rather a marker for increased vulnerability for somatoform illnesses in general. Functional dizziness can occur as a secondary disorder after a structural vestibular syndrome (Dieterich & Staab, 2017). Hence, understanding the vulnerability factors would allow clinicians to recognise the need for prevention measures or to optimise therapy. Standardised clinical/psychological measures have been already been found to be predictive: increased neuroticism was for example shown to be a risk factor for somatoform dizziness (Dieterich & Staab, 2017). The advantage of using such standardised questionnaires is that they are often cheap and easy to analyse. Considering that functional

neuroimaging requires extensive resources in terms of time, costs and expertise, I am therefore not suggesting that fMRI measures should be included into general clinical practice. Instead, further clinical research involving fMRI will help us to understand disease mechanisms and follow treatment success in somatoform dizziness. Recent developments in measuring of individual differences in functional networks (see Section 5.4) may advance this field in the near future.

Artificial vestibular stimulation has become a popular treatment in a variety of clinical disorders. It was shown to improve postural performance in patients with vestibular disorders such as vestibulopathy (Iwasaki et al., 2014), other neurological disorders (e.g. Parkinson's (Samoudi et al., 2015)) and even in healthy participants (Hilliard et al., 2019; Wuehr et al., 2018). In Chapter 3 I show that no whole brain functional network changes occur during GVS. The therapeutic benefit of GVS is thus probably not related to network changes (at least not in healthy participants). It should be noted however, that in most cases, noisy GVS was used in these clinical studies and thus differs from the stimulus used in Chapter 3. Noisy GVS (also termed stochastic GVS) is a stimulation with randomly fluctuating currents with an overall mean of zero (Hilliard et al., 2019) that is usually presented at current strengths below the individuals' perceptual threshold. Stochastic resonance is the proposed mechanism for the therapeutic effect of noisy GVS. Stochastic resonance is a phenomenon in signal detection by which a signal that is too weak to be detected can be increased by adding randomly fluctuating low-level noise. By introducing an optimal amount of noise to a non-linear system the signal variance is increased and signal transmission or detection performance is improved, instead of impaired (Garrett, Kovacevic, McIntosh, & Grady, 2011; McDonnell & Abbott, 2009). Evidence for stochastic resonance in the brain has been found at the neuronal level (McDonnell & Abbott, 2009), and interestingly, also at the network level, where noise induced (neural) signal synchronisation can allow for rapid establishment and dissolvement of coherence (Avena-Koenigsberger, Misic, & Sporns, 2017). Considering these findings, noisy GVS may cause a change in functional network organization, unlike the lack of network reconfiguration found in in Chapter 3. This would correspond to the behavioural findings reported by Wilkinson et al. (2008), who found improvements in visual memory recall only after noisy GVS, but not after GVS with a constant amplitude in healthy participants. The results presented in Chapter 3 would provide a relevant baseline in healthy participants if such a study were to be executed.

Understanding the physiological effects of microgravity is important to conduct safe missions and for appropriate interventions to avoid long-term adverse effects or accidents.

For example, a simple vibrotactile feedback device improved performance of tilt perception in astronauts, which is deteriorated temporarily after return to earth (Clément, Reschke, & Wood, 2018). This device provides a potential means to help astronauts during landing (Clément et al., 2018). In terms of whole brain structural changes, significant shifts in CSF and expansion of ventricles were reported in astronauts shortly after return to earth, but with trends towards improvements or compensation at follow-up scans (Jillings et al., 2020; Van Ombergen et al., 2019). In Chapter 4 I presented the additional finding that a small, but significant increase of MR visible perivascular spaces in astronauts occurs shortly after the return from space, but that this effect normalises in the follow up scans. Altogether this suggest that the connective tissue properties in the interstitial circulation of the brain adapts in response to space travel. The lack of gravity thus results in accumulation of fluid in the brain which further causes a swelling of the perivascular spaces. Although these changes do not appear to have a long-term negative impact on the brain, it is not clear whether there is accumulation effect from multiple space missions or how the duration of space travel impacts physiology. This is particularly important since the National Aeronautics and Space Administration (NASA) and other space agencies are considering Mars missions which may last up to 3 years. Furthermore, considering that structural changes found in Chapter 4 were highly variable across astronauts even before their mission, it is important to consider individual factors such as amount of training and sleep quality in future analyses.

In summary, advances in vestibular neuroimaging research not only provide an understanding of how vestibular perception is modulated by different contexts but it can also be relevant for clinical practice. It provides support for specific treatments, by pointing towards possibilities for interventions and provides measures for monitoring treatment success or severity of the underlying condition. To be of significance for clinical practice though, clear benchmark values still need to be determined. This can be achieved by increasing our understanding of individual factors impacting vestibular perception. Additionally, we will need to move the focus of our research from descriptive to predictive markers derived from neuroimaging studies. Possible approaches will be discussed in the next two sections.

5.3 Network neuroscience methodology

One problematic aspect of network neuroscience is the correlative or descriptive nature of most studies. The goal should instead be to develop and test theories about the brain's information processing (Bassett et al., 2020; Bertolero & Bassett, 2020). Advanced

neuroimaging analysis techniques have been developed which go beyond simple brain mapping and aim at understanding the underlying mechanisms. Specifically, two (not mutually exclusive) analysis methods have been of particular interest recently: 1) task-based functional connectivity and 2) time-varying functional connectivity.

The former approach compares and contrasts functional networks different states (such as tasks). In Chapter 2 and Chapter 3 I analysed functional network properties during task paradigms, as well as in task-free states and by this could derive additional information about perceptual processing. Recent studies differ in their verdict regarding the added informational value from such task-based connectivity studies. Whilst some suggest functional connectivity derived from task-based study designs provides additional information (Di & Biswal, 2019) and can help to predict phenotypes (Greene et al., 2020), other studies suggest that task-states contribute little to explaining the variance in functional connectivity, arguing that the most important organisational features in the brain are explained by stable individual factors (Gratton et al., 2018). Despite the potentially small contributions, I found meaningful task-related network changes in both Chapter 2 and Chapter 3 and would thus argue that task-based functional connectivity is relevant for deepening our understanding about the brain.

Either way, brain dynamics are not limited to a distinct small number of states such as task and rest. Instead, the acquired BOLD time-series can be resolved further to smaller time-scales (ranging from several seconds up to few minutes). For each of the smaller time-windows network properties can be computed, thus allowing to investigate dynamic network changes. Such time-varying functional connectivity analyses have revealed that network organisation in resting-state paradigms is highly dynamic and that interindividual differences in these dynamics are indicative of traits as well as psychiatric and neurological conditions (Lurie et al., 2019). The number of studies using time-varying functional connectivity has increased significantly in recent years, providing a wide number of methodological approaches and considerations (Lurie et al., 2019). For example, several networks can be represented by means of a multi-layer network. This approach also allows the direct comparison of networks determined with different imaging modalities, such as structural and functional MRI for example (Sizemore & Bassett, 2018). Additional informational value can also be extracted by using algebra-topological methods, which allow going beyond the description of links to the descriptions of higher-order network shapes (Sizemore, Phillips-Cremins, Ghrist, & Bassett, 2019). Exploring network organisation in this time-resolved manner may thus provide more information about healthy and dysfunctional vestibular processing.

5.4 Interindividual differences

It is common practice in neuroscience, and particularly in fMRI research, to collect data from a large sample size, which is then normalised to a group averaged brain in order to allow for generalisation. Using this method, potentially meaningful individual differences can be overlooked. An impression of just how much the added value of an individualised data analysis can be was provided by Gordon et al. (2017). In an innovative data set, they collected over 10 hours of functional and multiple structural MRI data from overall ten participants which allowed to thoroughly study spatial and functional network variability. Indeed, using these data from highly sampled individuals, previously unknown individual differences could be described. In terms of regions involved in vestibular perception, Gordon et al. (2017) for example revealed that V5/MT+ was part of the lateral visual network in seven participants and not strongly connected to the dorsal attentional network in these subjects, contrary to previous studies suggesting an important role in the attentional networks. This approach was also found to be informative for understanding the contribution of the cerebellum to higher-order vestibular information processing (further discussed in Section 5.5). In order to advance our understanding of the vestibular system it would be thus important to determine both functional and structural heterogeneity by using an individualistic approach by analysing data from highly-sampled individuals. Highly sampling of patients may also be useful for individualised diagnosis, for example for biomarkers or surgical planning (Gratton et al., 2018). Despite the amount of time necessary for data acquisition, fMRI does not bear risks of radiation and is non-invasive (in contrast to positron emission tomography and X-ray computed tomography) (Gordon et al., 2017), making MRI a safe tool for such surgical planning.

Interindividual differences also contribute to performance in astronauts (Clément et al., 2020). It would be important to understand relevant factors to select suitable candidates for space missions or to set appropriate interventions in case anomalies are detected. In Chapter 4 the astronauts tested showed a high variance of enlarged perivascular spaces even before they go to space. Since there was no clear association with previous mission experience, the reason for this could be that some individuals were better than others in terms of coping with astronaut training, or space travel, or both. For instance the individual responses and vulnerabilities to sleep deprivation are of particular relevance for the perivascular changes found in Chapter 4. Lymphatic clearance in the brain occurs mainly during sleep (Bakker et al., 2016), the lack of which can lead to increased perivascular spaces. Sleep deficiency is prevalent not only during space missions but also during the training before the mission (Barger et al., 2014). Those astronauts with

particularly low sleep levels in pre-mission training may show smaller effects during space flight than those that slept better.

5.5 The role of the cerebellum

The cerebellum has been often ignored in human neuroimaging studies or considered as one homogenous structure, although it contains four times the amount of cells in the cerebral cortex (Andersen, Korbo, & Pakkenberg, 1992). The cerebellum is not only a key structure that integrates vestibular information for motor function and self-motion perception, but it is also involved in a wide range of cognitive and behavioural functions (Baumann et al., 2015; Buckner, 2013; King et al., 2019). Considering this diversity of functions, the cerebellum is thought to be a structure generally important for predicting events and subsequently for modulating neural signals (Baumann et al., 2015; Marek et al., 2018).

In Chapter 2 I showed that cerebellar connectivity is strongly decreased during a symptom-provoking stimulus in patients with functional dizziness. Cerebellar connectivity is also weakened in a number of other conditions which are characterised by impairments in sensory processing such as schizophrenia (Chen et al., 2013; Ding et al., 2019), attention-deficit disorder and autism (Sathyanesan et al., 2019). This corroborates the notion that a dysfunction of cerebellum is related to deficient sensory processing and dysfunctional behavioural modulation. In future it will be important to differentiate between the subregions of the cerebellum in order to get a better understanding of the involved mechanisms.

In the task activation analysis in Chapter 3, I confirmed the long-held notion that nodulus and uvula are uniquely involved in the processing self-motion. Since only cortical connectivity was the focus of the study and infratentorial signal-to-noise ratio was insufficient, functional connectivity of the cerebellum was not explored further. In addition, the amount of both resting-state and task data would have probably not sufficed to achieve reliable results: in a resting-state fMRI study using high sampling of individuals, Marek et al. (2018) found that for reliable quantification of functional connectivity in the cerebellum, double the quantity of cortical data are necessary. This means, longer fMRI sessions are needed to quantify connectivity of the cerebellum. The same study also revealed that the network representation was highly variable amongst individuals. Hence, future studies investigating cerebellar connectivity during vestibular processing should also consider highly sampling individual participants to obtain stable results. Using

optimised fMRI sequences achieving high temporal signal to noise ration across the whole brain would be also an option, if high sampling is not possible.

The cerebellum was also structurally and functionally affected by microgravity. An upward cerebellar shift, in addition to the whole brain displacement was proposed by Jillings et al. (2020): they found a decrease in the space along the cerebellar tentorium (the dura mater between the cerebellum and the inferior portion of the occipital lobes). A similar effect was also found by Roberts et al. (2017), who describe a decrease of the supravermian cistern in astronauts (i.e. a decrease of the subarachnoid space above the cerebellar vermis). I made the unique observation of enlarged perivascular spaces in the cerebellum of some space travellers, further strengthening the notion that fluid accumulates in this portion of the brain as well.

5.6 Technological advances to study vestibular system

In order to gain a full understanding of the underlying neural processes involved in vestibular perception, imaging the brain during physical motion would be necessary to gather a realistic account of all the involved proprioceptive, visual and motor signals. Although GVS causes subjective motion perception, it is important to note that this vestibular stimulation activates all of the otolith organ and all of the semi-circular canal afferents on one side, while simultaneously inhibiting activation of all the vestibular organs on the contralateral side. As Kwan et al. (2019) rightly notes, this type of activation pattern (i.e. the simultaneous activation of otolith and semi-circular canal afferents) does not have a physiological motion equivalent and is thus indeed artificial. Furthermore, the neuronal response of the afferents differs to their responses to natural motion, possibly because GVS bypasses the mechanotransduction of the vestibular organs (Kwan et al., 2019).

Unfortunately, exposure to virtual environments without active motion is also not ideal for understanding self-motion. It has been shown, that motor signals generated during voluntary behaviour influence sensory processing at the level of the vestibular nuclei neurons (Cullen & Taube, 2017). In animal studies it has also been shown that neuronal firing differs in central brain structures involved with navigation, depending on whether movement was passive or active (Winter, Mehlman, Clark, & Taube, 2015). It can be thus expected that brain function in humans will to a certain extend also differ during active motion.

Whilst active motion is currently not possible during MR acquisition, it is possible during electroencephalography (EEG), which only provides low spatial resolution however. Technological advances in the more distanced future may be developed. For example, Boto et al. (2018) recently reported the development of a wearable magnetoencephalography (MEG) device, making it possible to perform more naturalistic tasks whilst brain activity is recorded. In contrast to MRI, which only allows the recording of a neurophysiological proxy of neuronal activity, MEG is a direct measure of neural currents (although only signals from dendrites located on the surface of the brain and at right angles to the walls of the sulci can be detected (Baars & Gage, 2013)). In contrast to EEG, MEG has better spatial resolution. This method would thus allow unconstrained head movement, more naturalistic paradigms involving realistic input from the vestibular system would thus be possible. Naturalistic locomotion would not be possible (yet) with this method however. So far, human vestibular research is thus restricted to use methods which approximate naturalistic self-motion and combine the results with experimental evidence from animal studies.

5.7 Conclusion

The processing of vestibular information is ubiquitous in our daily lives, in all movement as well as at rest, when the vestibular system recognizes gravity. Under most circumstances, we are not consciously aware of our vestibular processing, however there are a number of contexts, both artificial and natural that demonstrate how important our vestibular sense is by throwing us literally out of balance when the system is out of accord. In this thesis I have shown that a whole-brain approach is insightful for studying vestibular perception. By applying network neuroscience approaches to chronic vestibular patients and during artificial vestibular stimulation, I explored brain function during long and short-term state changes vestibular perception. I found functional network differences in individuals experiencing chronic dizziness without structural origin which fit to the notion that this condition is of somatoform origin. I also characterised functional brain changes during artificial vestibular stimulation in healthy participants and surprisingly found no cortical reorganisation, possibly reflecting the subconscious nature of vestibular processing. In addition, I showed that medium-term exposure to microgravity also affects the brain's structure supporting the notion of a cephalic fluid shift during microgravity. This finding contributes towards a better understanding of the effect microgravity has on the brain, which is important for designing safe missions to space. Overall, exploring whole brain network organisation and the change of thereof during vestibular perception in different context provides novel insights about the underlying neural processes.

6. References

Abbott, N. J., Pizzo, M. E., Preston, J. E., Janigro, D., & Thorne, R. G. (2018). The role of brain barriers in fluid movement in the CNS: is there a 'glymphatic' system? *Acta Neuropathol, 135*(3), 387-407. doi:10.1007/s00401-018-1812-4

Andersen, B. B., Korbo, L., & Pakkenberg, B. (1992). A quantitative study of the human cerebellum with unbiased stereological techniques. *Journal of Comparative Neurology, 326*(4), 549-560.

Angelaki, D. E., & Cullen, K. E. (2008). Vestibular system: the many facets of a multimodal sense. *Annu Rev Neurosci, 31*, 125-150. doi:10.1146/annurev.neuro.31.060407.125555

Anstis, S., Verstraten, F. A., & Mather, G. (1998). The motion aftereffect. *Trends Cogn Sci, 2*(3), 111-117. doi:10.1016/s1364-6613(98)01142-5

Avena-Koenigsberger, A., Misic, B., & Sporns, O. (2017). Communication dynamics in complex brain networks. *Nat Rev Neurosci, 19*(1), 17-33. doi:10.1038/nrn.2017.149

Baars, B. J., & Gage, N. M. (2013). Chapter 5 - Brain imaging. In B. J. Baars & N. M. Gage (Eds.), *Fundamentals of Cognitive Neuroscience* (pp. 109-140). San Diego: Academic Press.

Baggio, H. C., Segura, B., & Junque, C. (2015). Resting-state functional brain networks in Parkinson's disease. *CNS neuroscience & therapeutics, 21*(10), 793-801. doi:10.1111/cns.12417

Bakker, E. N., Bacskai, B. J., Arbel-Ornath, M., Aldea, R., Bedussi, B., Morris, A. W., . . . Carare, R. O. (2016). Lymphatic Clearance of the Brain: Perivascular, Paravascular and Significance for Neurodegenerative Diseases. *Cell Mol Neurobiol, 36*(2), 181-194. doi:10.1007/s10571-015-0273-8

Barger, L. K., Flynn-Evans, E. E., Kubey, A., Walsh, L., Ronda, J. M., Wang, W., . . . Czeisler, C. A. (2014). Prevalence of sleep deficiency and use of hypnotic drugs in astronauts before, during, and after spaceflight: an observational study. *The Lancet Neurology, 13*(9), 904-912. doi:10.1016/s1474-4422(14)70122-x

Barlow, H. B., & Hill, R. M. (1963). Evidence for a Physiological Explanation of the Waterfall Phenomenon and Figural After-effects. *Nature, 200*(4913), 1345-1347. doi:10.1038/2001345a0

Barmack, N. H. (2003). Central vestibular system: vestibular nuclei and posterior cerebellum. *Brain research bulletin, 60*(5-6), 511-541.

Bassett, D. S., Cullen, K. E., Eickhoff, S. B., Farah, M. J., Goda, Y., Haggard, P., . . . Ueda, H. R. (2020). Reflections on the past two decades of neuroscience. *Nat Rev Neurosci*. doi:10.1038/s41583-020-0363-6

Bassett, D. S., & Sporns, O. (2017). Network neuroscience. *Nature Neuroscience, 20*(3), 353-364. doi:10.1038/nn.4502

Bastian, M., Heymann, S., & Jacomy, M. (2015). Gephi: an open source software for exploring and manipulating networks. International AAAI Conference on Weblogs and Social Media [Internet]. 2009. *There is no corresponding record for this reference.[Google Scholar]*.

Baumann, O., Borra, R. J., Bower, J. M., Cullen, K. E., Habas, C., Ivry, R. B., . . . Sokolov, A. A. (2015). Consensus paper: the role of the cerebellum in perceptual processes. *Cerebellum, 14*(2), 197-220. doi:10.1007/s12311-014-0627-7

Bear, M. F., Connors, B. W., & Paradiso, M. A. (2007). Neuroscience: Exploring the brain.

Bertolero, M. A., & Bassett, D. S. (2020). On the Nature of Explanations Offered by Network Science: A Perspective From and for Practicing Neuroscientists. *Top Cogn Sci*. doi:10.1111/tops.12504

Biswal, B. B., Kylen, J. V., & Hyde, J. S. (1997). Simultaneous assessment of flow and BOLD signals in resting-state functional connectivity maps. *NMR in Biomedicine, 10*(4-5), 165-170. doi:10.1002/(SICI)1099-1492(199706/08)10:4/5<165::AID-NBM454>3.0.CO;2-7

Bolt, T., Nomi, J. S., Rubinov, M., & Uddin, L. Q. (2017). Correspondence between evoked and intrinsic functional brain network configurations. *Hum Brain Mapp, 38*(4), 1992-2007. doi:10.1002/hbm.23500

Borra, E., & Luppino, G. (2017). Functional anatomy of the macaque temporo-parieto-frontal connectivity. *Cortex, 97*, 306-326. doi:https://doi.org/10.1016/j.cortex.2016.12.007

Boto, E., Holmes, N., Leggett, J., Roberts, G., Shah, V., Meyer, S. S., . . . Brookes, M. J. (2018). Moving magnetoencephalography towards real-world applications with a wearable system. *Nature, 555*(7698), 657-661. doi:10.1038/nature26147

Brandt, T. (2013). *Vertigo: its multisensory syndromes*: Springer Science & Business Media.

Brandt, T., & Dieterich, M. (2017). The dizzy patient: don't forget disorders of the central vestibular system. *Nat Rev Neurol, 13*(6), 352-362. doi:10.1038/nrneurol.2017.58

Brandt, T., Huppert, T., Hüfner, K., Zingler, V. C., Dieterich, M., & Strupp, M. (2010). Long-term course and relapses of vestibular and balance disorders. *Restorative neurology and neuroscience, 28*(1), 69-82.

Buckner, Randy L. (2013). The Cerebellum and Cognitive Function: 25 Years of Insight from Anatomy and Neuroimaging. *Neuron, 80*(3), 807-815. doi:https://doi.org/10.1016/j.neuron.2013.10.044

Bullmore, E., & Sporns, O. (2009). Complex brain networks: graph theoretical analysis of structural and functional systems. *Nat Rev Neurosci, 10*(3), 186-198. doi:10.1038/nrn2575

Büttner, U., & Buettner, U. W. (1978). Parietal cortex (2v) neuronal activity in the alert monkey during natural vestibular and optokinetic stimulation. *Brain research, 153*(2), 392-397. doi:https://doi.org/10.1016/0006-8993(78)90421-3

Caballero-Gaudes, C., & Reynolds, R. C. (2017). Methods for cleaning the BOLD fMRI signal. *Neuroimage, 154*, 128-149. doi:https://doi.org/10.1016/j.neuroimage.2016.12.018

Chafee, M. V., Averbeck, B. B., & Crowe, D. A. (2007). Representing Spatial Relationships in Posterior Parietal Cortex: Single Neurons Code Object-Referenced Position. *Cerebral Cortex, 17*(12), 2914-2932. doi:10.1093/cercor/bhm017

Chen, A., DeAngelis, G. C., & Angelaki, D. E. (2010). Macaque parieto-insular vestibular cortex: responses to self-motion and optic flow. *Journal of Neuroscience, 30*(8), 3022-3042. Retrieved from https://www.ncbi.nlm.nih.gov/pmc/articles/PMC3108058/pdf/zns3022.pdf

Chen, A., DeAngelis, G. C., & Angelaki, D. E. (2011). Convergence of vestibular and visual self-motion signals in an area of the posterior sylvian fissure. *The Journal of neuroscience : the official journal of the Society for Neuroscience, 31*(32), 11617-11627. doi:10.1523/JNEUROSCI.1266-11.2011

Chen, Y.-L., Tu, P.-C., Lee, Y.-C., Chen, Y.-S., Li, C.-T., & Su, T.-P. (2013). Resting-state fMRI mapping of cerebellar functional dysconnections involving multiple large-scale networks in patients with schizophrenia. *Schizophrenia Research, 149*(1), 26-34. doi:https://doi.org/10.1016/j.schres.2013.05.029

Clément, G., Reschke, M. F., & Wood, S. J. (2018). Vibrotactile Feedback Improves Manual Control of Tilt After Spaceflight. *Front Physiol, 9*, 1850. doi:10.3389/fphys.2018.01850

Clément, G. R., Boyle, R. D., George, K. A., Nelson, G. A., Reschke, M. F., Williams, T. J., & Paloski, W. H. (2020). Challenges to the central nervous system during human spaceflight missions to Mars. *Journal of neurophysiology, 123*(5), 2037-2063.

Cole, M. W., Bassett, D. S., Power, J. D., Braver, T. S., & Petersen, S. E. (2014). Intrinsic and task-evoked network architectures of the human brain. *Neuron, 83*(1), 238-251. doi:10.1016/j.neuron.2014.05.014

Cottereau, B. R., Smith, A. T., Rima, S., Fize, D., Héjja-Brichard, Y., Renaud, L., . . . Durand, J.-B. (2017). Processing of Egomotion-Consistent Optic Flow in the Rhesus Macaque Cortex. *Cerebral Cortex, 27*(1), 330-343. doi:10.1093/cercor/bhw412

Culham, J. C., Dukelow, S. P., Vilis, T., Hassard, F. A., Gati, J. S., Menon, R. S., & Goodale, M. A. (1999). Recovery of fMRI activation in motion area MT following storage of the motion aftereffect. *J Neurophysiol, 81*(1), 388-393. doi:10.1152/jn.1999.81.1.388

Cullen, K. E., & Taube, J. S. (2017). Our sense of direction: progress, controversies and challenges. *Nat Neurosci, 20*(11), 1465-1473. doi:10.1038/nn.4658

Curthoys, I., & MacDougall, H. (2012). What Galvanic Vestibular Stimulation Actually Activates. *Frontiers in Neurology, 3*(117). doi:10.3389/fneur.2012.00117

Di, X., & Biswal, B. B. (2019). Toward task connectomics: examining whole-brain task modulated connectivity in different task domains. *Cerebral Cortex, 29*(4), 1572-1583.

Dieterich, M., & Staab, J. P. (2017). Functional dizziness: from phobic postural vertigo and chronic subjective dizziness to persistent postural-perceptual dizziness. *Current opinion in neurology, 30*(1), 107-113.

Ding, Y., Ou, Y., Pan, P., Shan, X., Chen, J., Liu, F., . . . Guo, W. (2019). Cerebellar structural and functional abnormalities in first-episode and drug-naive patients with schizophrenia: A meta-analysis. *Psychiatry Research: Neuroimaging, 283*, 24-33. doi:https://doi.org/10.1016/j.pscychresns.2018.11.009

Ebata, S., Sugiuchi, Y., Izawa, Y., Shinomiya, K., & Shinoda, Y. (2004). Vestibular projection to the periarcuate cortex in the monkey. *Neurosci Res, 49*(1), 55-68. doi:10.1016/j.neures.2004.01.012

Eickhoff, S. B., Yeo, B. T. T., & Genon, S. (2018). Imaging-based parcellations of the human brain. *Nat Rev Neurosci, 19*(11), 672-686. doi:10.1038/s41583-018-0071-7

Fitzpatrick, R. C., & Day, B. L. (2004). Probing the human vestibular system with galvanic stimulation. *J Appl Physiol (1985), 96*(6), 2301-2316. doi:10.1152/japplphysiol.00008.2004

Forbes, P. A., Luu, B. L., Van der Loos, H. M., Croft, E. A., Inglis, J. T., & Blouin, J.-S. (2016). Transformation of vestibular signals for the control of standing in humans. *Journal of Neuroscience, 36*(45), 11510-11520.

Furman, J. M., & Cass, S. P. (1999). Benign paroxysmal positional vertigo. *New England Journal of Medicine, 341*(21), 1590-1596.

Garrett, D. D., Kovacevic, N., McIntosh, A. R., & Grady, C. L. (2011). The importance of being variable. *J Neurosci, 31*(12), 4496-4503. doi:10.1523/JNEUROSCI.5641-10.2011

Goldberg, J. M., Smith, C. E., & Fernandez, C. (1984). Relation between discharge regularity and responses to externally applied galvanic currents in vestibular nerve afferents of the squirrel monkey. *Journal of neurophysiology, 51*(6), 1236-1256. doi:10.1152/jn.1984.51.6.1236

Goldberg, J. M., Wilson, V. J., Cullen, K. E., Angelaki, D. E., Broussard, D. M., Buttner-Ennever, J., . . . Minor, L. B. (2012). *The vestibular system: a sixth sense*: Oxford University Press.

Gordon, E. M., Laumann, T. O., Gilmore, A. W., Newbold, D. J., Greene, D. J., Berg, J. J., . . . Sun, H. (2017). Precision functional mapping of individual human brains. *Neuron, 95*(4), 791-807. e797.

Gratton, C., Laumann, T. O., Nielsen, A. N., Greene, D. J., Gordon, E. M., Gilmore, A. W., . . . Petersen, S. E. (2018). Functional Brain Networks Are Dominated by Stable Group and Individual Factors, Not Cognitive or Daily Variation. *Neuron, 98*(2), 439-452 e435. doi:10.1016/j.neuron.2018.03.035

Greene, A. S., Gao, S., Noble, S., Scheinost, D., & Constable, R. T. (2020). How Tasks Change Whole-Brain Functional Organization to Reveal Brain-Phenotype Relationships. *Cell Reports, 32*(8), 108066. doi:https://doi.org/10.1016/j.celrep.2020.108066

Guldin, W., & Grüsser, O. (1998). Is there a vestibular cortex? *Trends in neurosciences, 21*(6), 254-259.

Guldin, W. O., Akbarian, S., & Grüsser, O. J. (1992). Cortico-cortical connections and cytoarchitectonics of the primate vestibular cortex: a study in squirrel monkeys (Saimiri sciureus). *J Comp Neurol, 326*(3), 375-401. doi:10.1002/cne.903260306

Hallgren, E., Kornilova, L., Fransen, E., Glukhikh, D., Moore, S. T., Clément, G., . . . Wuyts, F. L. (2016). Decreased otolith-mediated vestibular response in 25 astronauts induced by long-duration spaceflight. *Journal of neurophysiology, 115*(6), 3045-3051. doi:10.1152/jn.00065.2016

Helmchen, C., Machner, B., Rother, M., Spliethoff, P., Göttlich, M., & Sprenger, A. (2020). Effects of galvanic vestibular stimulation on resting state brain activity in patients with bilateral vestibulopathy. *Hum Brain Mapp, 41*(9), 2527-2547. doi:10.1002/hbm.24963

Hilliard, D., Passow, S., Thurm, F., Schuck, N. W., Garthe, A., Kempermann, G., & Li, S.-C. (2019). Noisy galvanic vestibular stimulation modulates spatial memory in young healthy adults. *Scientific Reports, 9*(1), 9310. doi:10.1038/s41598-019-45757-0

Hinghofer-Szalkay, H. (2011). Gravity, the hydrostatic indifference concept and the cardiovascular system. *Eur J Appl Physiol, 111*(2), 163-174. doi:10.1007/s00421-010-1646-9

Hitier, M., Besnard, S., & Smith, P. F. (2014). Vestibular pathways involved in cognition. *Front Integr Neurosci, 8*, 59. doi:10.3389/fnint.2014.00059

Indovina, I., Riccelli, R., Chiarella, G., Petrolo, C., Augimeri, A., Giofrè, L., . . . Passamonti, L. (2015). Role of the insula and vestibular system in patients with chronic subjective dizziness: an fMRI study using sound-evoked vestibular stimulation. *Frontiers in Behavioral Neuroscience, 9*, 334.

Iwasaki, S., Yamamoto, Y., Togo, F., Kinoshita, M., Yoshifuji, Y., Fujimoto, C., & Yamasoba, T. (2014). Noisy vestibular stimulation improves body balance in bilateral vestibulopathy. *Neurology, 82*(11), 969-975.

Jillings, S., Van Ombergen, A., Tomilovskaya, E., Rumshiskaya, A., Litvinova, L., Nosikova, I., . . . Manko, O. (2020). Macro-and microstructural changes in cosmonauts' brains after long-duration spaceflight. *Science Advances, 6*(36), eaaz9488.

Kim, S. M., Hong, J. S., Min, K. J., & Han, D. H. (2019). Brain Functional Connectivity in Patients With Somatic Symptom Disorder. *Psychosom Med, 81*(3), 313-318. doi:10.1097/PSY.0000000000000681

King, M., Hernandez-Castillo, C. R., Poldrack, R. A., Ivry, R. B., & Diedrichsen, J. (2019). Functional boundaries in the human cerebellum revealed by a multi-domain task battery. *Nature Neuroscience, 22*(8), 1371-1378. doi:10.1038/s41593-019-0436-x

Klingner, C. M., Axer, H., Brodoehl, S., & Witte, O. W. (2016). Vertigo and the processing of vestibular information: a review in the context of predictive coding. *Neuroscience & Biobehavioral Reviews, 71*, 379-387.

Kwan, A., Forbes, P. A., Mitchell, D. E., Blouin, J. S., & Cullen, K. E. (2019). Neural substrates, dynamics and thresholds of galvanic vestibular stimulation in the behaving primate. *Nat Commun, 10*(1), 1904. doi:10.1038/s41467-019-09738-1

Lathers, C. M., Charles, J. B., Elton, K. F., Holt, T. A., Mukai, C., Bennett, B. S., & Bungo, M. W. (1989). Acute hemodynamic responses to weightlessness in humans. *J Clin Pharmacol, 29*(7), 615-627. doi:10.1002/j.1552-4604.1989.tb03390.x

Lee, H., Xie, L., Yu, M., Kang, H., Feng, T., Deane, R., . . . Benveniste, H. (2015). The Effect of Body Posture on Brain Glymphatic Transport. *J Neurosci, 35*(31), 11034-11044. doi:10.1523/JNEUROSCI.1625-15.2015

Lehnen, N., Schröder, L., Henningsen, P., Glasauer, S., & Ramaioli, C. (2019). Deficient head motor control in functional dizziness: Experimental evidence of central sensory-motor dysfunction in persistent physical symptoms. In *Progress in brain research* (Vol. 249, pp. 385-400): Elsevier.

Lopez, C., & Blanke, O. (2011). The thalamocortical vestibular system in animals and humans. *Brain Research Reviews, 67*(1-2), 119-146. doi:10.1016/j.brainresrev.2010.12.002

Lopez, C., Blanke, O., & Mast, F. W. (2012). The human vestibular cortex revealed by coordinate-based activation likelihood estimation meta-analysis. *Neuroscience, 212*, 159-179. doi:10.1016/j.neuroscience.2012.03.028

Lurie, D. J., Kessler, D., Bassett, D. S., Betzel, R. F., Breakspear, M., Kheilholz, S., . . . Calhoun, V. D. (2019). Questions and controversies in the study of time-varying functional connectivity in resting fMRI. *Network Neuroscience, 4*(1), 30-69. doi:10.1162/netn_a_00116

Mader, T. H., Gibson, C. R., Pass, A. F., Kramer, L. A., Lee, A. G., Fogarty, J., . . . Sargsyan, A. (2011). Optic disc edema, globe flattening, choroidal folds, and hyperopic shifts observed in astronauts after long-duration space flight. *Ophthalmology, 118*(10), 2058-2069.

Marek, S., Siegel, J. S., Gordon, E. M., Raut, R. V., Gratton, C., Newbold, D. J., . . . Dosenbach, N. U. F. (2018). Spatial and Temporal Organization of the Individual Human Cerebellum. *Neuron, 100*(4), 977-993 e977. doi:10.1016/j.neuron.2018.10.010

McDonnell, M. D., & Abbott, D. (2009). What is stochastic resonance? Definitions, misconceptions, debates, and its relevance to biology. *PLoS Comput Biol, 5*(5), e1000348. doi:10.1371/journal.pcbi.1000348

Mestre, H., Kostrikov, S., Mehta, R. I., & Nedergaard, M. (2017). Perivascular spaces, glymphatic dysfunction, and small vessel disease. *Clin Sci (Lond), 131*(17), 2257-2274. doi:10.1042/CS20160381

Mestre, H., Mori, Y., & Nedergaard, M. (2020). The Brain's Glymphatic System: Current Controversies. *Trends Neurosci, 43*(7), 458-466. doi:10.1016/j.tins.2020.04.003

Morita, H., Kaji, H., Ueta, Y., & Abe, C. (2020). Understanding vestibular-related physiological functions could provide clues on adapting to a new gravitational environment. *The Journal of Physiological Sciences, 70*(1), 17. doi:10.1186/s12576-020-00744-3

Nashner, L. M., & Wolfson, P. (1974). Influence of head position and proprioceptive cues on short latency postural reflexes evoked by galvanic stimulation of the human labyrinth. *Brain research, 67*(2), 255-268.

Nelson, E. S., Mulugeta, L., & Myers, J. G. (2014). Microgravity-induced fluid shift and ophthalmic changes. *Life (Basel, Switzerland), 4*(4), 621-665. doi:10.3390/life4040621

Popp, P., Wulff, M., Finke, K., Ruhl, M., Brandt, T., & Dieterich, M. (2017). Cognitive deficits in patients with a chronic vestibular failure. *J Neurol, 264*(3), 554-563. doi:10.1007/s00415-016-8386-7

Purkinje, J. E. (1820). Beyträge zur näheren Kenntniss des Schwindels aus heautognostischen Daten. *Medicinische Jahrbücher des kaiserlich königlich österreichischen Staates, 6*(II), 79-125.

Querner, V., Krafczyk, S., Dieterich, M., & Brandt, T. (2000). Patients with somatoform phobic postural vertigo: the more difficult the balance task, the better the balance performance. *Neuroscience letters, 285*(1), 21-24.

Rasmussen, M. K., Mestre, H., & Nedergaard, M. (2018). The glymphatic pathway in neurological disorders. *The Lancet Neurology, 17*(11), 1016-1024. doi:10.1016/s1474-4422(18)30318-1

Roberts, D. R., Albrecht, M. H., Collins, H. R., Asemani, D., Chatterjee, A. R., Spampinato, M. V., . . . Antonucci, M. U. (2017). Effects of Spaceflight on

Astronaut Brain Structure as Indicated on MRI. *New England Journal of Medicine, 377*(18), 1746-1753. doi:10.1056/NEJMoa1705129

Rorden, C. (2020). MRIcroGL. Retrieved from https://www.nitrc.org/projects/mricrogl

Rozzi, S., Calzavara, R., Belmalih, A., Borra, E., Gregoriou, G. G., Matelli, M., & Luppino, G. (2005). Cortical Connections of the Inferior Parietal Cortical Convexity of the Macaque Monkey. *Cerebral Cortex, 16*(10), 1389-1417. doi:10.1093/cercor/bhj076

Rubinov, M., & Sporns, O. (2010). Complex network measures of brain connectivity: uses and interpretations. *Neuroimage, 52*(3), 1059-1069. doi:10.1016/j.neuroimage.2009.10.003

Rühl, R. M., Bauermann, T., Dieterich, M., & zu Eulenburg, P. (2018). Functional correlate and delineated connectivity pattern of human motion aftereffect responses substantiate a subjacent visual-vestibular interaction. *Neuroimage, 174*, 22-34.

Samoudi, G., Jivegård, M., Mulavara, A. P., & Bergquist, F. (2015). Effects of Stochastic Vestibular Galvanic Stimulation and LDOPA on Balance and Motor Symptoms in Patients With Parkinson's Disease. *Brain Stimulation: Basic, Translational, and Clinical Research in Neuromodulation, 8*(3), 474-480. doi:10.1016/j.brs.2014.11.019

Sathyanesan, A., Zhou, J., Scafidi, J., Heck, D. H., Sillitoe, R. V., & Gallo, V. (2019). Emerging connections between cerebellar development, behaviour and complex brain disorders. *Nat Rev Neurosci, 20*(5), 298-313. doi:10.1038/s41583-019-0152-2

Schaefer, A., Kong, R., Gordon, E. M., Laumann, T. O., Zuo, X.-N., Holmes, A. J., . . . Yeo, B. T. (2018). Local-global parcellation of the human cerebral cortex from intrinsic functional connectivity MRI. *Cerebral Cortex, 28*(9), 3095-3114.

Scheperjans, F., Hermann, K., Eickhoff, S. B., Amunts, K., Schleicher, A., & Zilles, K. (2007). Observer-Independent Cytoarchitectonic Mapping of the Human Superior Parietal Cortex. *Cerebral Cortex, 18*(4), 846-867. doi:10.1093/cercor/bhm116

Schlindwein, P., Mueller, M., Bauermann, T., Brandt, T., Stoeter, P., & Dieterich, M. (2008). Cortical representation of saccular vestibular stimulation: VEMPs in fMRI. *Neuroimage, 39*(1), 19-31.

Schneider, E., Glasauer, S., & Dieterich, M. (2002). Comparison of human ocular torsion patterns during natural and galvanic vestibular stimulation. *Journal of neurophysiology, 87*(4), 2064-2073.

Schniepp, R., Boerner, J. C., Decker, J., Jahn, K., Brandt, T., & Wuehr, M. (2018). Noisy vestibular stimulation improves vestibulospinal function in patients with bilateral vestibulopathy. *J Neurol, 265*(Suppl 1), 57-62. doi:10.1007/s00415-018-8814-y

Schniepp, R., Wuehr, M., Huth, S., Pradhan, C., Brandt, T., & Jahn, K. (2014). Gait characteristics of patients with phobic postural vertigo: effects of fear of falling, attention, and visual input. *Journal of neurology, 261*(4), 738-746.

Shinder, M. E., & Taube, J. S. (2010). Differentiating ascending vestibular pathways to the cortex involved in spatial cognition. *J Vestib Res, 20*(1), 3-23. doi:10.3233/VES-2010-0344

Sizemore, A. E., & Bassett, D. S. (2018). Dynamic graph metrics: Tutorial, toolbox, and tale. *Neuroimage, 180*(Pt B), 417-427. doi:10.1016/j.neuroimage.2017.06.081

Sizemore, A. E., Phillips-Cremins, J. E., Ghrist, R., & Bassett, D. S. (2019). The importance of the whole: Topological data analysis for the network neuroscientist. *Netw Neurosci, 3*(3), 656-673. doi:10.1162/netn_a_00073

Smith, A. T., Greenlee, M. W., DeAngelis, G. C., & Angelaki, D. E. (2017). Distributed Visual–Vestibular Processing in the Cerebral Cortex of Man and Macaque. *Multisensory Research, 30*(2), 91-120. doi:10.1163/22134808-00002568

Smith, A. T., Wall, M. B., & Thilo, K. V. (2012). Vestibular inputs to human motion-sensitive visual cortex. *Cereb Cortex, 22*(5), 1068-1077. doi:10.1093/cercor/bhr179

Sporns, O., Tononi, G., & Kötter, R. (2005). The Human Connectome: A Structural Description of the Human Brain. *PLOS Computational Biology, 1*(4), e42. doi:10.1371/journal.pcbi.0010042

Tanaka, K., Nishimura, N., & Kawai, Y. (2017). Adaptation to microgravity, deconditioning, and countermeasures. *J Physiol Sci, 67*(2), 271-281. doi:10.1007/s12576-016-0514-8

Toschi, N., Kim, J., Sclocco, R., Duggento, A., Barbieri, R., Kuo, B., & Napadow, V. (2017). Motion sickness increases functional connectivity between visual motion and nausea-associated brain regions. *Auton Neurosci, 202*, 108-113. doi:10.1016/j.autneu.2016.10.003

van den Heuvel, M. P., & Hulshoff Pol, H. E. (2010). Exploring the brain network: a review on resting-state fMRI functional connectivity. *Eur Neuropsychopharmacol, 20*(8), 519-534. doi:10.1016/j.euroneuro.2010.03.008

Van Ombergen, A., Heine, L., Jillings, S., Roberts, R. E., Jeurissen, B., Van Rompaey, V., . . . Wuyts, F. L. (2017). Altered functional brain connectivity in patients with visually induced dizziness. *NeuroImage. Clinical, 14*, 538-545. doi:10.1016/j.nicl.2017.02.020

Van Ombergen, A., Jillings, S., Jeurissen, B., Tomilovskaya, E., Rumshiskaya, A., Litvinova, L., . . . Wuyts, F. L. (2019). Brain ventricular volume changes induced by long-duration spaceflight. *Proc Natl Acad Sci U S A, 116*(21), 10531-10536. doi:10.1073/pnas.1820354116

Van Wezel, R., & Britten, K. (2002). Multiple uses of visual motion. The case for stability in sensory cortex. *Neuroscience, 111*(4), 739-759.

Wall, M. B., & Smith, A. T. (2008). The Representation of Egomotion in the Human Brain. *Current Biology, 18*(3), 191-194. doi:https://doi.org/10.1016/j.cub.2007.12.053

Wilkinson, D., Nicholls, S., Pattenden, C., Kilduff, P., & Milberg, W. (2008). Galvanic vestibular stimulation speeds visual memory recall. *Experimental brain research, 189*(2), 243-248. doi:10.1007/s00221-008-1463-0

Wilkinson, D., Zubko, O., Sakel, M., Coulton, S., Higgins, T., & Pullicino, P. (2014). Galvanic vestibular stimulation in hemi-spatial neglect. *Frontiers in Integrative Neuroscience, 8*(4). doi:10.3389/fnint.2014.00004

Winter, S. S., Mehlman, M. L., Clark, B. J., & Taube, J. S. (2015). Passive Transport Disrupts Grid Signals in the Parahippocampal Cortex. *Curr Biol, 25*(19), 2493-2502. doi:10.1016/j.cub.2015.08.034

Wuehr, M., Boerner, J. C., Pradhan, C., Decker, J., Jahn, K., Brandt, T., & Schniepp, R. (2018). Stochastic resonance in the human vestibular system - Noise-induced facilitation of vestibulospinal reflexes. *Brain Stimul, 11*(2), 261-263. doi:10.1016/j.brs.2017.10.016

Wuehr, M., Brandt, T., & Schniepp, R. (2017). Distracting attention in phobic postural vertigo normalizes leg muscle activity and balance. *Neurology, 88*(3), 284-288.

Yoder, R. M., & Taube, J. S. (2014). The vestibular contribution to the head direction signal and navigation. *Frontiers in Integrative Neuroscience, 8*, 32. Retrieved from https://www.frontiersin.org/article/10.3389/fnint.2014.00032

Zink, R., Bucher, S., Weiss, A., Brandt, T., & Dieterich, M. (1998). Effects of galvanic vestibular stimulation on otolithic and semicircular canal eye movements and perceived vertical. *Electroencephalography and clinical neurophysiology, 107*(3), 200-205.

zu Eulenburg, P., Caspers, S., Roski, C., & Eickhoff, S. B. (2012). Meta-analytical definition and functional connectivity of the human vestibular cortex. *Neuroimage, 60*(1), 162-169. doi:10.1016/j.neuroimage.2011.12.032

zu Eulenburg, P., Stephan, T., Dieterich, M., & Ruehl, R. M. (2020). The human vestibular cortex. *ScienceOpen Posters*.

Acknowledgements

"Well I've come so far to get here…"
Villagers

… and that I finally "arrived" is due to some very important people who have supported me throughout my PhD. First and foremost, I want to thank Dr. Virginia Flanagin for the supervision and for always giving me the freedom to follow my interests throughout my PhD. I want to thank Prof. Peter zu Eulenburg for the support and frequent enthusiasm. I also want to thank my RTG supervisor Prof. Thomas Geyer and TAC member Prof. Michael Ewers for support.

I want to thank all the people from the old and new Forschungshaus. Special thanks to Kathrin, Christopher, Nisha, and Theresa for being great office mates. Thommy, thank you for your kind and patient technical support. I also want to thank Isi, Angela and Kahina for the lovely spontaneous chats. Maxine, thank you for your scientific support and for your shared enthusiasm for jogging, good food and the arts.

I want to mention how vital the GSN & RTG was for not only my academic success, but also for my general wellbeing. I therefore want to thank Prof. Benedikt Grothe, Prof. Christian Leibold and Lena Bittl for supporting me and for being flexible enough to support my academic choices. Many thanks also to Stefanie Bosse and Verena Winkler for always supporting me with the greatest enthusiasm, I have always left your offices in a better mood. Catherine Botheroyd-Hobohm, thank you for organising all these memorable GSN events, you significantly contributed towards making Munich feel like my second home to me. I particularly want to thank Renate Herzog for definitely going above and beyond her work at the GSN office by helping out in a housing emergency – you helped me during this incredibly stressful time and I am very grateful for that!

"Home, is where I want to be, but I guess I'm already there"
Talking Heads

A lot of people indirectly contributed to this thesis by being there for me and by making Munich feel like a second home to me. Although words are not enough to express my gratitude, I will hereby at least attempt this impossible endeavour.

Lili, thank you for being such a reliable, understanding, and supportive friend. I do not think I would have managed to keep my sanity throughout the pandemic isolation without you. Thank you for your frequent motivational words which definitely helped me in getting this thesis actually done.

Veronika, it is somewhat crazy that we know each other since day one of our GSN PhD journey! Thank you for always being enthusiastic and interested, for asking and listening. Also thank you for being a reliable traveling, dancing and sports companion.

Ksenia, I am grateful for all the shared time: for those travels, the dancing, the fancy meals and drinks in restaurants and on balconies while discussing music and art.

Gabriel, muchas gracias for your friendship: for always making me laugh and for all the scientific, but more importantly, for all the emotional support.

Aurore, merci beaucoup for your friendship and for always being interested in my wellbeing!

Becky, notable founding member of the secret society with questionable rules which shall not be named, thank you for always coming up with the most random ideas, but at the same time also for being there to talk about all the seriousness going on in our lives.

Uri, Jaime & Alex, you all left Munich way too early in my opinion, but you have been an integral part regardless since day one at the GSN – thank you for being there and for making me laugh frequently.

Danke dir Sophie fürs schöne langjährige Zusammenwohnen. Marina, auch dir danke ich fürs Zusammenwohnen (wenn auch unter erschwerten Bedingungen) und für die regelmäßige Konzertbegleitung.

Definitely worthy of an honourable mention is the swanky apartment (aka. Veronika, Anna, Martin & Sara) – thank you for hosting me frequently and for making me feel like it is my Zweitwohnsitz.

Thanks to the 6-month-society (well, 6-month-ish-society) aka. Isi, Kathrin, Nisha & Alicia for the travels to Norway & Austria, and hopefully many more in the future.

To the lovely ladies from the Soapbox Science Munich Team, thank you for being passionate about feminism and for all the hard work you put into smashing the patriarchy, one step at a time.

Thank you to the Neurocamp Team for making this project actually work and for giving me the opportunity to share my enthusiasm for science.

I also want to generally thank all the lovely and kind people from the GSN 2013 cohort for cooking the most delicious dinners and for throwing the best parties.

Wo stehst du mit deiner Kunst, Baby?
Pauls Jets

Danke an Moritz, Andi & Vilim für die regelmäßige Theater- und Kulturbegleitung und für all die inspirierten Gespräche vor und nach den Vorstellungen.

Danke an ElChorazon, dass ihr mir einen Grund gegeben habt, um mich auf Montage zu freuen und dass ich durch euch für ein paar Stunden meinen Kopf von der Wissenschaft befreien konnte um meine Noten zu treffen.

„Wenn es soweit ist, werden wir es wissen (…) und es wird in Ordnung sein“
Die Heiterkeit

Das wichtigste kommt ja immer zum Schluss. Daher gehört der allergrößte Dank meiner Familie. Mama & Papa, danke, dass ihr mich immer unterstützt und dass ihr mir immer zur Seite steht. Danke, dass ihr es niemals leid werdet, mein Selbstwertgefühl aufzubauen und mir zu sagen, dass alles gut wird. Danke an Matthi, Babi, Opa Gerhard und an die gesamte Müller-Laber Familie, dass ihr mich trotz jahrelanger geographischer Distanz am Familiengeschehen teilhaben lässt. Ich bin mir bewusst, dass es etwas Besonderes ist, eine so liebe Familie zu haben. Ihr gebt mir das nötige Fundament, ohne welches diese Arbeit niemals entstanden wäre.

Curriculum Vitae: Judita Huber

HIGHER EDUCATION

Since 11/2016	**Ludwig-Maximilians-Universität**, Munich, DE Graduate School for Systemic Neurosciences (GSN) & RTG 2175: Perception in Context and its Neural Basis *PhD Systemic Neuroscience*
10/2013 – 10/2016	**Ludwig-Maximilians-Universität**, Munich, DE Graduate School for Systemic Neurosciences (GSN) *MSc Systemic Neuroscience*
09/2009 – 06/2013	**University of St Andrews**, St Andrews, UK *BSc (Honours) Psychology*

RESEARCH EXPERIENCE

Since 11/2016 — **Neurologische Forschung, Klinikum der Universität München, Ludwig-Maximilians-Universität, Munich, DE**

- *PhD Project:* "Individual differences in brain connectivity of the human vestibular network"

03/2019 – 05/2019 — **Complex Traits Genetics, Center for Neurogenomics and Cognitive Research, Vrije Universiteit,** Amsterdam, NL

- *Research Project:* "The functional connectome of the human vestibular system"

12/2014 – 10/2016 — **Neuroimaging Center, Technische Universität**, Munich, DE

- *MSc Project: "*Association of local neuronal activity with functional connectivity in the mouse, measured by means of simultaneous optical fiber calcium activity and resting-state functional imaging (rs-fMRI)"

10/2014 – 11/2014 — **Neuroimaging Center, Technische Universität,** Munich, DE

- *Research Project:* "Structural integrity and connectivity in coma patients"

02/2014 – 04/2014 — **Max Planck Institute of Psychiatry,** Munich, DE

- *Research Project:* The effect of trimethylhiazolin (fox odour) on the accumulation of nasally applied manganese using MRI

06/2012 – 08/2012 — **Austrian Institute of Economic Research (WIFO),** Vienna, AT

- *Scientific Assistant (part-time)* for *'WWWforEurope'*

06/2012 — **Neurorehabilitation Center Meidling,** Vienna, AT

- *Internship:* Therapy of people with traumatic brain injury

07/2008 – 08/2008 — **Austrian Institute of Technology (AIT),** Seibersdorf, AT

- *Internship at Institute of Bioresources: "*Protein Microarrays as a possible diagnostic tool for sepsis"

STIPENDS, AWARDS & WORKSHOPS

02/2019	**Exchange Stipend of the Network of European Neuroscience Schools (NENS)** for research stay at Vrije Universiteit Amsterdam
12/2017	**Workshop "The Senses: Cross-species Perspectives from Science and Art"** (organised by BIOTOPIA museum & GSN)
10/2017	**Boehringer Ingelheim Travel Stipend** for attending FENS CAJAL Neuroscience Training in Bordeaux
07/2017	**LMU Travel Stipend** for attending LERU Summer School on the topic of Citizen Science (UTH Zürich)
09/2016	**Leadership Seminar** (organised by Common Purpose & Studienstiftung)
09/2015	**9th Zurich Summer School on Biomedical Imaging** (ETH Zürich)
03/2015 – 09/2016	**Stipend of the Studienstiftung des Deutschen Volkes**
2010, 2011 & 2013	**Dean's List Award of University of St Andrews**

OTHER WORK EXPERIENCE & VOLUNTEERING

11/2017 – 10/2020 **Soapbox Science Munich**, *Organiser*

- Annual science communication event with the goal to increase visibility of women in science
- Tasks included event organisation (both as a 'physical' and as virtual event) and social media content management

10/2017 – 10/2020 **Neurocamp,** *Academic Content Officer*

- Annual two-week long neuroscience summer school for 16-18 year old students
- Tasks included conception and organisation of academic curriculum, contacting of lecturers

2014 – 2018 **Kids Brain Day,** *Organiser*

- Annual event for communication of neuroscience to children
- Event organisation, coordination of other volunteers, conception of activities appropriate for 6-10 year olds

Since 2013 **Akademický Spolek**, *Social Media Officer*

- Czech Academic Society in Vienna organising regular lectures and networking events for the Czech minority
- Social Media Content Management, Event Organisation

SKILLS

Programming & Software	MATLAB (Advanced), R (basic), Python (basic); Git (basic); Adobe Illustrator, MS Office
Languages	Native languages: German & Czech, English (C2), Slovak (B2), Spanish (A1)

Publication

Huber, J, Flanagin, VL, Popp, P, zu Eulenburg, P, Dieterich, M. Network changes in patients with phobic postural vertigo. *Brain Behav*. 2020; 10:e01622. https://doi.org/10.1002/brb3.1622

Affidavit

Hiermit versichere ich an Eides statt, dass ich die vorliegende Dissertation „The Impact of Vestibular Modulations on Whole Brain Structure and Function in Humans“ selbstständig angefertigt habe, mich außer der angegebenen keiner weiteren Hilfsmittel bedient und alle Erkenntnisse, die aus dem Schrifttum ganz oder annähernd übernommen sind, als solche kenntlich gemacht und nach ihrer Herkunft unter Bezeichnung der Fundstelle einzeln nachgewiesen habe.

I hereby confirm that the dissertation „The Impact of Vestibular Modulations on Whole Brain Structure and Function in Humans“ is the result of my own work and that I have only used sources or materials listed and specified in the dissertation.

München, den 08.10.2020

_____

Judita Huber

Declaration of author contribution

Huber, J., Flanagin, V.L., Popp, P., zu Eulenburg, P., Dieterich, M.*. Network changes in patients with phobic postural vertigo. Brain Behav. 2020*
JH conceived the analysis, analysed and interpreted the data, wrote the manuscript, and created the figures. VLF provided support with data analysis, and drafted and reviewed the manuscript and figures. PP acquired the data. PzE conceived the analysis, interpreted the data, and drafted and reviewed the manuscript and figures. MD conceived and designed the study, and drafted and reviewed the manuscript and figures. * PzE and MD have contributed equally.

Huber, J., Flanagin, V.L., Ruehl, R.M., zu Eulenburg, P. The modulation of human brain networks by means of vestibular stimulation (in preparation).
JH conceived the analysis, preprocessed the data for the functional connectivity analysis, analysed, and interpreted the data, wrote the manuscript, and created the figures. VLF provided support with data analysis, reviewed the manuscript and figures. RMR acquired the data. PzE conceived the experiment and the analysis, preprocessed the data for the task-based analysis, interpreted the data, and reviewed the manuscript and figures.

Huber, J., Jillings, S., Jeurissen, B., Tomilovskaya E., Rumshiskaya, A., Litvinova, L., Nosikova, I., Pechenkova, E., Kozlovskaya, I. B., Petrovichev, V., Rukavishnikov, I., Sunaert, S., Parizel, P.M., Sinitsyn, V., Sijbers, J., Annen, J., Laureys, S., Van Ombergen, A., and Wuyts, F. L., zu Eulenburg, P. Quantitative analysis of perivascular spaces in long-duration space flyers (in preparation).
JH analysed and interpreted the data, wrote the manuscript, and created the figures. F.W. conceived the experiment and acquired funding together with SL, VS, IK, PP, and SS. BJ, PP, FW, VS, SS, and JS designed the experiment. SJ, AVO, FW, ET, AR, LL, IN, EP, and IK collected the data. PzE conceived the analysis, preprocessed the data, interpreted the data, and reviewed the manuscript and figures.

Judita Huber	Date, Place
(First Author)	
Dr. Virginia L. Flanagin	Date, Place
(Supervisor)	